U.S. Department
of Transportation
**Federal Railroad
Administration**

Thermal Response of a Small Scale Cask-Like Test Article to Three Different High Temperature Environments

**Office of Research and Development
Washington, D.C. 20590**

R. S. Longenbaugh
L. C. Sanchez
A. R. Mahoney

Sandia National Laboratories
Albuquerque, New Mexico

DOT/FRA/ORD-90/01

February 1990
Final Report

This document available to the U.S. public through the National Technical Information Service, Springfield, VA 22161.

NOTICE

This document is disseminated under the sponsorship of the Department of Transportation in the interest of information exchange. The United States Government assumes no liability for its contents or use thereof.

NOTICE

The United States Government does not endorse products or manufacturers. Trade or manufacturers' names appear herein solely because they are considered essential to the object of this report.

Technical Report Documentation Page

1. Report No.	2. Government Accession No.	3. Recipient's Catalog No.
DOT/FRA/ORD-90/01		

4. Title and Subtitle	5. Report Date
Thermal Response of a Small Scale Cask-Like Test Article to Three Different High Temperature Environments	February 1990
	6. Performing Organization Code
	8. Performing Organization Report No.
7. Author(s)	
R. S. Longenbaugh; L. C. Sanchez; A. R. Mahoney*	
9. Performing Organization Name and Address	10. Work Unit No. (TRAIS)
Transportation Systems Technology and Analysis Division Sandia National Laboratories Albuquerque, NM 87185	11. Contract or Grant No. DTFR53-86-X-00035
	13. Type of Report and Period Covered Final
12. Sponsoring Agency Name and Address	14. Sponsoring Agency Code
Federal Railroad Administration Office of Research and Development 400 Seventh Street, SW Washington, DC 20590	RRS-32

15. Supplementary Notes

* Thermophysical Properties Division

16. Abstract

This report describes the test series conducted to assess the thermal response of a small scale, cask-like test article to three different thermal environments: an 800°C, 30-minute radiant heat environment; an 870°C, 100-minute radiant heat environment; and an enclosed engulfing fire environment of approximately 100-minute duration. Results indicated that the average total heat input to a cask-like test article was 140 MJ/m^2 for an 870°C, 100-minute radiant heat environment; 88 MJ/m^2 for an 800°C, 30-minute radiant heat environment; and 125 MJ/m^2 for enclosed engulfing fire for an approximate 100-minute duration. Results are specific to the test article geometry that was tested and are not applicable to real shipping cask geometries.

17. Key Words	18. Distribution Statement
thermal response; radiant heat environment; small scale cask-like test article	Document is available to the public from the National Technical Information Service Springfield, Virginia 22161

19. Security Classif. (of this report)	20. Security Classif. (of this page)	21. No. of Pages	22. Price
Unclassified	Unclassified	125	

METRIC CONVERSION FACTORS

Approximate Conversions to Metric Measures

Symbol	When You Know	Multiply by	To Find	Symbol
		LENGTH		
in	inches	*2.6	centimeters	cm
ft	feet	30	centimeters	cm
yd	yards	0.9	meters	m
mi	miles	1.6	kilometers	km
		AREA		
in^2	square inches	6.5	square centimeters	cm^2
ft^2	square feet	0.09	square meters	m^2
yd^2	square yards	0.8	square meters	m^2
mi^2	square miles	2.6	square kilometers	km^2
	acres	0.4	hectares	ha
		MASS (weight)		
oz	ounces	28	grams	g
lb	pounds	0.45	kilograms	kg
	short tons (2000 lb)	0.9	tonnes	t
		VOLUME		
tsp	teespoons	5	milliliters	ml
Tbsp	tablespoons	15	milliliters	ml
fl oz	fluid ounces	30	milliliters	ml
c	cups	0.24	liters	l
pt	pints	0.47	liters	l
qt	quarts	0.95	liters	l
gal	gallons	3.8	liters	l
ft^3	cubic feet	0.03	cubic meters	m^3
yd^3	cubic yards	0.76	cubic meters	m^3
		TEMPERATURE (exact)		
°F	Fahrenheit temperature	5/9 (after subtracting 32)	Celsius temperature	°C

*1 in. = 2.54 cm (exactly). For other exact conversions and more detail tables see NBS Misc. Publ. 286, Units of Weight and Measures. Price $2.25 SD Catalog No. C13 10 286.

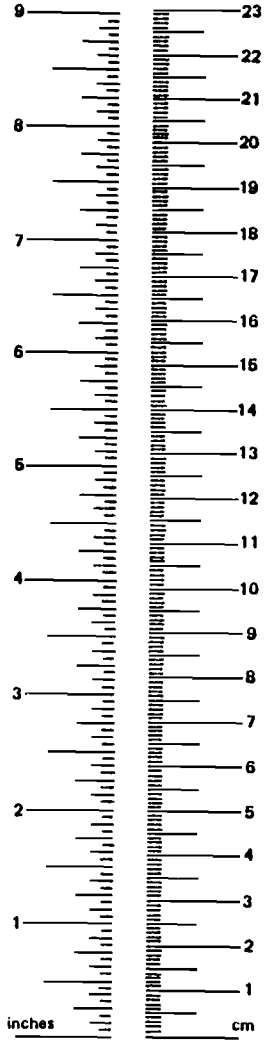

Approximate Conversions from Metric Measures

Symbol	When You Know	Multiply by	To Find	Symbol
		LENGTH		
mm	millimeters	0.04	inches	in
cm	centimeters	0.4	inches	in
m	meters	3.3	feet	ft
m	meters	1.1	yards	yd
km	kilometers	0.6	miles	mi
		AREA		
cm^2	square centimeters	0.16	square inches	in^2
m^2	square meters	1.2	square yards	yd^2
km^2	square kilometers	0.4	square miles	mi^2
ha	hecteres (10,000 m^2)	2.5	acres	
		MASS (weight)		
g	grams	0.035	ounces	oz
kg	kilograms	2.2	pounds	lb
t	tonnes (1000 kg)	1.1	short tons	
		VOLUME		
ml	milliliters	0.03	fluid ounces	fl oz
l	liters	2.1	pints	pt
l	liters	1.06	quarts	qt
l	liters	0.26	gallons	gal
m^3	cubic meters	36	cubic feet	ft^3
m^3	cubic meters	1.3	cubic yards	yd^3
		TEMPERATURE (exact)		
°C	Celsius temperature	9/5 (then add 32)	Fahrenheit temperature	°F

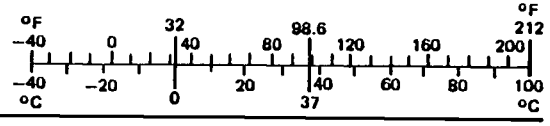

ACKNOWLEDGEMENTS

The authors acknowledge the contributions of Brian Joseph and David Humphreys (6322), along with David Schulze, Lawrence Kent, Mark Schieder, Keri Sobolik, and Joseph Bonner (7537), in the preparation and conducting of this test series. Contributions by Ned Keltner (7537) and Edward Hensel (NMSU) during the initial planning stages of this project deserve significant recognition. Also, special thanks goes to Marvin Moss, Gregory Haseman, and Peter Roth (1824) for providing excellent support in determining material properties.

TABLE OF CONTENTS

LIST OF FIGURES

APPENDIX A

APPENDIX B

APPENDIX C

APPENDIX D

LIST OF TABLES

APPENDIX C

APPENDIX D

NOMENCLATURE

α	absorptance
ε	surface emittance
$\bar{Y}$	estimate of the true mean
Y_i	sample of observations
n	number of observations
s	standard deviation
$\lvert\Delta T\rvert$	absolute difference in temperature
$\bar{T}_i$	average temperature of two tests at time i
σ	one sigma error bound
$\lvert\overline{\Delta T}\rvert$	mean absolute difference in temperature

1. BACKGROUND

Sandia National Laboratories, Albuquerque (SNLA) characterized the thermal response of a cask-like test article to three different thermal environments. This work was initiated for the Department of Transportation/Federal Railroad Administration (DOT/FRA).

The work includes the following tasks:

(1) Design a cask-like test article and quantify its response in different thermal environments.

(2) Assess the thermal response of a test article when exposed to an 800°C, 30-minute radiant heat environment; an 870°C, 100-minute radiant heat environment; and an engulfing fire environment for approximately 100 minutes.

(3) Perform a comparative analysis of (1) the 800°C and 870°C radiant heat environments and (2) the radiant heat environments and the engulfing fire environment.

(4) Assess the repeatability of the radiant heat test environment.

2. INTRODUCTION

To characterize the thermal response of a cask-like test article, SNLA performed a series of tests, exposing a specifically designed test article to three different thermal environments. Five tests were conducted in this test series: two 800°C, 30-minute radiant heat tests; two 870°C, 100-minute radiant heat tests; and one engulfing fire test for approximately 100 minutes. This report describes the testing and presents the results of the test series.

The purpose of the test series was to assess the response of the test article in a thermal environment and to use the response to define the environment. The intent of the first experiment was to characterize the response of the test article to the 10CFR71 thermal environment. This is a theoretical environment, however, and cannot be obtained identically in the real world. Due to slight convective heat losses and the thermal mass of the test article, it was not possible to maintain a uniform environment temperature of 800°C. Similarly, it is difficult to maintain a single value of emissivity and absorptivity as they vary with temperature and substrate. During the testing, it was determined that test performance is highly dependent upon the configuration and the thermal mass of the test article. The test article used in this test series had sufficient thermal mass to alter both the radiant heat environment and the engulfing fire environment. Therefore, the results of this test series are specific to the test article used in this test series.

3. TEST ARTICLE DESIGN

Several test article designs incorporating "cask-like" features were considered. Cask-like features incorporated in the test article include cylindrical cross section and thick wall design. Since the test article would be used in different thermal environments, the design had to be simple. A simple test article design is essential in obtaining an accurate temperature response. One must keep in mind that an object with sufficient thermal mass will interact and alter the local environment surrounding it. The larger the thermal mass, the larger the heat-sink effect. Gregory [1] says that "the

heat transfer to a test item in an engulfing fire can be highly dependent on the properties of the test item itself."

3.1 Determination of Test Article Dimensions

The dimensions of the test article were determined by satisfying the following design constraints:

(1) The test article must fit within the existing radiant heat test facility shroud that has an inner diameter of 0.6096 m (24 in.).

(2) The test article should have enough thermal mass such that steady-state conditions are approached at the end of a step change radiant heat environment i.e., from ambient conditions to 870°C for a 100-minute period.

(3) The surface absorptance of the test article should satisfy $\alpha \geq 0.8$ (minimal requirement in accordance with 10CFR71 regulations [2]).

The dimensions of the test article were determined by performing forward parametric study simulations of the test article using the thermal heat transfer code QTRAN [3] and using boundary conditions defined in (2) above. The forward parametric simulations were run assuming a one-dimensional radial geometry with gap radiation between the radiant heat shroud and the outer surface of the test article. The accuracy of QTRAN is not considered during this analysis. For a complete description of its performance, see [4,5,6,7]. The resultant dimensions of the test article are shown in Figure 3.1-1.

The test article was fabricated of 1010/1020 mild steel and packed with Cera-Blanket insulation. Appendix A contains the thermal property data for the mild steel and the insulation used for the test article. The outer surface of the test article was coated with PYROMARK 2500 paint. An analysis was performed by the Thermophysical Properties Division of Sandia National Laboratories (SNL) to determine the thermal radiative properties of PYROMARK 2500 on a mild steel substrate (see Appendix B). Results indicated that the

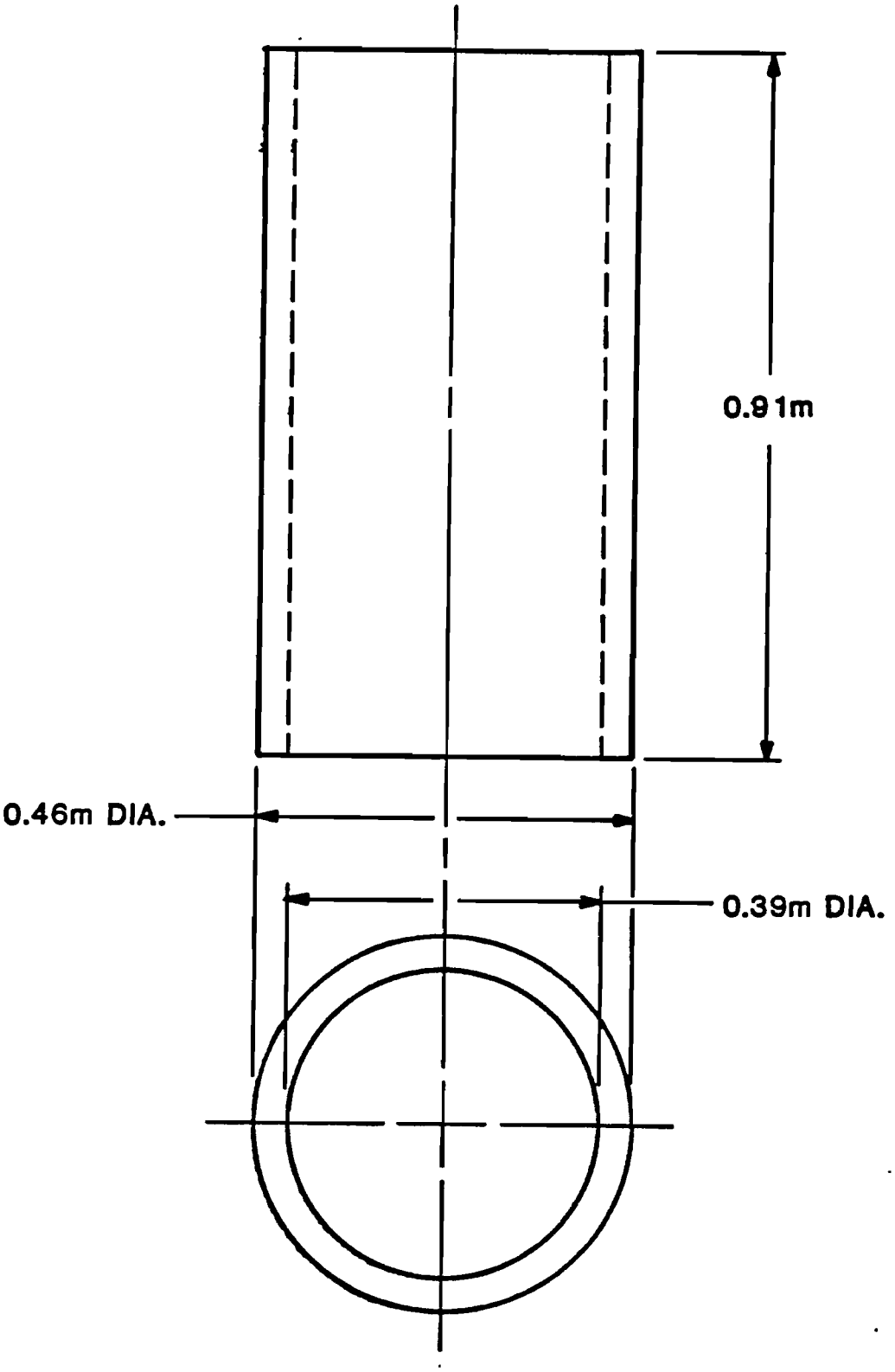

Figure 3.1-1 Diagram of Test Article

surface absorptance of the test article was greater than 0.8 for the entire range of surface temperatures experienced.

3.2 Determination of Thermocouple Placement

After the test article dimensions were finalized, a sensitivity analysis was performed (an experimental design procedure) to ensure that sufficient data would be obtained for post-test analysis. Even though the thermal environment within the radiant heat facility was close to one-dimensional, a transient, nonlinear, multidimensional inverse heat conduction analysis [8] was used to determine the number and location of sensors. The multi-dimensional data obtained was used as an experimental verification of a multidimensional inverse heat conduction code, MIDAS [8].

The primary instrumentation plane is an axial plane (center axial plane) approximately half-way (.46 m [18 in.]) between the upper and lower surface of the test article. The two secondary axial planes (top and bottom axial planes) equidistant (.23 m [9 in.]) from the primary instrumentation plane were used primarily to assess the presence of an axial temperature differential.

The sensors used in this test series were thermocouples. A total of 43 thermocouples were mounted on the test article at various locations (see Figure 3.2-1). Thermocouples 1 through 36 (TC1 through TC36) were intrinsic Type K and were mounted on the inner wall of the test article. This thermocouple, along with an insulated backface, provide an accurate temperature measurement [9]. TC1 through TC25 are mounted in the center axial plane, TC26 through TC30 are mounted in the top axial plane, and TC31 through TC36 are mounted in the bottom axial plane. Thermocouples 37 through 39 (TC37 through TC39), Type K standard 0.063-in. diameter, 304 stainless steel sheathed, were embedded in the insulating blanket. Four Nanmac Pencil Probe "eroding" Type K thermocouples (TC40 through TC43) were mounted in the inner wall in the center axial plane of the test article, as shown in Figure 3.2-1. Nanmac thermocouples provide an alternative method of obtaining surface temperatures. Data obtained from these thermocouples were used in a

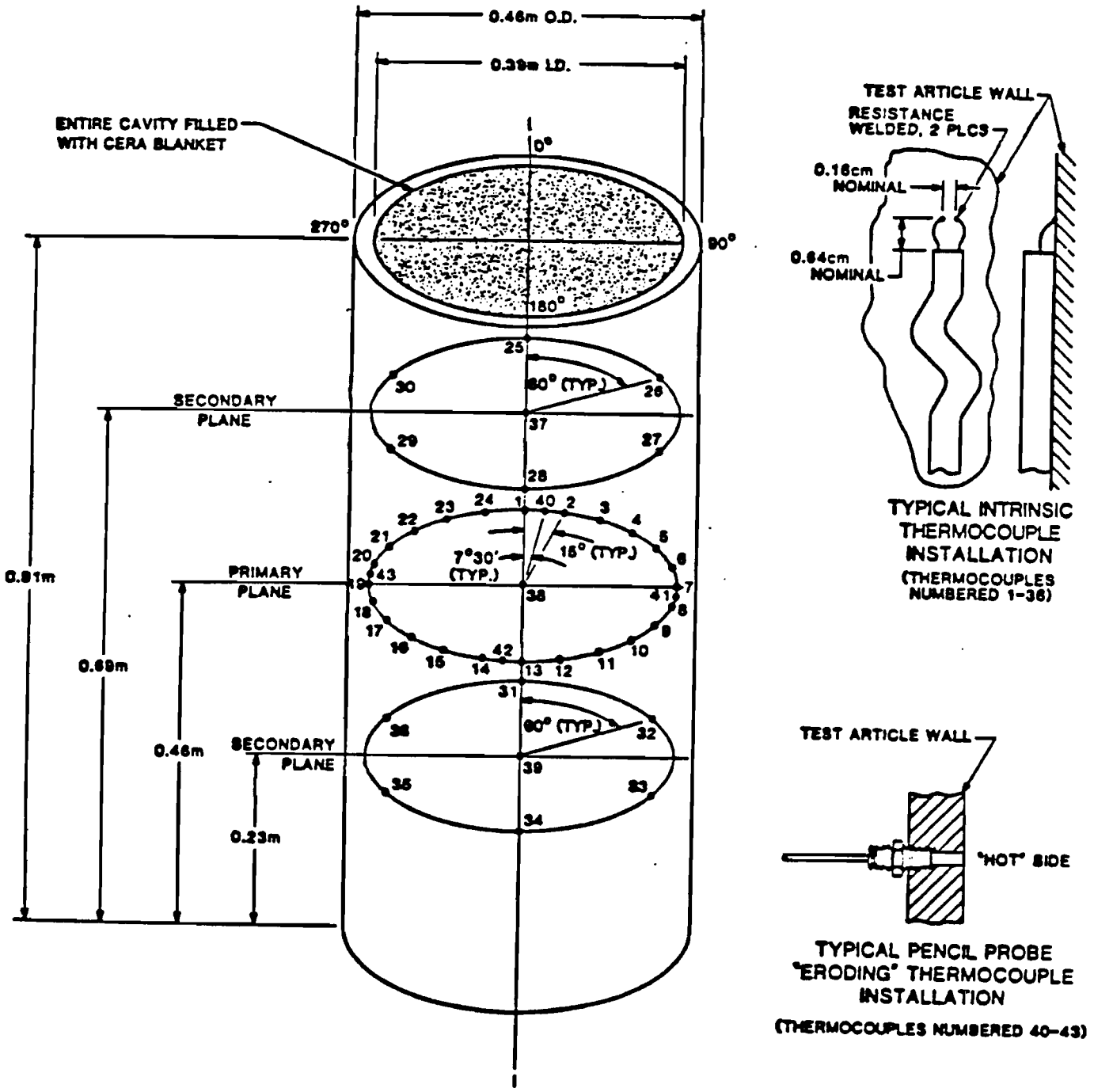

Figure 3.2-1 Test Article Thermocouple Locations

comparative analysis to better understand the accuracy of an inverse heat conduction method. Appendix C contains this analysis.

The leads from all 43 thermocouples were run axially down the inner surface of the steel wall and exited the article through the bottom opening. The top and bottom of the test article were heavily insulated using Fiber-Frax insulating board to reduce end loss effects.

4. TEST FACILITIES

Two test facilities were used for this test series: the SNLA Radiant Heat Facility and the SNLA Tenth Scale Enclosed Fire Facility. The Radiant Heat Facility is capable of achieving the required controlled thermal environment. The Tenth Scale Enclosed Fire Facility environment is not as predictably accurate as the radiant heat environment. A comparison of environment temperatures and their variability during testing is presented in Section 6.4.

4.1 Radiant Heat Facility

The test articles were exposed to a specified time- dependent thermal environment in the Radiant Heat Facility at SNLA. A schematic of the facility showing thermocouple locations is shown in Figure 4.1.1.

The Radiant Heat Facility consists of a 304 stainless steel cylindrical shroud with a 1.22 m (48 in.) long 0.61 m (24 in.) inner diameter. The entire inner surface of the shroud is painted with PYROMARK 2500 to provide a surface emittance of $\varepsilon \geq 0.9$ over the temperature range that was used during the test series (20°C-870°C). The outer surface of the shroud is heated by eight infrared quartz halogen lamp arrays to the test temperature. These arrays heat the shroud to the test temperature in less than two minutes. The lamps are mounted on water-cooled aluminum reflectors; the thin front surfaces are air cooled. Four Type K control thermocouples, as shown in Figure 4.1.1, control and monitor the shroud temperature.

4.2 Tenth Scale Enclosed Fire Facility

The engulfing fire environment was provided by the Tenth Scale Enclosed Fire Facility at SNLA. The Tenth Scale Facility is an aboveground, pyramidal structure. The outer walls of the facility are water cooled when a test is in

TC	LOCATION	
STC1	LEVEL 0.05	0°
STC2	LEVEL 0.15	0°
STC3		90°
STC4		180°
STC5		270°
STC6	LEVEL 0.30	0°
STC7	LEVEL 0.46	0°
STC8	LEVEL 0.61	0°
STCC1		
STC20	LEVEL 0.61	45°
STC9	LEVEL 0.61	90°
STCC2		
STC21	LEVEL 0.61	135°
STC10	LEVEL 0.61	180°
STCC3		
STC22	LEVEL 0.61	225°
STC11	LEVEL 0.61	270°
STCC4		
STC23	LEVEL 0.61	315°
STC12	LEVEL 0.76	0°
STC13	LEVEL 0.91	0°
STC14	LEVEL 1.07	0°
STC15		90°
STC16		180°
STC17		270°
STC18	LEVEL 1.17	0°
STC19	TOP	

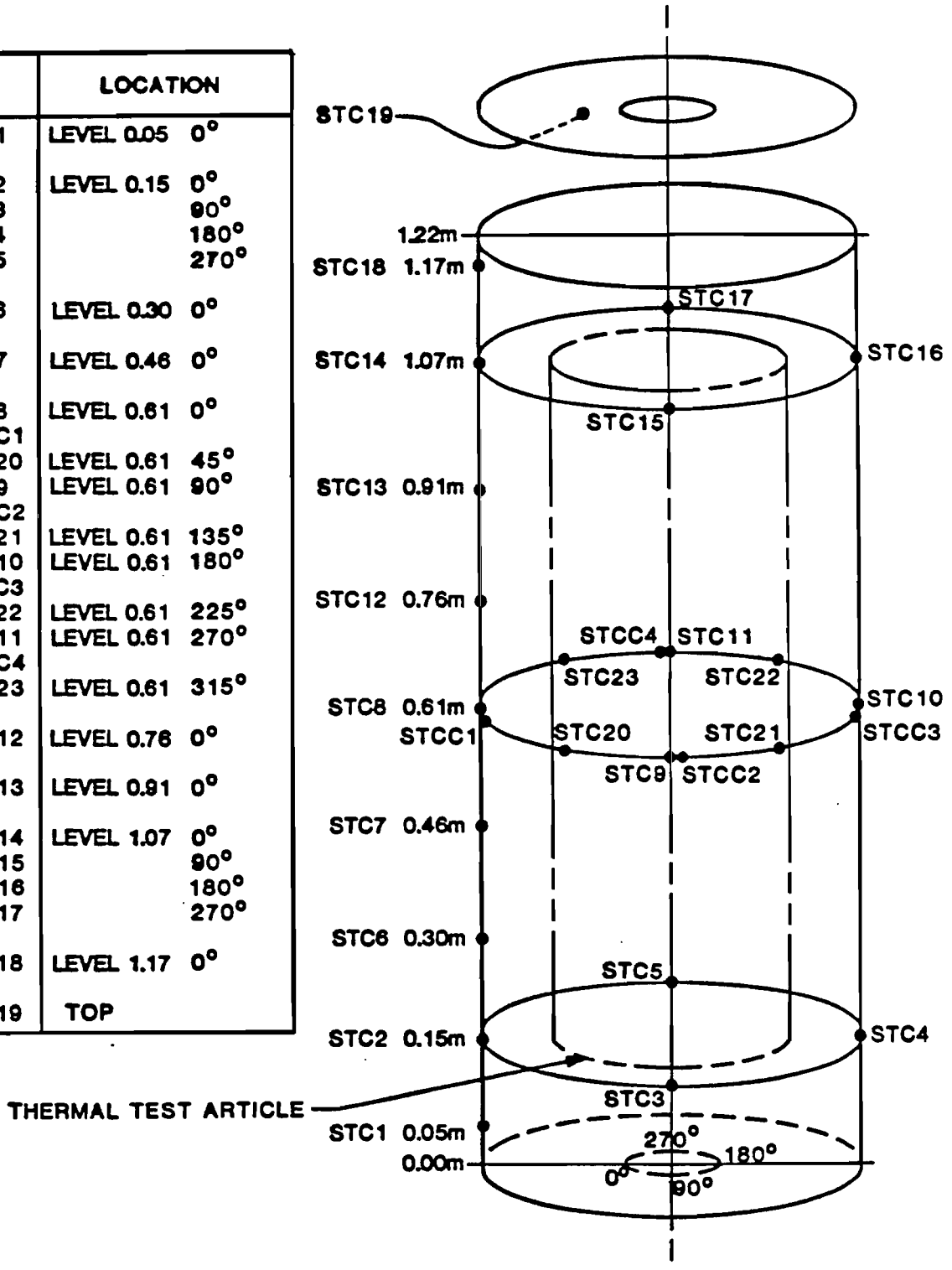

Figure 4.1-1 Diagram of the SNLA Radiant Heat Facility Test Shroud

progress. Figure 4.2.1 is a side view of the Tenth Scale Facility. The base of the structure is 7.9 m (26 ft.) by 7.9 m (26 ft.) and tapers to the stack assembly, which is 0.91 m (3 ft.) by 1.8 m (6 ft.) by 4.3 m (14 ft.) tall. The total height of the structure is 8.8 m (29 ft.). The mass flow rates are 2.27 kg/sec (300 lb/min) of air and 0.098 kg/sec (13 lb/min) of fuel. The average stack exit temperature is 870°C.

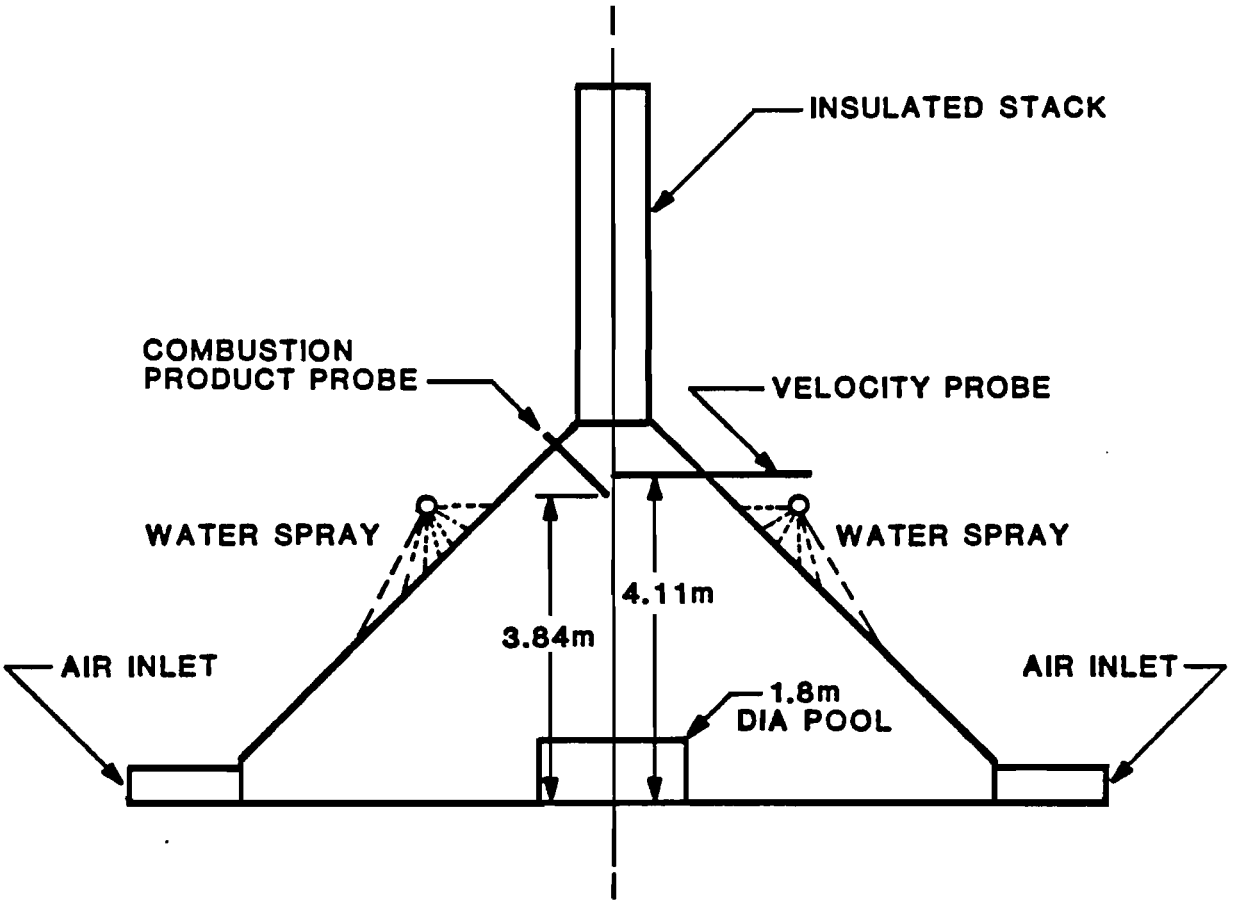

Figure 4.2-1 Diagram of the SNLA Tenth Scale Enclosed Fire Facility

5.0 EXPERIMENTAL TEST SEQUENCE

Four tests were performed at the Radiant Heat Facility, and one test was performed at the Tenth Scale Enclosed Fire Facility. The test matrix in Table 5.1 outlines the experimental test series. Tests 1, 3, and 5 were performed to characterize the response of the test article to an 800°C, 30-minute radiant heat environments; an 870°C, 100-minute radiant heat environment; and an engulfing fire environment, respectively, and to provide comparative results of the test article's response to the three different environments. Tests 2 and 4 were performed to assess the repeatability of the Tests 1 and 3, respectively.

TABLE 5.1

Test Matrix for Characterizing the Thermal Response of a Cask-Like Test Article

Test	Description
1	800°C, 30-minute Radiant Heat Test
2	800°C, 30-minute Radiant Heat Test
3	870°C, 100-minute Radiant Heat Test
4	870°C, 100-minute Radiant Heat Test
5	Engulfing Fire Test, approximated 100 minutes

6.0 RESULTS

The results from the test series include temperature histories for each thermal environment and temperature profiles and surface heat flux as a function of time and surface temperature for the test article. As a measure of the variability of the environment, environment temperatures are averaged over time to determine the sample mean and sample standard deviation. The sample mean was determined using the following:

$$\bar{Y} = \sum_{i=1}^{n} \frac{Y_i}{n} \qquad 6.1$$

where

$\bar{Y}$ = the estimate of the true mean
Y_i = sample of observations
n = number of observations

The standard deviation of the sample, which supplies a measure of the spread or variability of the sample, was determined from:

$$s = \sqrt{\sum_{i=1}^{n} \frac{(Y_i - \bar{Y})^2}{n-1}} \qquad 6.2$$

where

$\bar{Y}$ = the estimate of the true mean
Y_i = sample of observations
$n-1$ = degrees of freedom

The test article surface heat flux values are estimates based on a one-dimensional inverse heat conduction analysis [10].

6.1 Tests 1 and 2: 800°C 30-Minute Radiant Heat Tests

6.1.1 Environment Temperature Results for Test 1

Figures 6.1-1 through 6.1-4 show temperature histories for the radiant heat shroud for Test 1. The data for three different axial heights and four circumferential locations are shown in Figures 6.1-1 through 6.1-3. Figure 6.1-4 shows shroud temperature histories for one circumferential position at three different axial heights. Refer to Figure 4.1-1 for thermocouple locations on the radiant heat test shroud.

Four control thermocouples, STCC1, STCC2, STCC3, and STCC4, were located next to thermocouples STC8, STC9, STC10, and STC11--all on the center axial plane. One controller was used for those thermocouples. Table 6.1-1 indicates mean environment temperatures with corresponding standard deviations for several shroud thermocouple locations. The interval for which temperatures are averaged starts when the shroud reached test temperature (approximately 2.5 minutes after start of temperature ramp up) and ended when the quartz lamps shut down.

All thermocouple locations on the center axial plane were within 9°C of the test temperature of 800°C. The mean temperature for this plane was 796°C. The circumferential standard deviation, or variability, for control plane thermocouples is 7°C, small relative to other axial locations. Thermocouples on the bottom axial plane (STC2 through STC5) yielded the lowest temperatures with a mean temperature of 735°C. The thermal mass of the test article, along

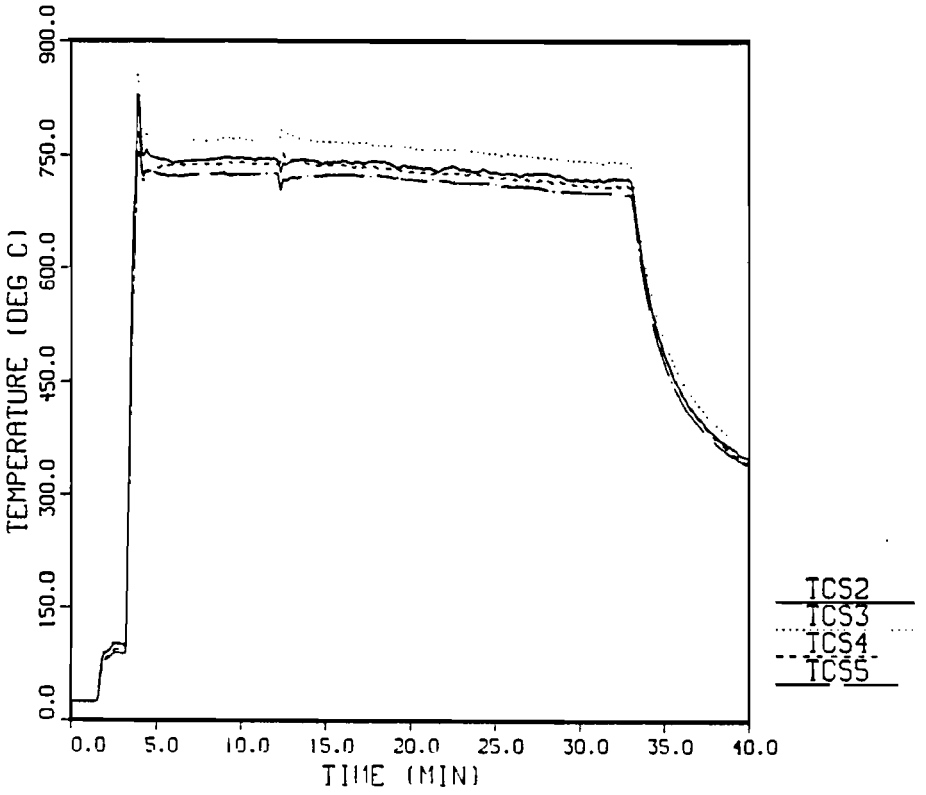

Figure 6.1-1 Radiant Heat Shroud Temperature Profile, Bottom Axial Plane

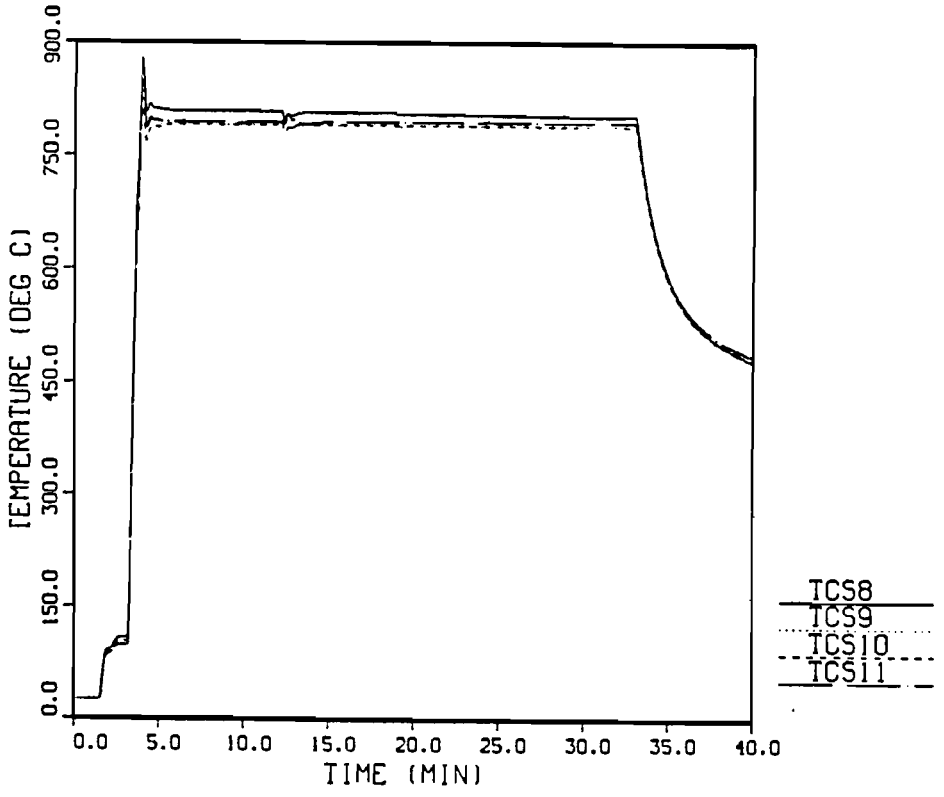

Figure 6.1-2 Radiant Heat Shroud Temperature Profile, Center Axial Plane

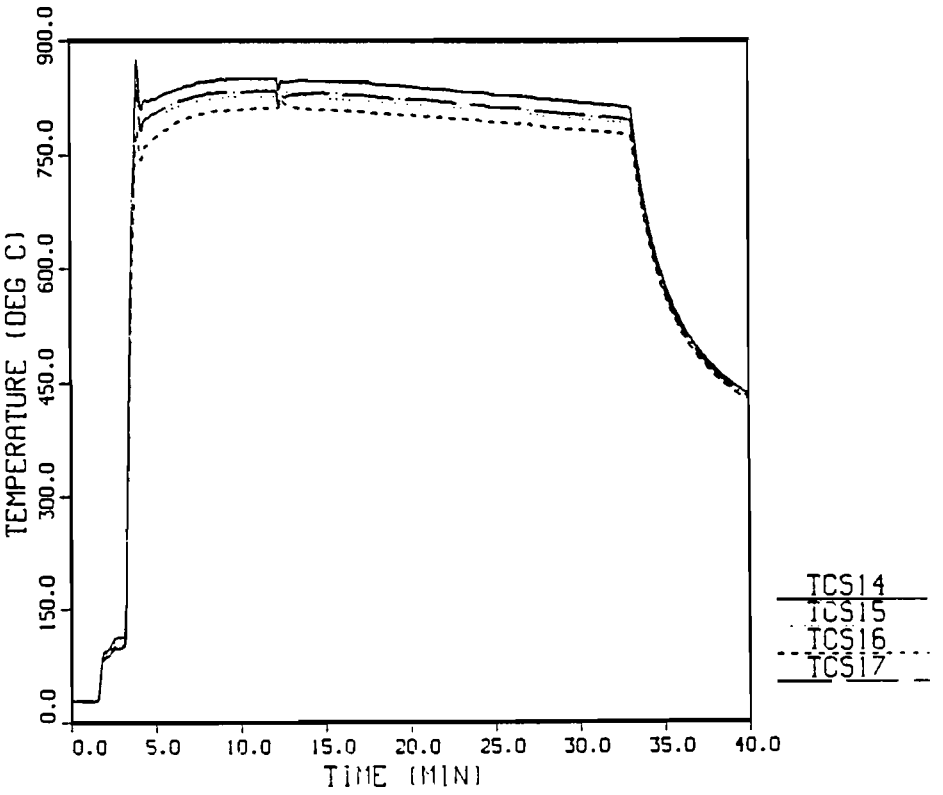

Figure 6.1-3 Radiant Heat Shroud Temperature Profile, Top Axial Plane

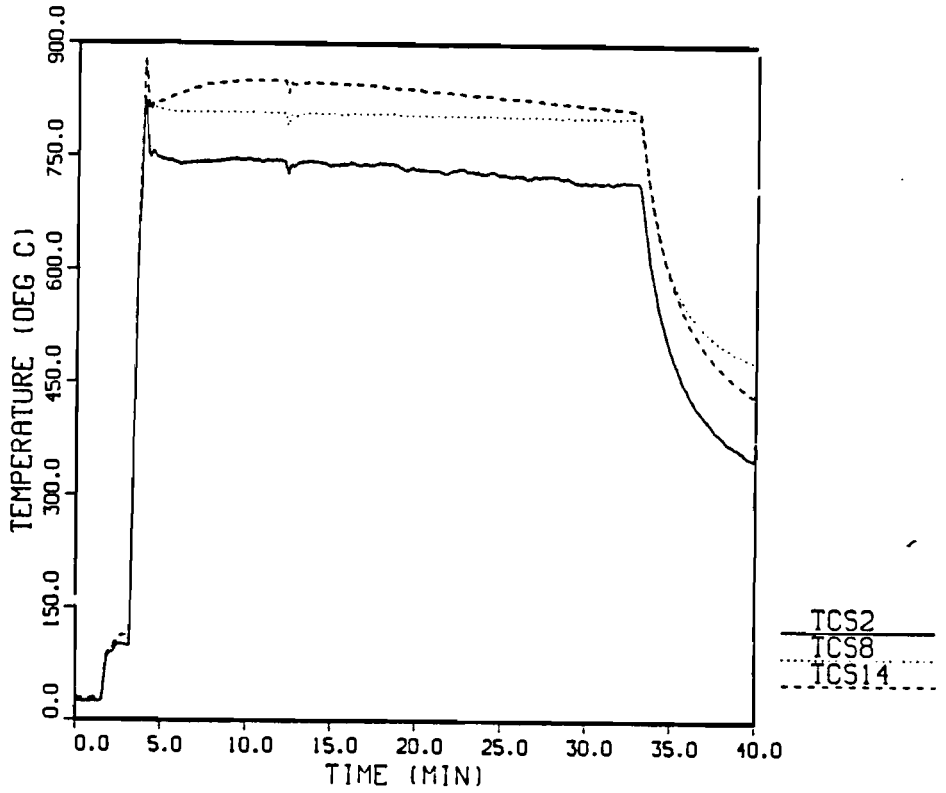

Figure 6.1-4 Radiant Heat Shroud Temperature Profile, Bottom, Center, and Top Axial Planes

TABLE 6.1-1

Sample Means and Estimated Standard Deviations for Selected Shroud Thermocouple Locations During Test 1

Thermocouple Location	$\bar{Y}$ (°C)	S (°C)
Bottom Axial Plane		
2	734.7	9.8
3	760.3	11.0
4	728.4	10.6
5	716.3	8.8
Circumferential Mean	734.9	18.6
Center Axial Plane		
8	806.5	2.7
9	791.1	2.1
10	791.6	1.9
11	795.4	2.0
Circumferential Mean	796.2	7.2
Top Axial Plane		
14	836.4	11.4
15	814.1	11.7
16	797.7	11.9
17	819.4	11.4
Circumferential Mean	816.9	15.9
TOTAL	$\bar{Y}$=782.7°C	S = 42.64°C

with convection losses and end loss effects, caused a reduction in the mean temperature of this plane. Circumferential temperature variability in the bottom axial plane is 19°C, approximately four times greater than circumferential temperature variability in the control (center) axial plane. Since the radiant heat facility is controlling temperature circumferentially in the center axial plane only, variabilities in other axial planes are to be expected. Controlling axially, as well as circumferentially, would reduce variabilities as well as provide a more uniform environment. Thermocouples on the top axial plane (STC14 through STC17) yielded the highest temperature with a mean temperature of 817°C. Variability of temperatures in the top axial plane was still large compared to that of the center axial plane.

Due to the lack of temperature control in the top and bottom plane of the shroud, the thermal mass of the test article, convection heat transfer losses, and end loss effects (end loss effects include conduction losses from the test article to the test stand), the environment temperature histories for the top and bottom axial planes approach an equilibrium temperature other than the target test temperature. This experimental phenomenon is characteristic of many control problems and is seen graphically in Figure 6.1-4, which shows the temperature profile for one circumferential location at the three different axial planes. For longer test times this effect becomes more severe. The equilibrium state that the top and bottom axial planes approach is highly dependent upon the thermal mass of the test article, convection losses, and end loss effects. The effect of this is a nonconstant environment temperature at all locations other than the control plane.

To determine an average temperature for the entire shroud, the sample means for all thermocouple locations shown in Table 6.1.1 were averaged. The result was an environment temperature of 783°C, 17°C under the target test temperature of 800°C. The axial variability was 43°C.

6.1.2 Test Article Temperatures Results for Test 1

Figures 6.1-5 through 6.1-8 show temperature profiles as a function of time for the test article (see Figure 3.2-1 for thermocouple locations). The same axial temperature variations are seen on the test article as on the test shroud. Figure 6.1-5 shows a circumferential temperature profile as a function of time for the center axial plane of the test article.

The maximum difference in temperature between any two thermocouples in the center axial plane was 24°C, which occurred between TC7 and TC13. TC7 was the hottest thermocouple on this plane, reaching 654°C. Figure 6.1-6 shows a circumferential temperature profile for the top axial plane of the test article. The maximum difference in temperature between any two thermocouples in this plane was approximately 22°C, which occurred between TC29 and TC26. TC26 reached a maximum temperature of 668°C, which was the hottest for this plane and for the entire test article. Figure 6.1-7 shows the circumferential temperature profile for the bottom axial plane. Temperatures were much more uniform in this plane with a maximum difference in temperature of only 6°C between TC31 and TC32. TC32 was the hottest thermocouple on this plane reaching, 608°C. Figure 6.1-8 shows the temperature difference between the three axial planes.

6.1.3 Surface Heat Flux Results for Test 1

The next evaluation of the test was the determination of surface heat flux. This heat flux represents the energy being conducted into the surface of the test article and includes both thermal radiation and convection. In a radiant heat environment, the test shroud is surrounded by cool ambient air. During a test, the hot shroud causes buoyancy forces in the test environment. These buoyancy forces entrain ambient air, causing convection cells to exist in the test environment. Because of this, convection is considered to be a loss of energy. In an engulfing fire environment, convection is considered to be a gain of energy because the test article is surrounded by the hot gasses of the fire that are at test temperature. The surface heat flux, however,

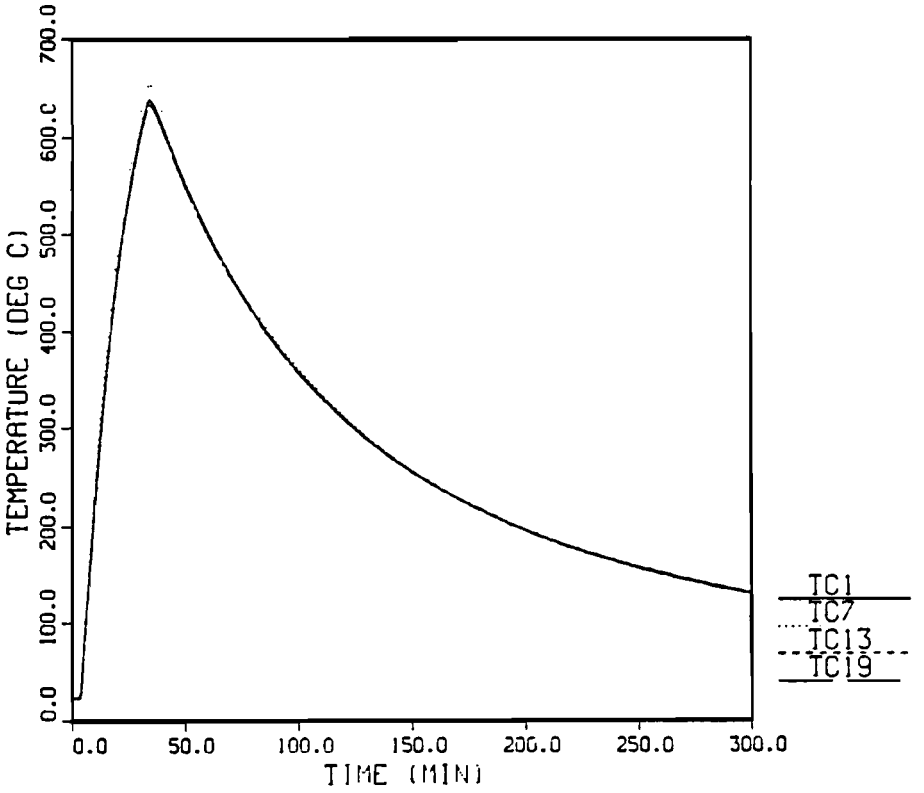

Figure 6.1-5 Test Article Temperature Profile, Center Axial Plane

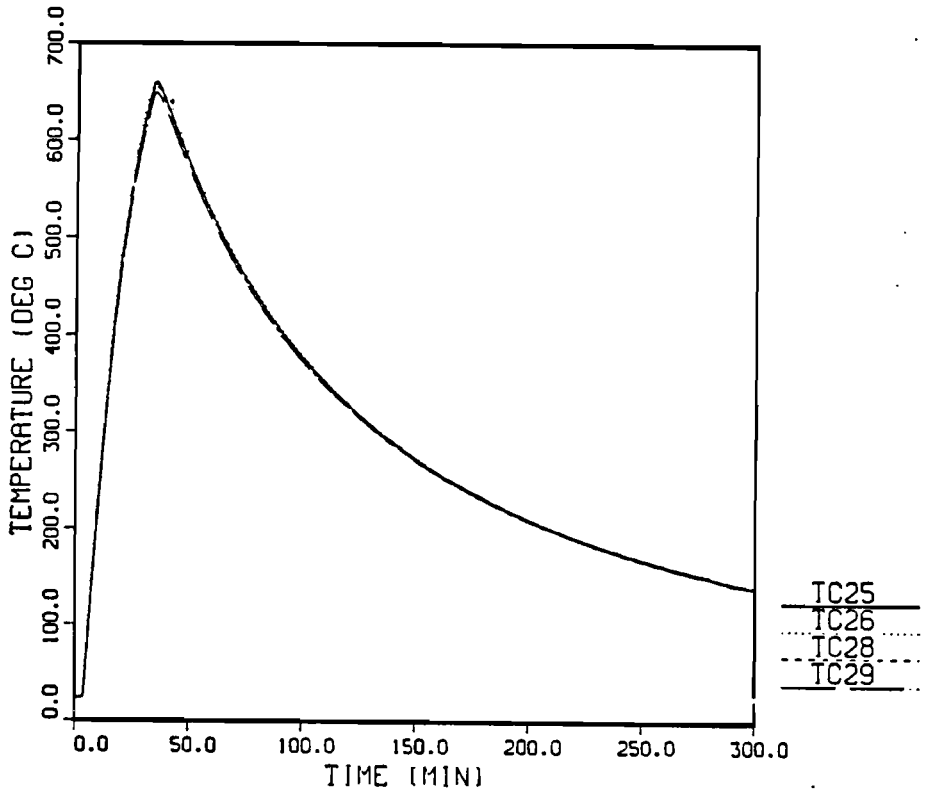

Figure 6.1-6 Test Article Temperature Profile, Top Axial Plane

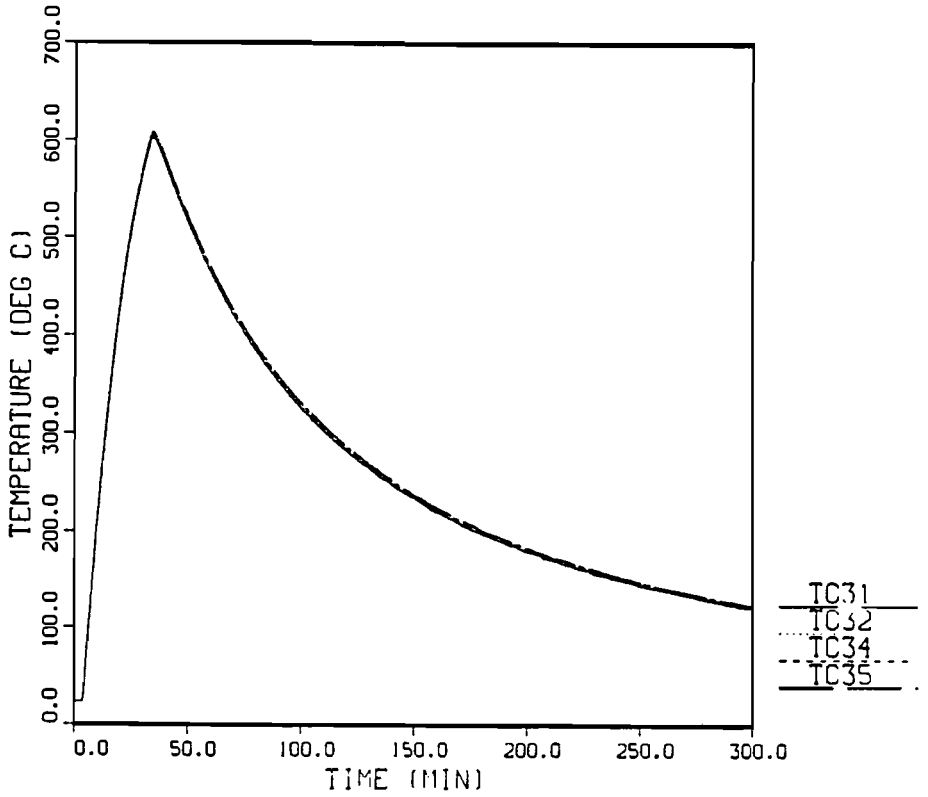

Figure 6.1-7 Test Article Temperature Profile, Bottom Axial Plane

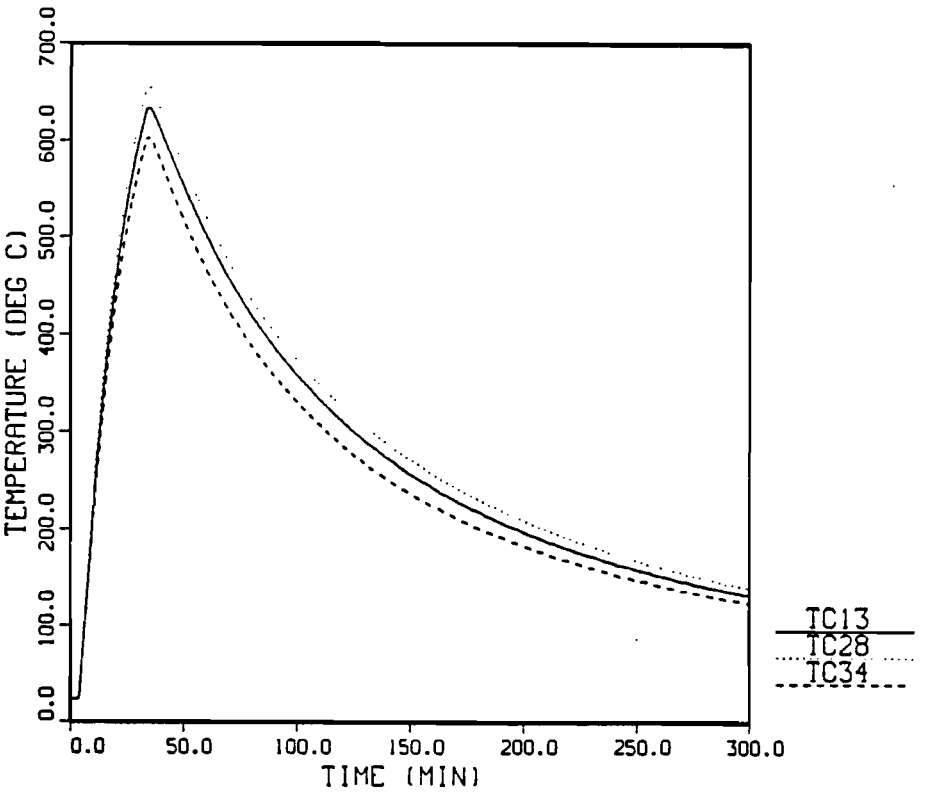

Figure 6.1-8 Test Article Temperature Profile, Bottom, Center, and Top Axial Planes

represents the total energy absorbed at the surface of the test article, regardless of the type of environment.

In a thermal environment, such as an engulfing fire or radiant heat environment, accurate direct measurements of surface temperature or surface heat flux are difficult to obtain. This problem is explained by Blackwell [11]. An alternative method of determining surface thermal conditions is to infer them from measurements made within the test article. This method is called the Inverse Heat Conduction Problem [10]. This problem can be explained by showing a cross section of the test article. Figure 6.1-9 shows this cross section with possible thermocouple locations P_1 and P_2. The inverse technique is used first to solve a standard boundary value problem between thermocouple locations P_1 and P_2, using P_1 and P_2 as boundary conditions. After the temperature distribution between P_1 and P_2 is calculated, the inverse technique is then used to determine the temperature at P_3.

If one could obtain an analytical expression for the temperature or flux histories at P_1 and P_2, an analytical expression could possibly be derived for the temperature history at P_3; but obtaining the expressions for P_1 and P_2 based upon experimental data is impossible due to the infinite number of high frequency components as explained by Hills and Hensel [10]:

"Due to the nature of data acquisition systems, one can never obtain measurements with infinite resolution and accuracy. One should not expect, therefore, to determine surface conditions with infinite resolution and accuracy. However, a method that can take smaller time steps without giving up stability can be expected, in general, to resolve finer temporal scale surface events. The relative effect of truncation on the surface condition estimates depends on the time-step size and the magnitude of the noise in the data. Often, the degradation in the estimates for the surface conditions due to the noisy interior temperature measurements is much larger than the effect of truncation error. One cannot hope to find a unique surface condition history using only interior measurements made at discrete times. There are an infinity of surface histories that will satisfy a finite set of measurements."

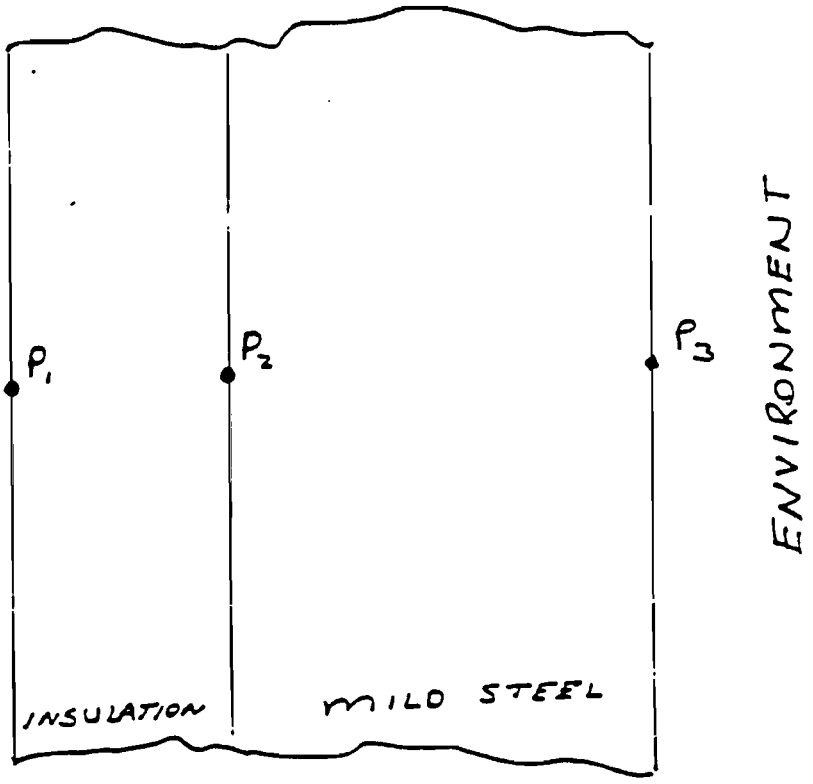

Figure 6.1-9 Cross Section of Test Article

Thus, an infinity of solutions can be reduced by several methods, including time weighted averaging and least squares approximating.

A one-dimensional geometry is used for all inverse heat conduction calculations. A representation of the finite difference mesh is shown in Figure 6.1-10. A sensitivity analysis was performed to determine the effect of mesh density on estimated surface conditions. The mesh density shown in Figure 6.1-10 minimized the discretization errors associated with finite difference approximations. Referring back to Figure 6.1-9, location P1 corresponds to node 1. Location P2 corresponds to node 11. Therefore, the standard boundary value problem is solved in the Cera Blanket insulation region. P3 corresponds to node 25. It is at this node that surface conditions are estimated. The inverse heat conduction problem is solved in the mild steel region between nodes 11 and 25.

The problem of uniqueness in inverse heat conduction analysis warrants the estimation of surface condition uncertainties. It is essential for this test series to estimate the surface condition uncertainties. Otherwise, the comparisons made to satisfy the objectives of the scope of work are less meaningful. A complete analysis of surface condition uncertainties (surface heat flux and surface temperature) is given in Appendix E. The uncertainty analysis evaluates not only the effects of random measurement noise errors but also the effects of errors in independent variables, such as material properties. Also an assessment of degradation of resolution of surface estimates as a function of filter strength is made. Biased or systematic errors are not considered in this analysis.

The local heat flux results are plotted using both time and surface temperature as the independent variable. The time-independent variable plots allow comparisons to be made only for the specific test article-environment configuration. In other words, these plots are specific to the geometry being tested. The surface temperature-independent variable plots allow comparisons of different thermal environments to be made in a more generic sense. This is

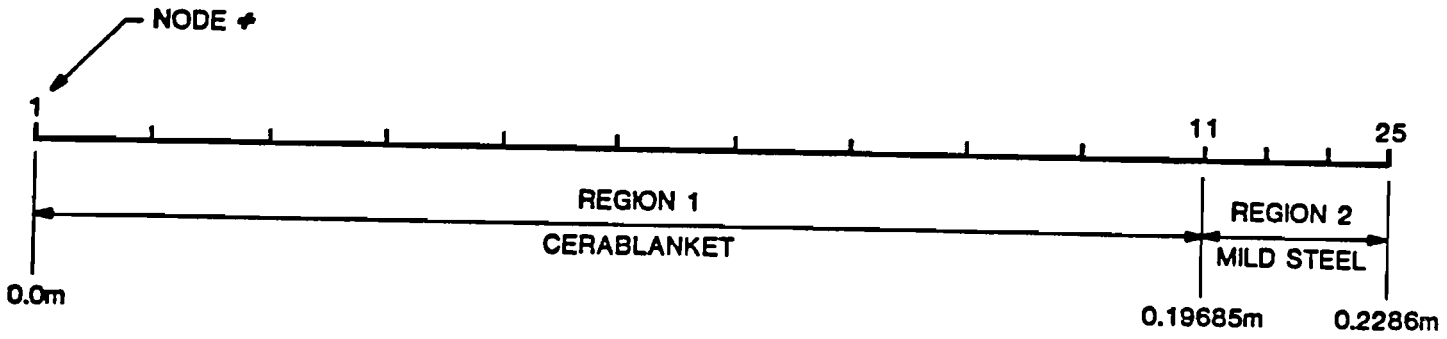

Figure 6.1-10 Finite Difference Mesh Used for Inverse Heat Conduction Analysis

not to say that comparisons can be made for any type of geometry (with any thermal mass), but rather that comparison of different thermal environments to regulatory-type environments can be made, in which thermal mass and geometry are not considered.

Only one thermocouple location from each axial plane is considered here. Thermocouple locations representing the maximum and minimum of each test are presented in Section 6.4. The information that is given is sufficient to describe test conditions and test article performance.

Figures 6.1-11 through 6.1-16 show the surface heat flux as a function of time and surface temperature for thermocouple locations TC1, TC25, and TC31. These curves are smooth relative to open pool fire data [12], indicating the absence of wind-induced variability and the highly turbulent nature inside the fire. The surface flux is in agreement with shroud temperature profiles shown earlier. Also, note that the surface flux did not approach zero flux indicating that the test article was still absorbing energy when the test was stopped. The sharp drop-off in both curves indicates when the quartz lamps were turned off and the test article started to cool. Data are analyzed only for the heat-up phase of the test.

The data presented in Figures 6.1-11 through 6.1-16 were calculated using a filter strength of 1 [10] to provide the best resolution. The reported estimated surface heat flux values and estimated surface temperatures were calculated using a filter strength of 2 due to large uncertainties encountered using a filter strength of 1. Appendix E explains filter strength details of the uncertainty analysis. The maximum estimated surface heat flux achieved at TC1 was 64.2 KW/m^2 at an estimated surface temperature of 124°C. The time-integrated heat flux is a representation of the total heat absorbed by the test article during the heat up phase of the test. At TC1 the integrated heat flux was calculated to be 88.62 MJ/m^2. The maximum estimated surface heat flux at TC25 was 67.3 KW/m^2 at an estimated surface temperature of 131.0°C. The time-integrated heat flux was 92.87 MJ/m^2. The maximum estimated surface

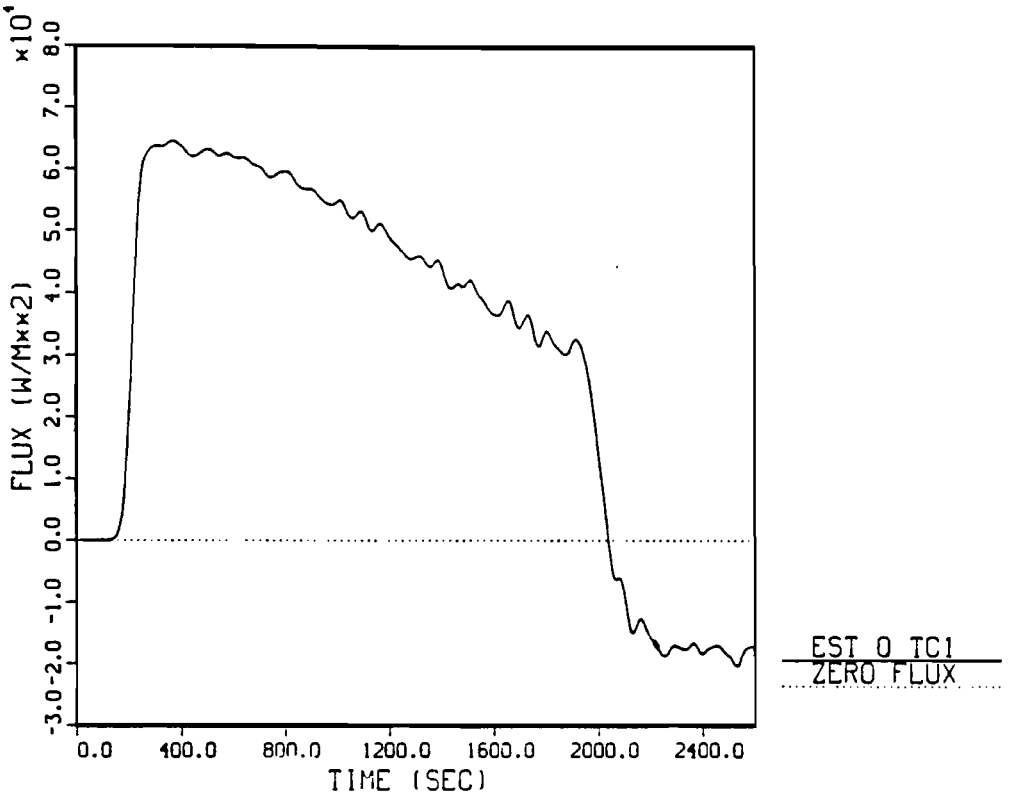

Figure 6.1-11 Local Surface Heat Flux History for TC1, Test 1

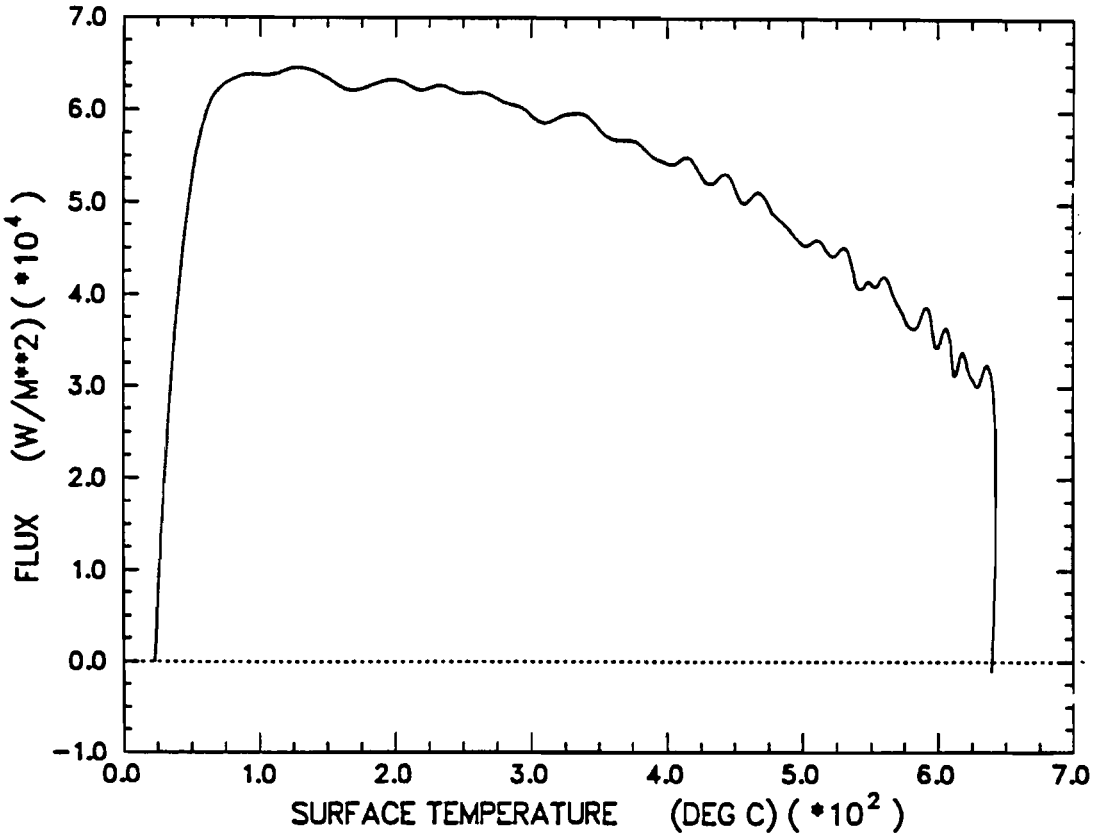

Figure 6.1-12 Local Surface Heat Flux as a Function of Surface Temperature for TC1, Test 1

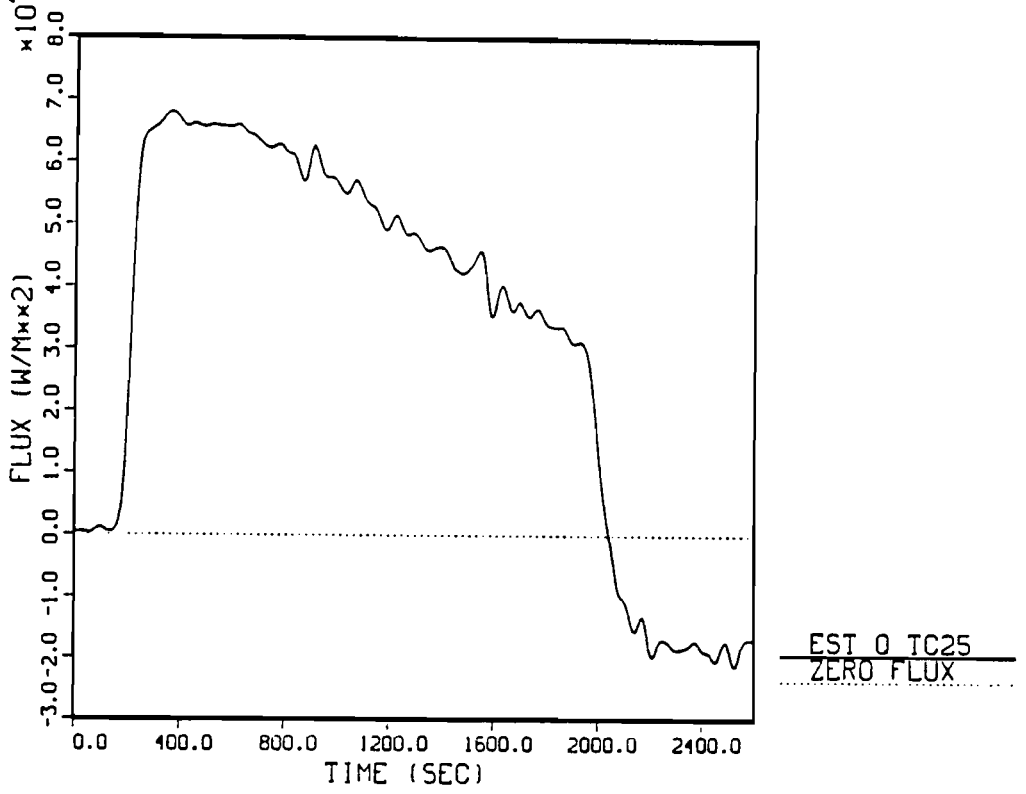

Figure 6.1-13 Local Surface Heat Flux History for TC25, Test 1

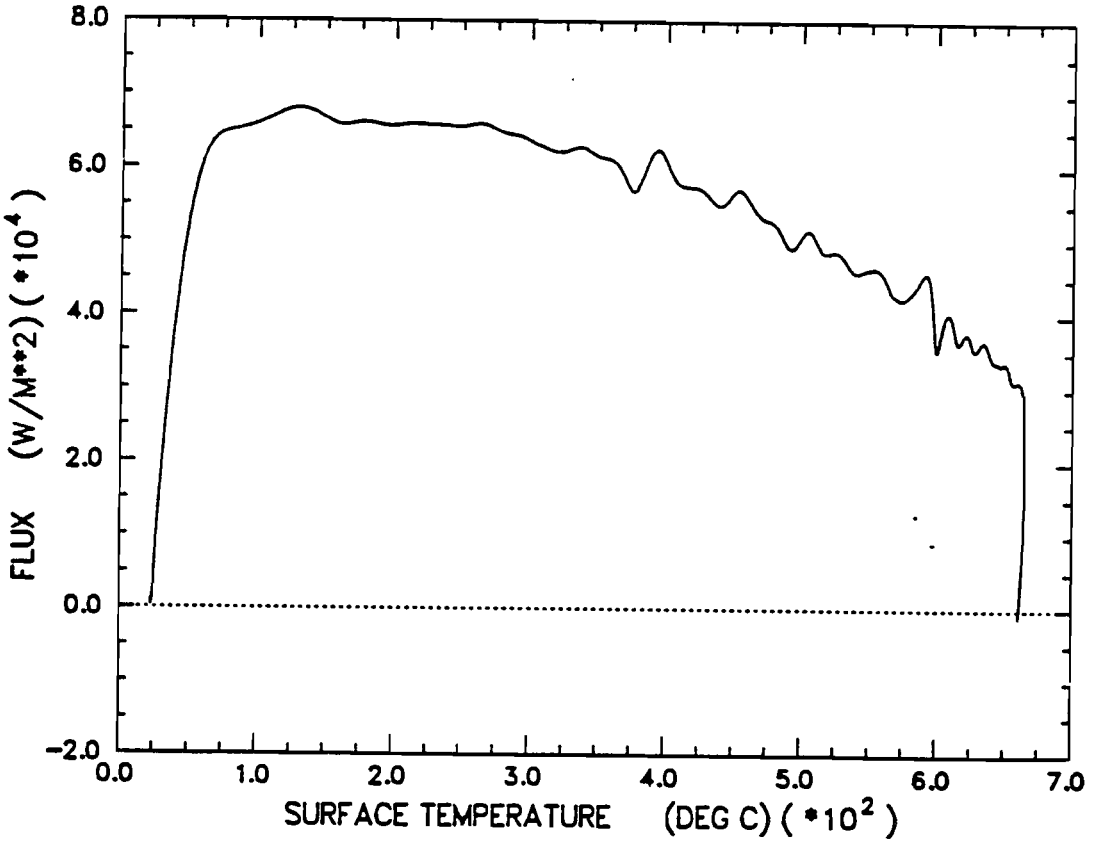

Figure 6.1-14 Local Surface/Heat Flux as a Function of Surface Temperature for TC25, Test 1

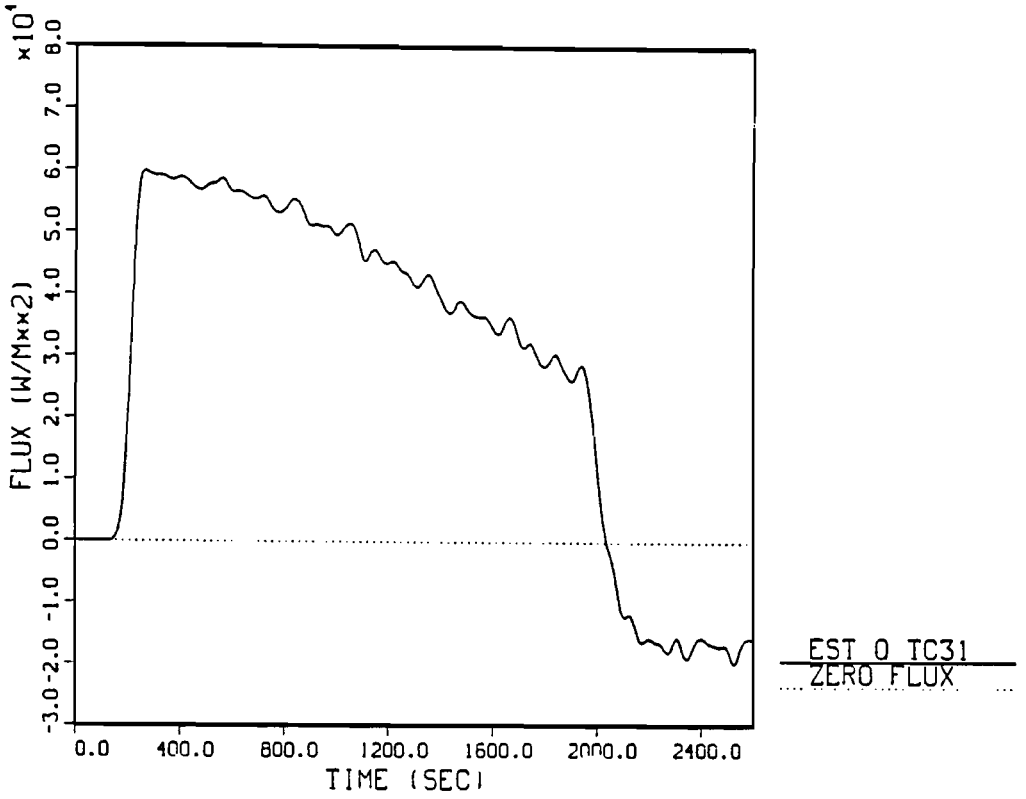

Figure 6.1-15 Local Surface Heat Flux History for TC31, Test 1

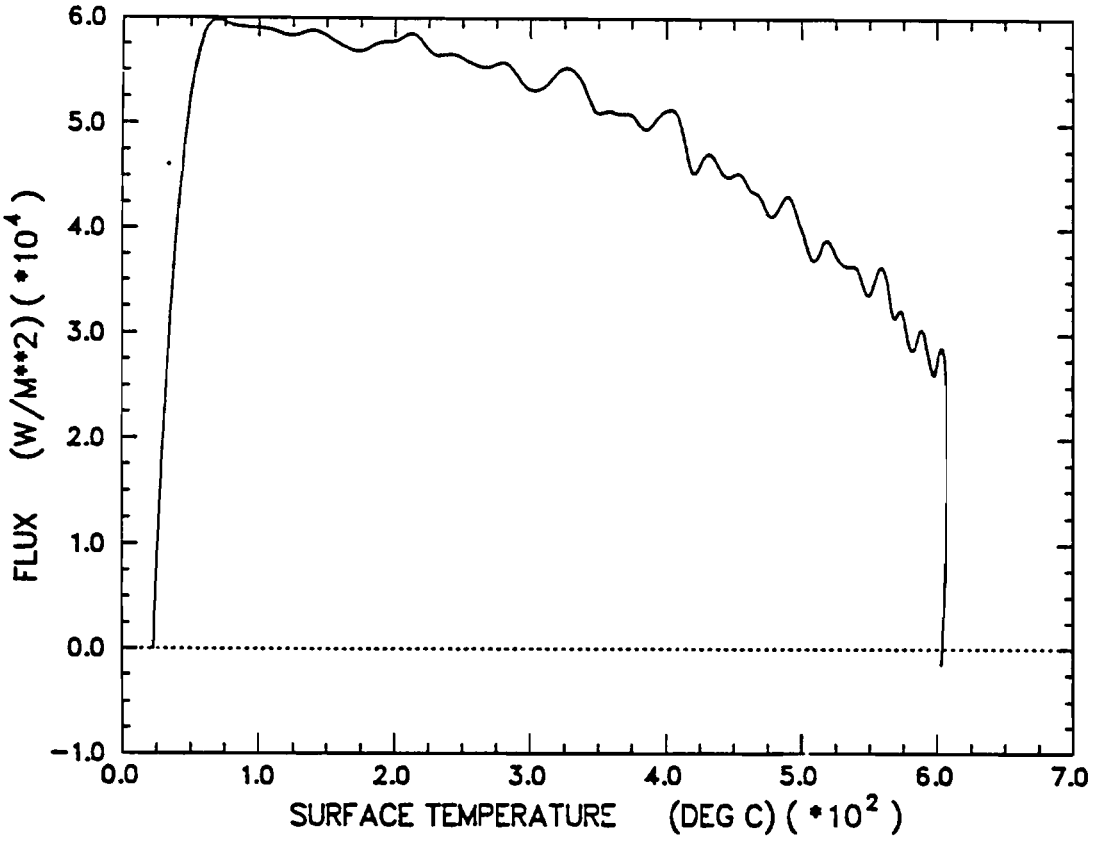

Figure 6.1-16 Local Surface Heat Flux as a Function of Surface Temperatures for TC31, Test 1

heat flux at TC31 was 59.0 KW/m² at a surface temperature of 98°C. The time-integrated heat flux was 81.81 MJ/m².

6.1.4 Test 2 Repeatability of 800°C, 30-Minute Radiant Heat Test

Test 2 was performed to assess the repeatability of the 800°C, 30-minute radiant heat test. The results of Test 2 are presented here to assess repeatability only.

Repeatability is expressed in several ways. First, Figures 6.1-17 through 6.1-19 show temperature histories for Tests 1 and 2 for three different thermocouple locations TC1, TC25 and TC31. Test 2 produced slightly higher temperatures than Test 1. This could be due to the initial ambient conditions of the test.

Secondly, Figures 6.1-20 through 6.1-22 show the one sigma error bound for both 800°C, 30-minute radiant heat tests for TC1, TC25, and TC31. The discontinuities in these figures correspond to experimental data that is rounded off to whole integers.

The temperature difference increases with increasing temperature. The one sigma error bound is calculated using the following equation:

$$\sigma = \sqrt{\frac{\sum_{i=1}^{n} (\bar{T}_i - T_i)^2}{n - 1}}, \qquad 6.1\text{-}1$$

where

$\bar{T}_i$ = average temperature of Tests 1 and 2 at time i
T_i = temperature from each test at time i.

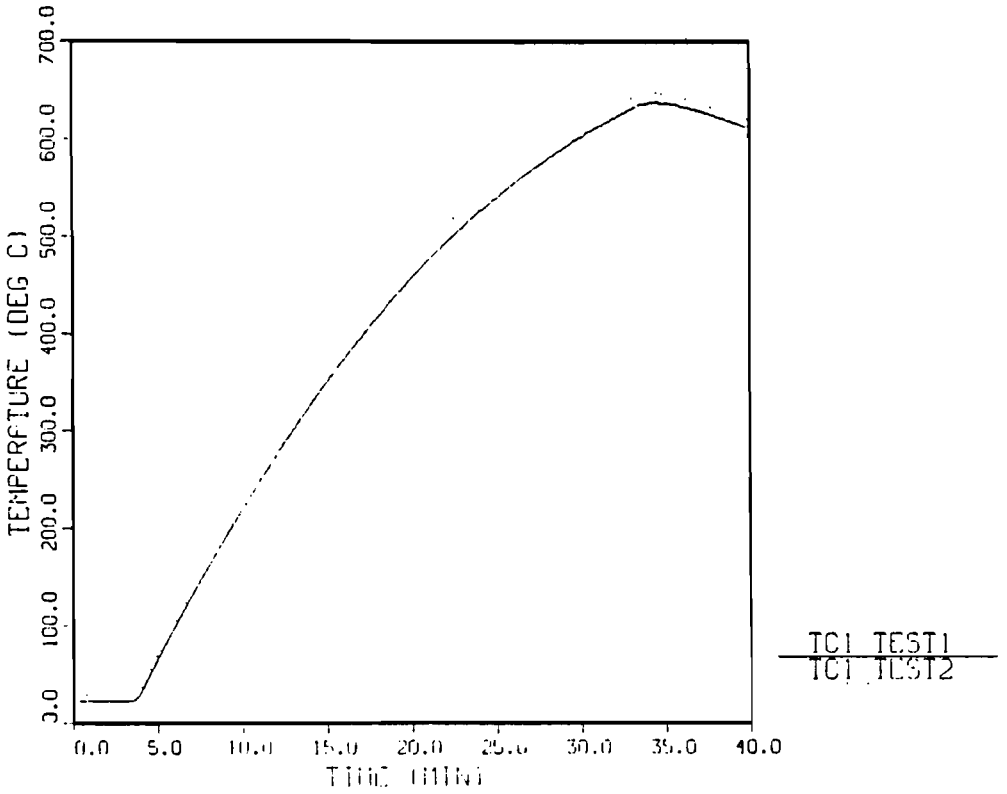

Figure 6.1-17 Temperature Profile for TC1, Tests 1 and 2

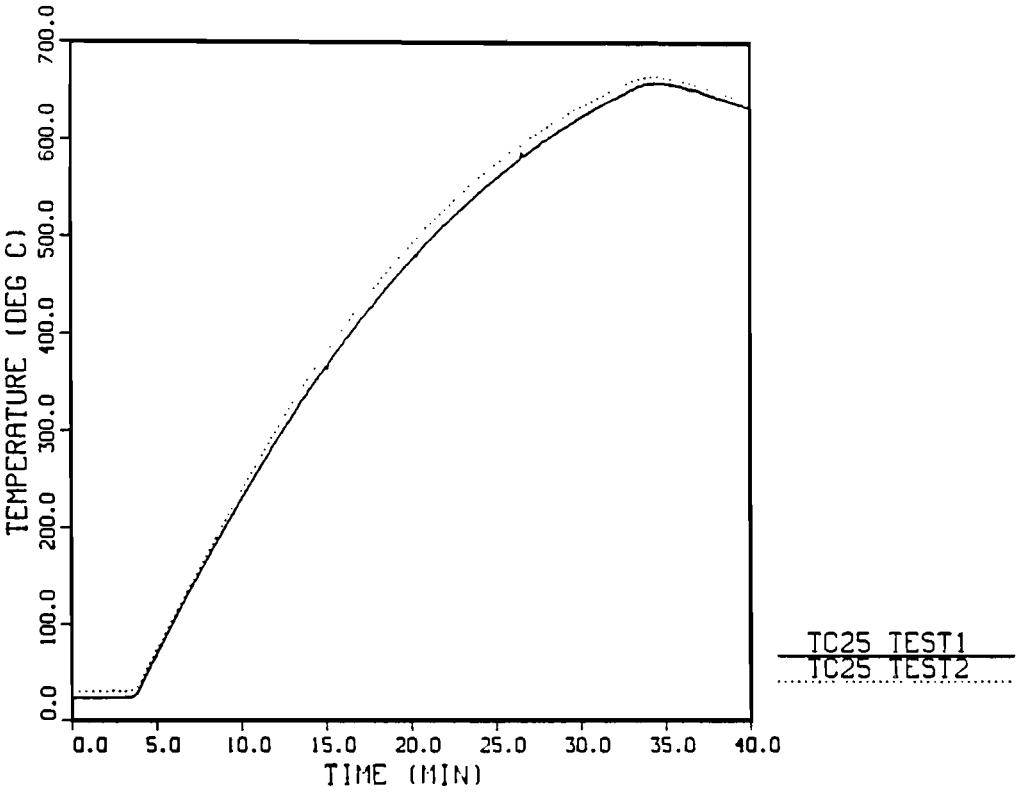

Figure 6.1-18 Temperature Profile for TC25, Tests 1 and 2

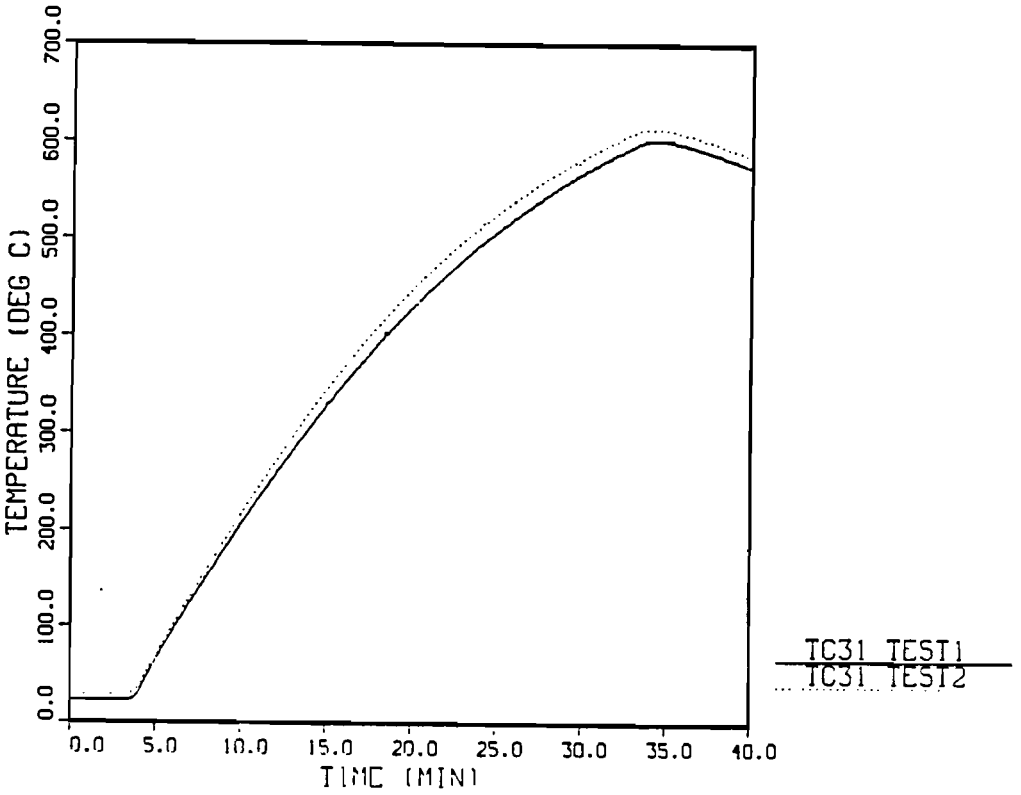

Figure 6.1-19 Temperature Profile for TC31, Tests 1 and 2

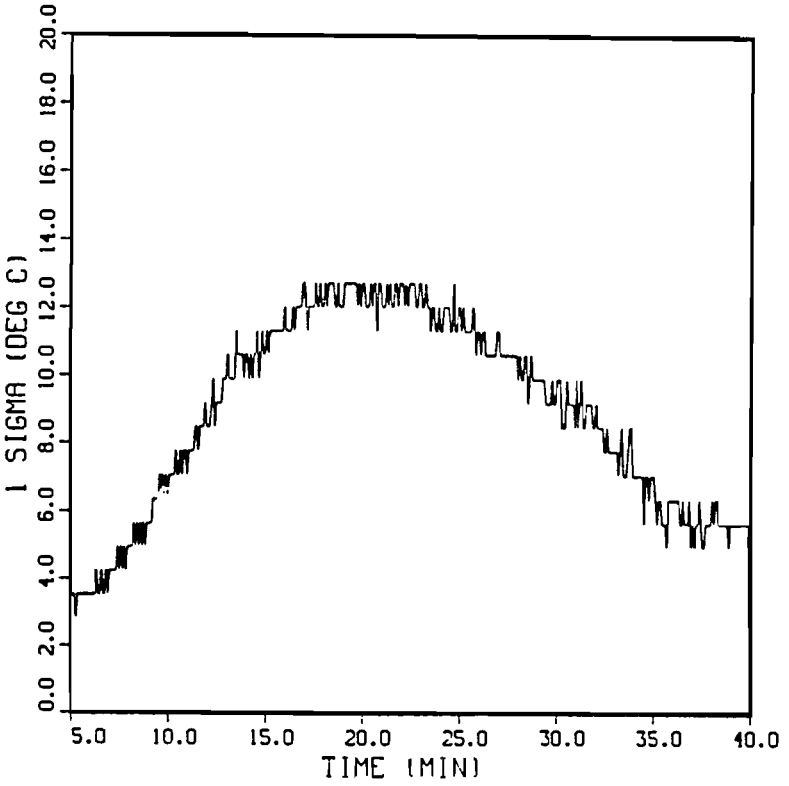

Figure 6.1-20 One Sigma Error Bound as a Function of Time for TC1, Tests 1 and 2

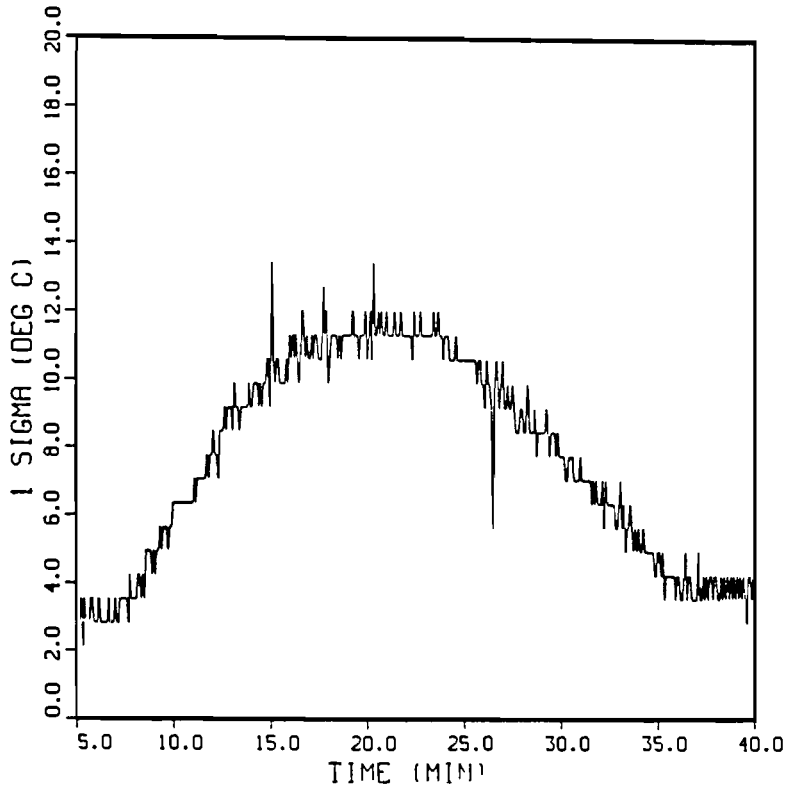

Figure 6.1-21 One Sigma Error Bound as a Function of Time for TC25, Tests 1 and 2

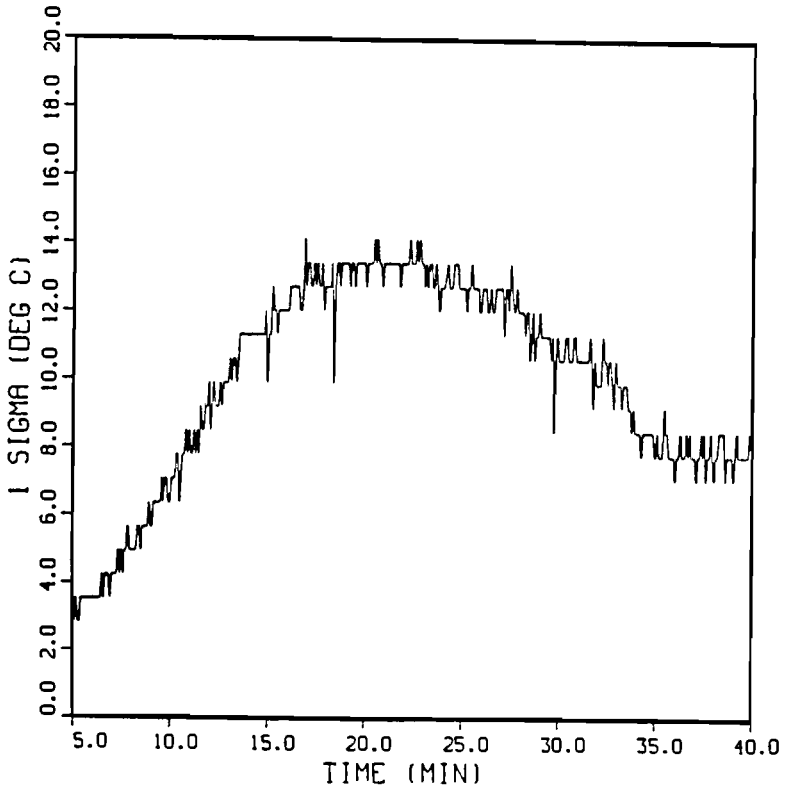

Figure 6.1-22 One Sigma Error Bound as a Function of Time for TC31, Tests 1 and 2

The one sigma error bounds are a measure of the error bound associated with the mean temperatures of both tests.

All curves shown start at five minutes because large temperature differences due to different ambient temperatures during pre-test data acquisition are not considered for repeatability assessment. Table 6.1-2 shows maximum temperatures for each test at thermocouple locations TC1, TC25, and TC31. Also included in this table are the maximum absolute difference in temperature and the estimated mean of the absolute difference. The estimated mean values have corresponding estimated standard deviations.

6.2 Results of the 870°C 100-Minute Radiant Heat Tests

6.2.1 Environment Temperature Results for Test 3

Figures 6.2-1 through 6.2-4 show temperatures histories for the radiant heat shroud for Test 3. The data for three different axial heights and four circumferential locations are shown in Figures 6.2-1 through 6.2-3. Figure 6.2-4 shows shroud temperature histories for one circumferential position at three different axial heights. Refer to Figure 4.1-1 for thermocouple locations on the radiant heat test shroud. Table 6.2-1 indicates mean environment temperatures at each axial location with corresponding standard deviations for several shroud thermocouple locations. The circumferential mean temperature with corresponding standard deviation is given for each axial plane. The interval for which temperatures were averaged started when the shroud reached test temperature (approximately 2.5 minutes after start of temperature ramp up) and ended when the quartz lamps shut down.

The mean temperature for the bottom axial plane was 784°C, 86°C below the target test temperature. The circumferential variability is 18°C, 2.8 times greater than the variability of the control (center axial) plane. The center axial plane produced a mean temperature of 867°C, only 3°C below the required test temperature. Circumferential variability is small at 6°C. The top axial plane yielded a mean temperature of 850°C with a circumferential variability

TABLE 6.1-2

Maximum Temperatures, Maximum Absolute Difference, and Mean Absolute Difference for Thermocouple Stations TC1, TC25, and TC31 for Both 800°C, 30-Minute Radiant Heat Tests

Thermocouple Station	Test #	Max Temperature (°C)	MAX $\lvert\Delta T\rvert$ (°C)	$\lvert\overline{\Delta T}\rvert$ [a] (°C)
TC1	1	638	18	13±4
	2	648		
TC25	1	659	17	12±4
	2	666		
TC31	1	602	20	15±4
	2	614		

[a] The plus or minus value represents the estimated standard deviation of the sample.

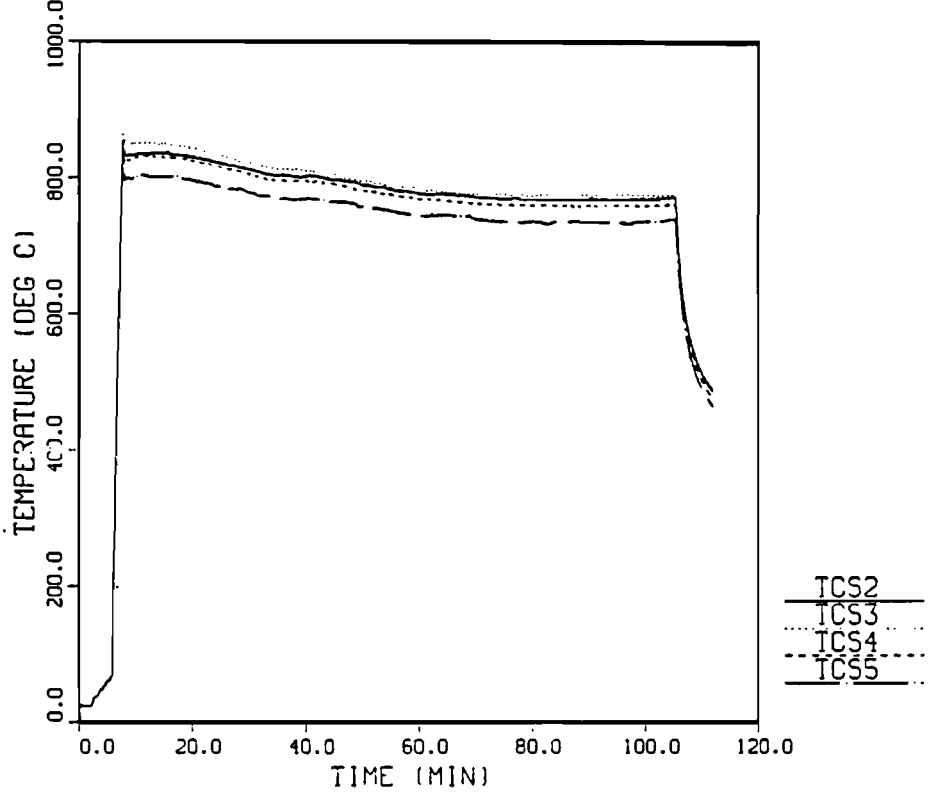

Figure 6.2-1 Radiant Heat Shroud Temperature Profile, Bottom Axial Plane, Test 3

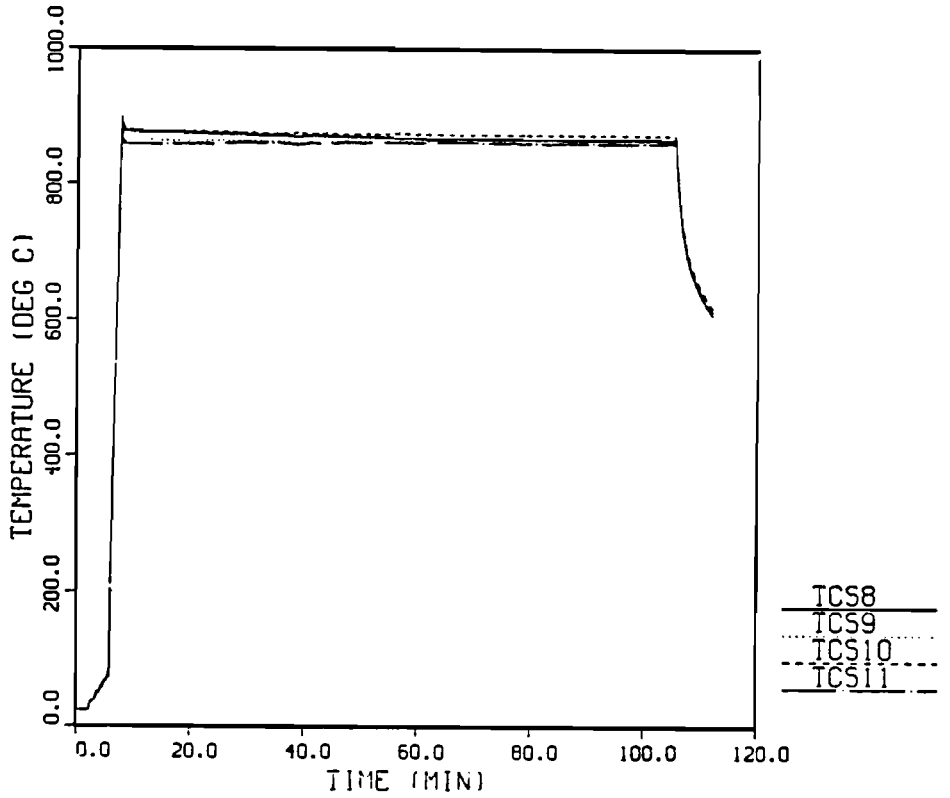

Figure 6.2-2 Radiant Heat Shroud Temperature Profile, Center Axial Plane, Test 3

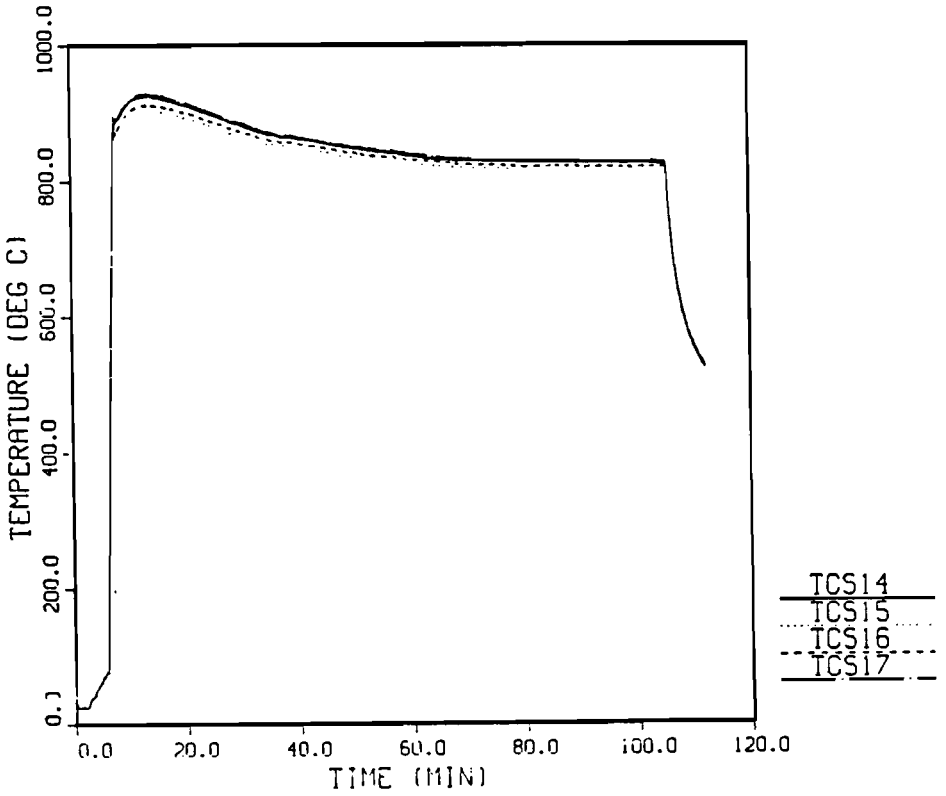

Figure 6.2-3 Radiant Heat Shroud Temperature Profile, Top Axial Plane, Test 3

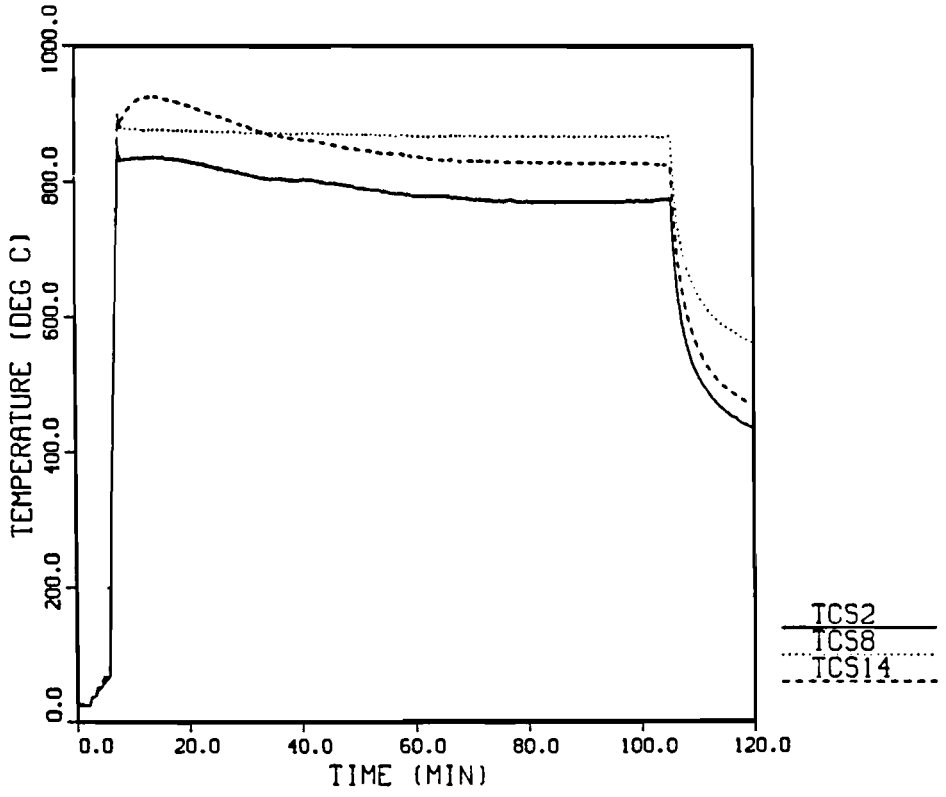

Figure 6.2-4 Radiant Heat Shroud Temperature Profile, Bottom, Center, and Top Axial Planes, Test 3

TABLE 6.2-1

Sample Mean ($\bar{Y}$) and Standard Deviation (S) Selected Shroud Thermocouple Locations During Test 3

Thermocouple Location	$\bar{Y}$ (°C)(a)	S (°C)
Bottom Axial Plane		
2	791.9	23.0
3	799.7	26.1
4	784.3	24.5
5	758.9	23.0
Circumferential Mean	783.7	17.7
Center Axial Plane		
8	869.8	3.5
9	862.9	1.2
10	874.5	1.2
11	860.5	1.2
Circumferential Mean	866.9	6.4
Top Axial Plane		
14	855.2	32.2
15	842.2	29.5
16	847.5	30.0
17	856.5	32.8
Circumferential Mean	850.4	6.73
TOTAL	$\bar{Y}$ = 833.7°C	S = 44.0°C

of 67°C. The overall mean environment temperature was calculated to be 834°C, which is 36°C below the target test temperature. The axial variability, 44°C, was much greater than any of the circumferential variabilities.

The same type of control phenomenon that was experienced during Test 1 was also present during Test 3. Figure 6.2.4 shows the temperature history of the test shroud at each axial plane. The apparent steady state condition described for Test 1 is more pronounced in Test 3 due to longer test times. Because of the longer test time, temperature variability at each thermocouple location (except the control plane) on the test shroud is much greater than temperature variability of Test 1.

6.2.2 Test Article Temperature Results for Test 3

Figure 6.2-5 through 6.2-8 show temperature profiles as a function of time for the test article. Refer to Figure 3.2-3 for thermocouple locations. The temperature profile for the axial center plane of the test article is shown in Figure 6.2-5. The maximum difference in temperature between any two thermocouples in the center axial plane was 10°C, which occurred between TC19 and TC13. TC13 was the hottest thermocouple on this plane reaching 847°C. The inflection point shown in all test article temperature histories is caused by a solid phase change that occurs at the Curie point, approximately 760°C, which is characteristic of the mild steel material. This temperature will not shift for a relatively large number of test cycles. Figure 6.2-6 shows the temperature profile for the top axial plane of the test article. The maximum difference in temperature between any two thermocouples in the top axial plane was approximately 8°C, which occurred between TC25 and TC28. TC28 reached a maximum temperature of 859°C, which was the hottest for this plane and for the entire test article. In Figure 6.2-7 the temperature profile for the bottom axial plane is shown. Temperatures were less uniform in this plane, with a maximum difference in temperature of 15°C between TC32 and TC35. TC35 was the hottest thermocouple on this plane reaching 815°C. Figure 6.2-8 graphically shows the temperature differences between the three axial planes. The maximum difference in temperature was 46°C.

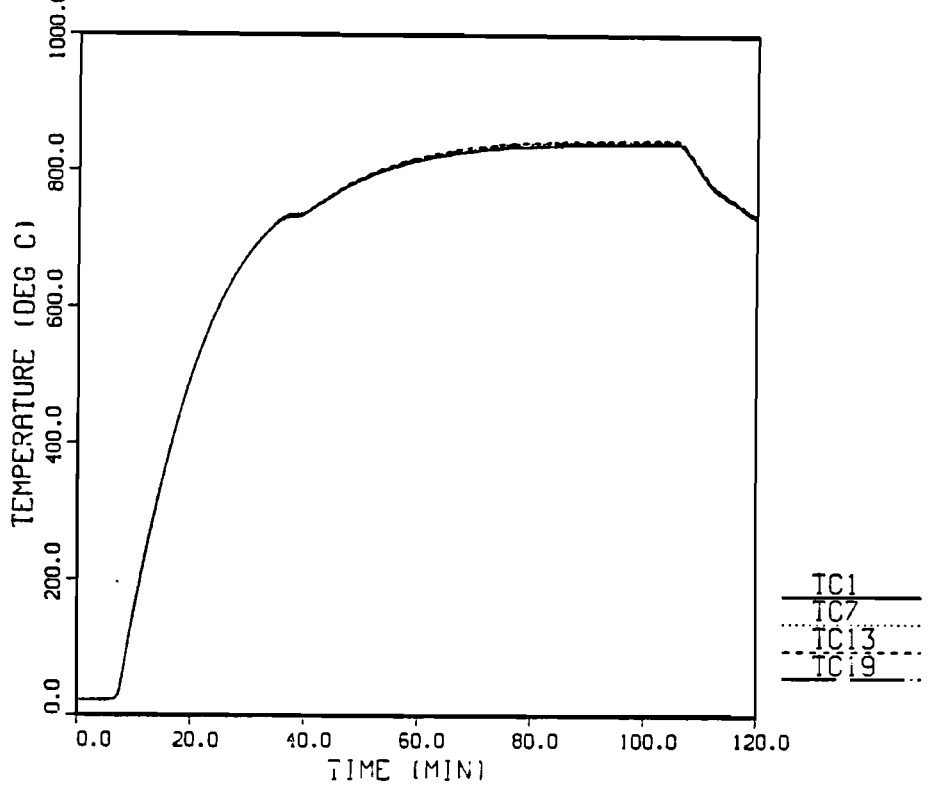

Figure 6.2-5 Test Article Temperature Profile, Center Axial Plane, Test 3

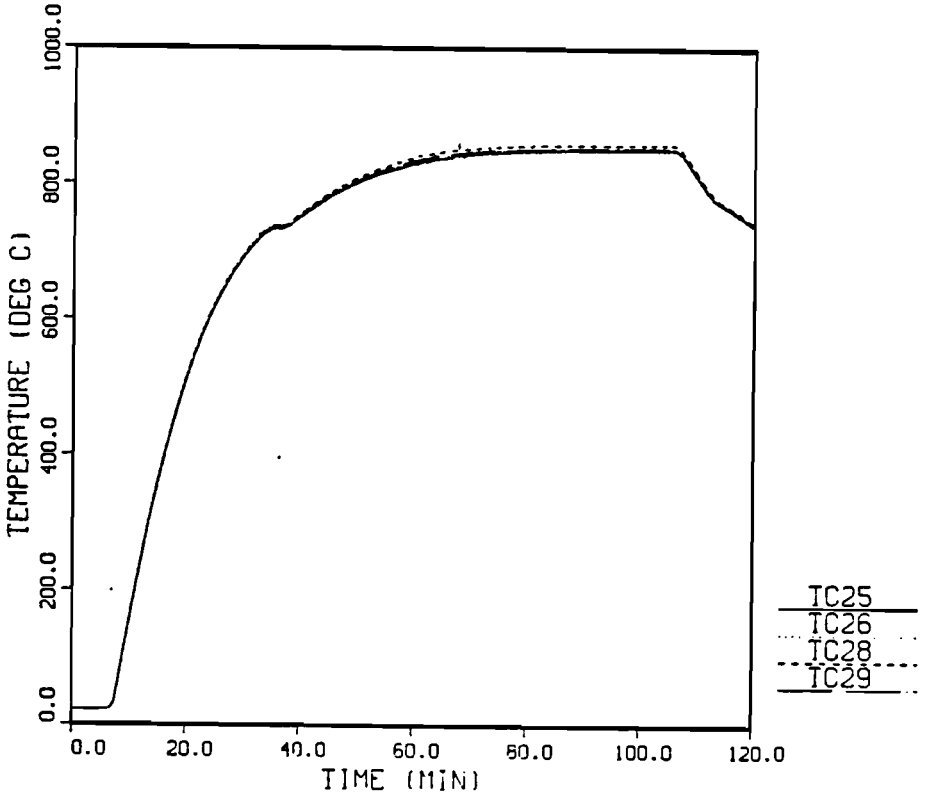

Figure 6.2-6 Test Article Temperature Profile, Top Axial Plane, Test 3

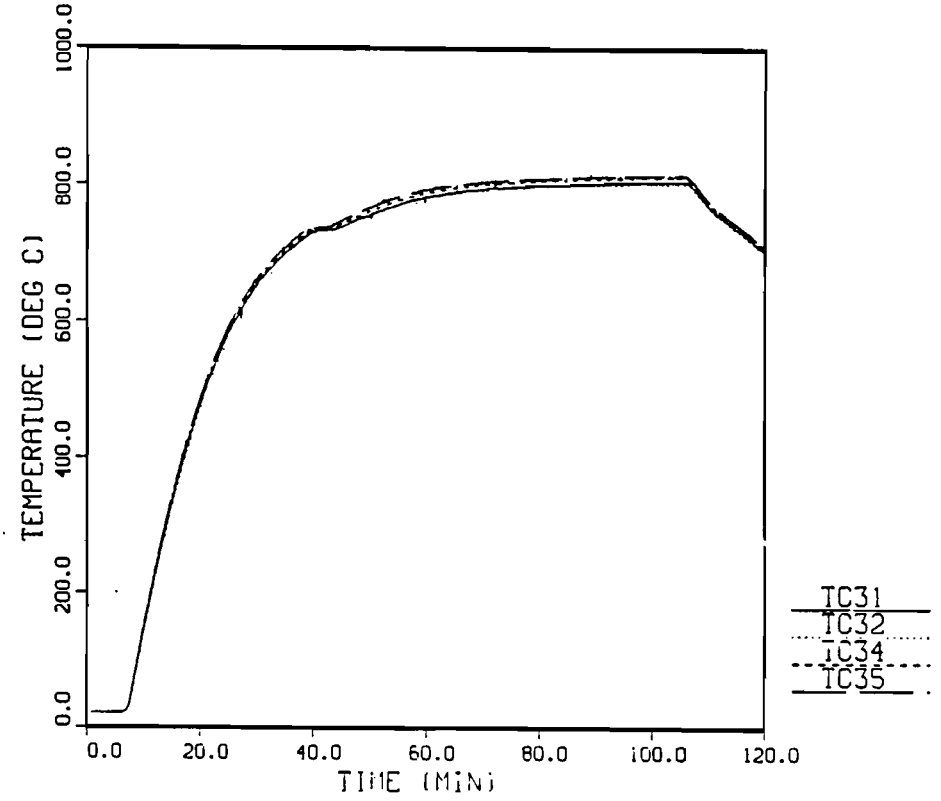

Figure 6.2-7 Test Article Temperature Profile, Bottom Axial Plane, Test 3

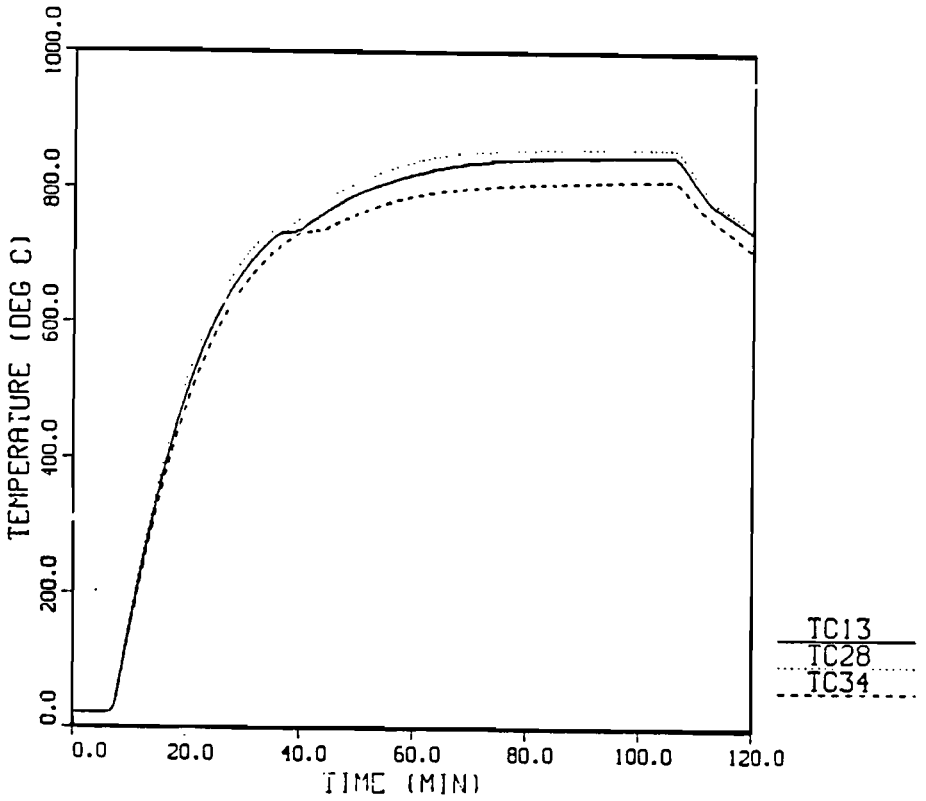

Figure 6.2-8 Test Article Temperature Profile, Bottom, Center, and Top Axial Planes, Test 3

6.2.3 Surface Heat Flux Results for Test 3

Figures 6.2-9 through 6.2-14 show the surface heat flux as a function of time and surface temperature for thermocouple locations TC1, TC25, and TC31. As in Test 1, the curves are smooth indicating the absence of wind induced variability and highly turbulent nature inside the fire. The fluctuations in the curves are caused primarily by the growth of measurement noise errors in the inverse region [10]. Appendix E discusses the effect of filter strength on these fluctuations. The data shown in the Figures 6.2-9 through 6.2-14 were calculated using a filter strength of 1 to provide the best resolution. The reported estimated surface heat flux values and estimated surface temperatures, along with their uncertainties, were calculated using a filter strength of 3. Appendix E explains the details of the uncertainty analysis. The curves also indicate that the surface heat flux approaches zero towards the end of the test, when test article temperatures are approaching their maximum values. It is at this point that the test article becomes saturated. This is analogous to a steady-state condition. The test article was designed to approach steady-state towards the end of the 100-minute test. The large fluctuation in surface heat flux shown in all curves occurs at the Curie point region. At this point the inverse heat conduction code became unstable. This unstable condition occurs because of rapidly varying material properties. For this reason it is important to have reliable material properties with high resolution in the curie point region. The maximum estimated surface heat flux at TC1 was 90.4 KW/m^2 for a surface temperature of 166°C. The time-integrated heat flux at TC1 was 142.02 MJ/m^2. The maximum flux at TC25 was 93.1 KW/m^2 for a surface temperature of 180°C. The time-integrated heat flux was 143.59 MJ/m^2. The maximum flux at TC31 was 85.3 KW/m^2 for a surface temperature of 155°C. The time-integrated heat flux was 134.92 MJ/m^2.

6.2.4 Test 4: Repeatability of 870°C, 100-Minute Radiant Heat Test

Test 4 was performed to assess the repeatability of the 870°C, 100-minute radiant heat test. Test 4 results are presented here to assess repeatability only.

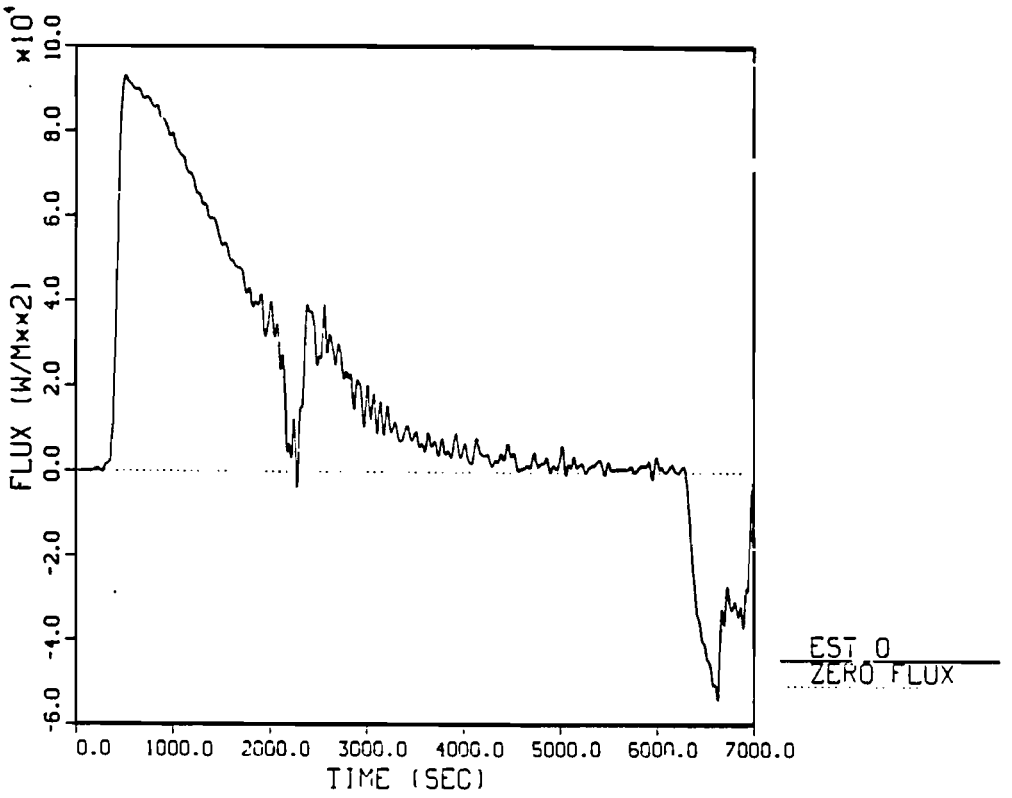

Figure 6.2-9 Local Surface Heat Flux History for TC1, Test 3

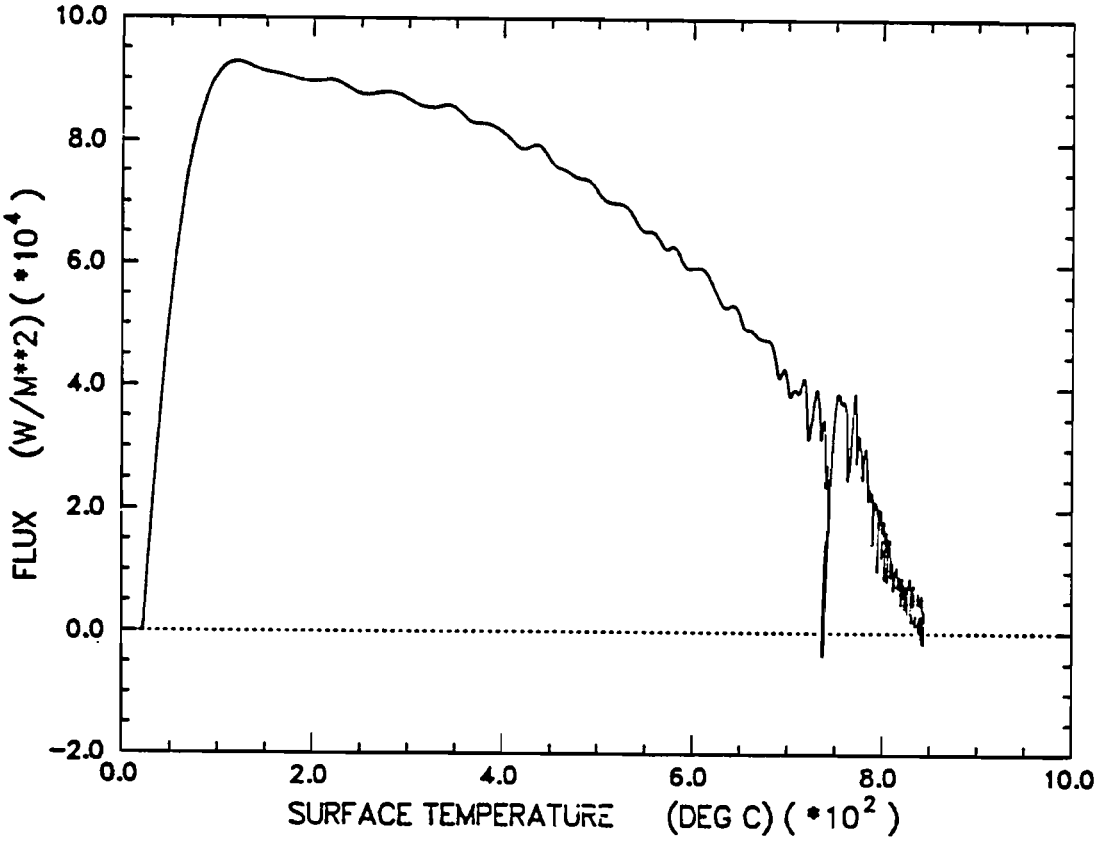

Figure 6.2-10 Local Surface Heat Flux as a Function of Surface Temperature for TC1, Test 3

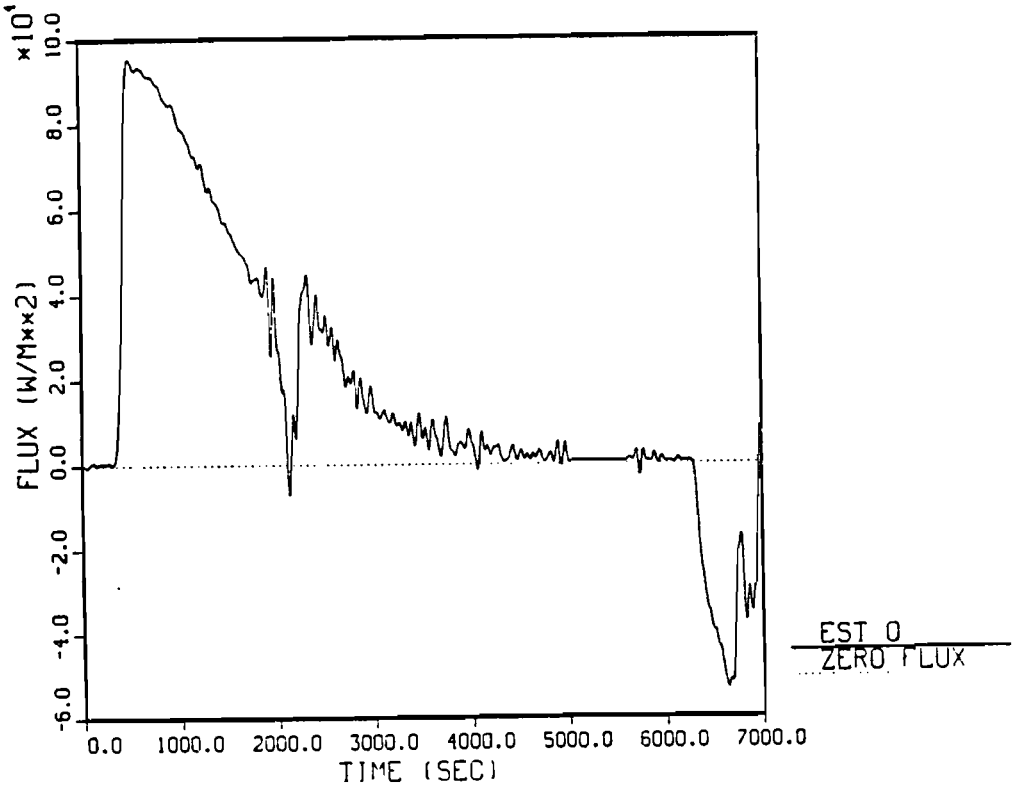

Figure 6.2-11 Local Surface Heat Flux History for TC25, Test 3

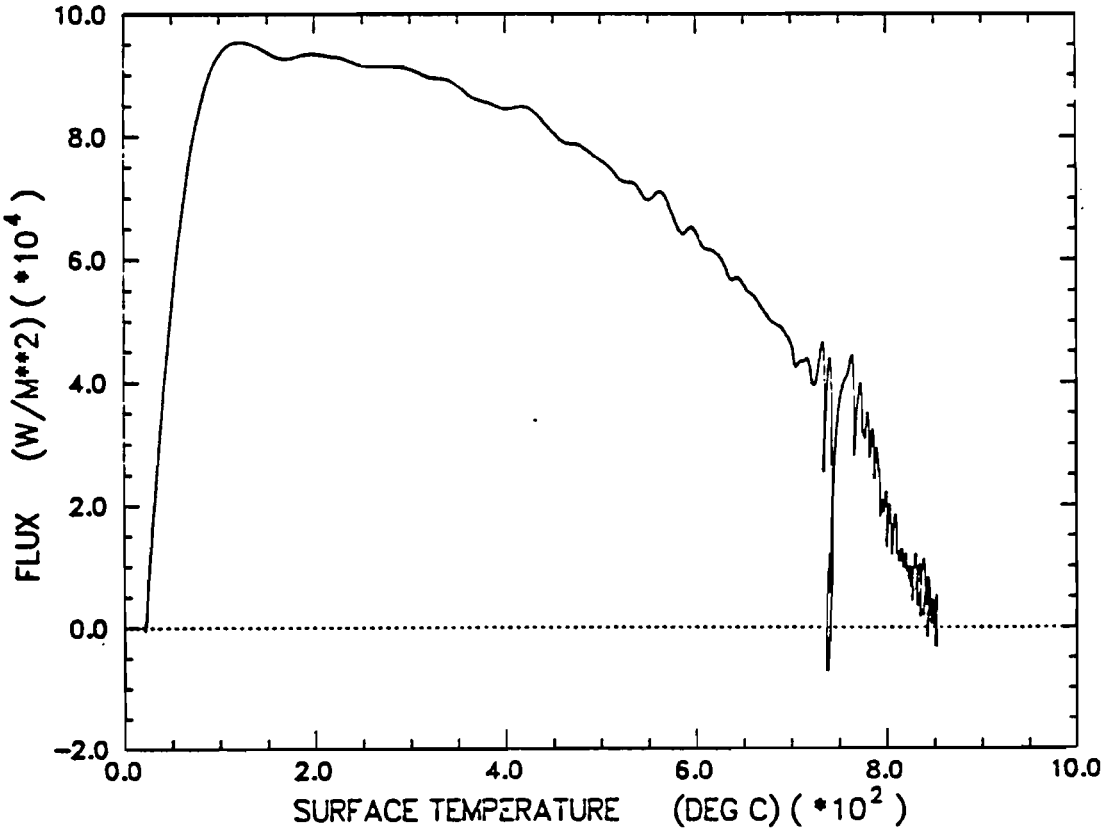

Figure 6.2-12 Local Surface Heat Flux as a Function of Surface Temperature for TC25, Test 3

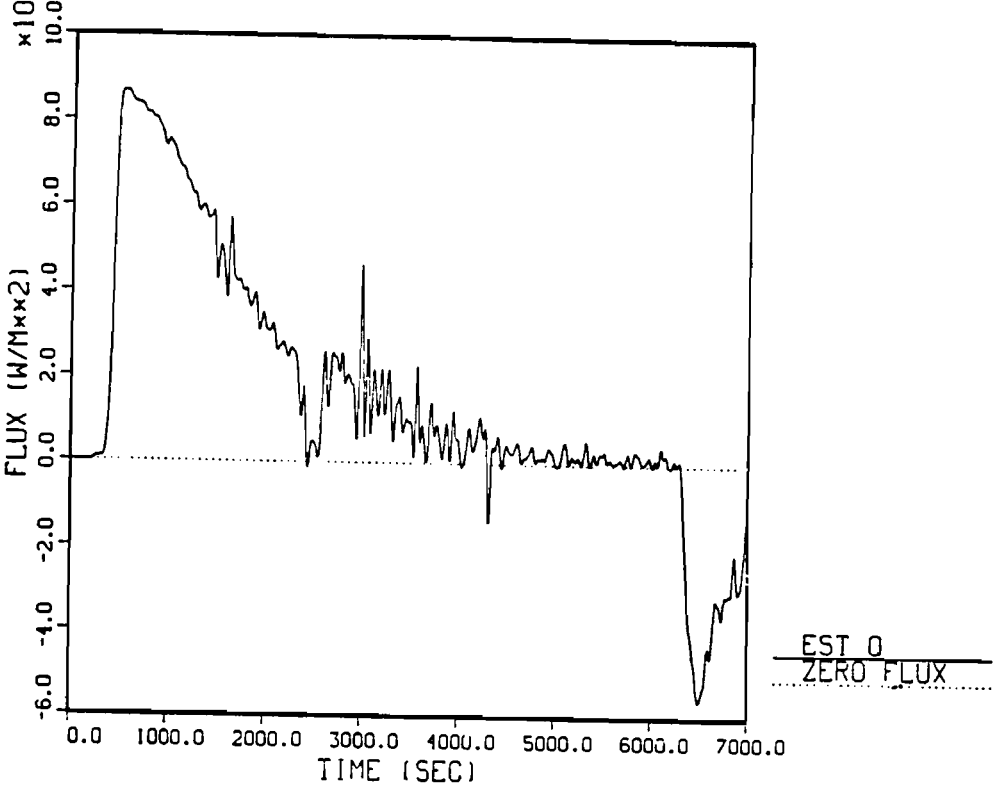

Figure 6.2-13 Local Surface Heat Flux History for TC315, Test 3

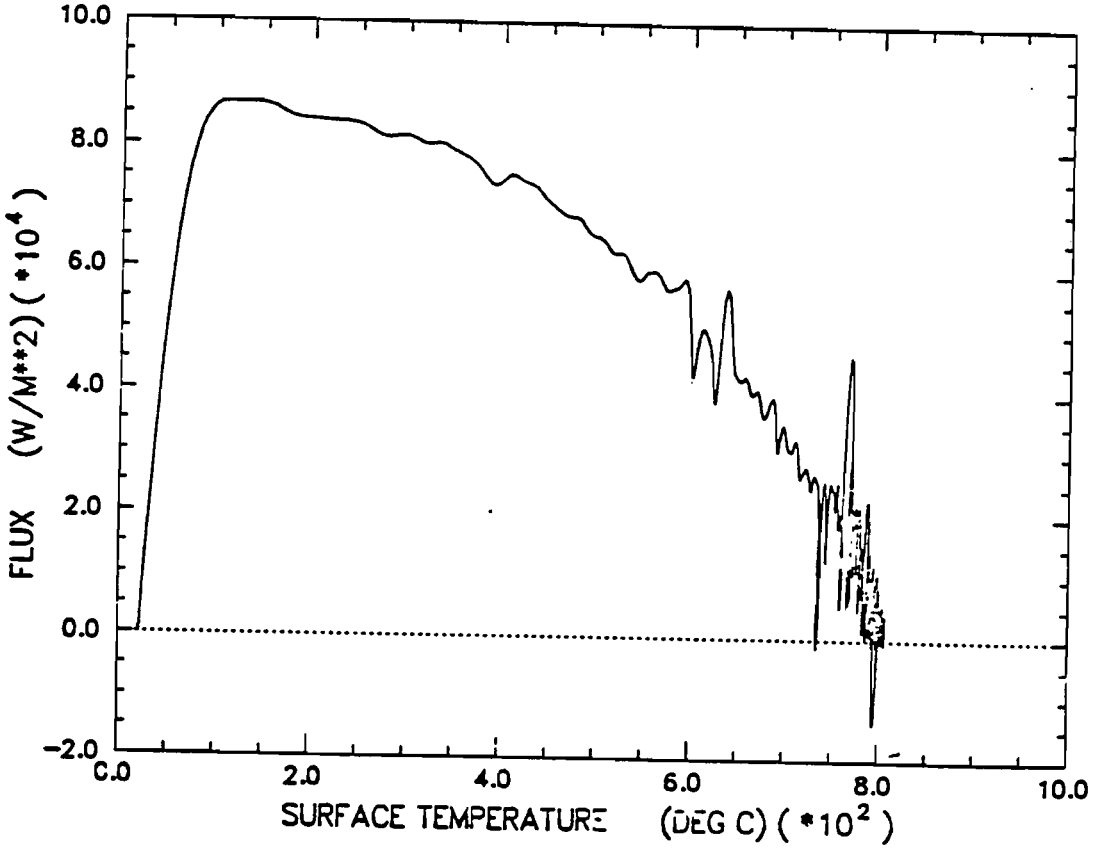

Figure 6.2-14 Local Surface Heat Flux as a Function of Surface Temperature for TC31, Test 3

Figures 6.2-15 through 6.2-17 show temperature histories for Tests 3 and 4 for three different thermocouple locations TC1, TC25, and TC31. Figures 6.2-18 through 6.2-20 show the one sigma error bound for Tests 3 and 4 for TC1, TC25, and TC31. The discontinuities in these figures correspond to experimental data that is rounded off to whole integers.

Table 6.2-2 shows maximum temperatures, maximum absolute difference, and mean absolute difference for TC1, TC25, and TC31 for both tests. In general, the one sigma error bound for the 870°C, 100-minute radiant heat test, was much lower than for the 800°C, 30-minute radiant heat tests.

6.3 Results of the Engulfing Fire Test

6.3.1 Environment Temperature Results for Test 5

Figure 6.3-1 shows the location of the instrumentation poles relative to the test article within the Tenth Scale Enclosed Pool Fire Facility. Figure 6.3-2 through 6.3-5 show flame temperature histories from the instrumentation poles for Test 5. The data for three axial heights and four circumferential directions are shown in Figures 6.3-2 through 6.3-4. Figure 6.3-5 shows flame temperature histories for one circumferential position at three different axial heights. Table 6.3-1 summarizes mean flame temperatures at each thermocouple location with corresponding one sigma standard deviation. Also included in this table are mean temperatures for each axial plane as well as the mean temperature for the entire test.

The bottom axial plane produced a mean temperature of 854°C. The circumferential variability was 17°C. The center axial plane produced a mean temperature of 897°C. Circumferential variability of 26°C was relatively large compared to the center control plane of the radiant heat facility shroud. The top axial plane yielded a mean temperature of 908°C with a circumferential variability of 11°C. The overall mean environment temperature was calculated to be 886°C. The axial variability, 30°C, was slightly greater than the circumferential variabilities.

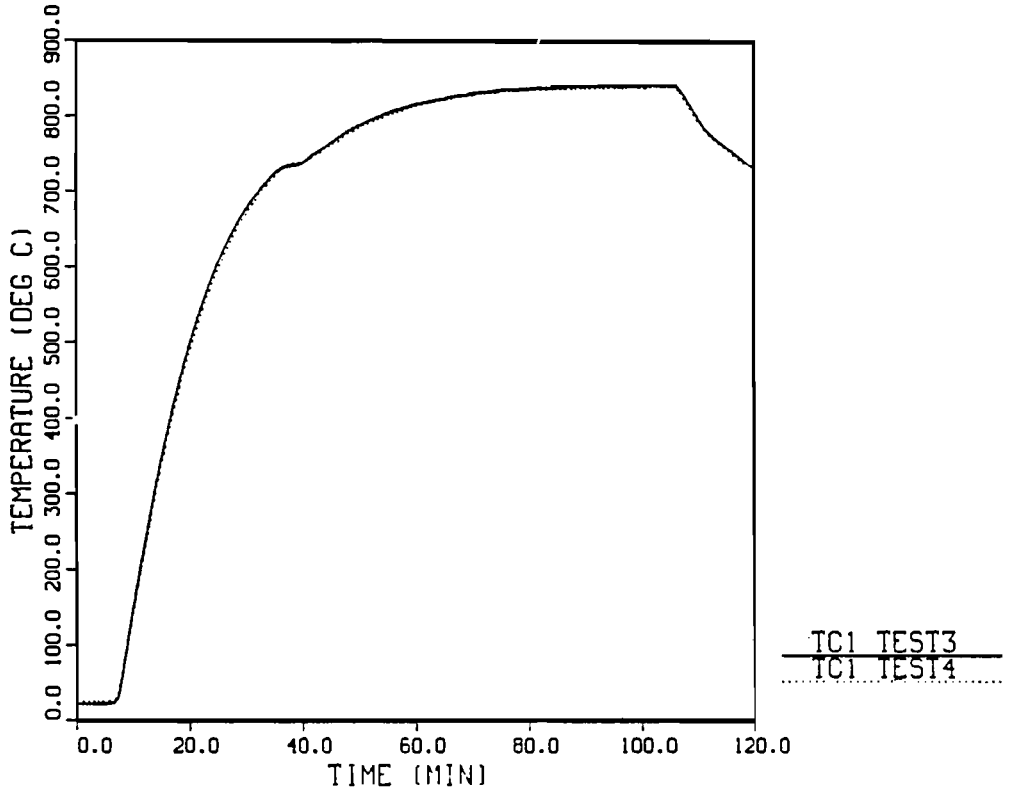

Figure 6.2-15 Temperature Profile for TC1, Tests 3 and 4

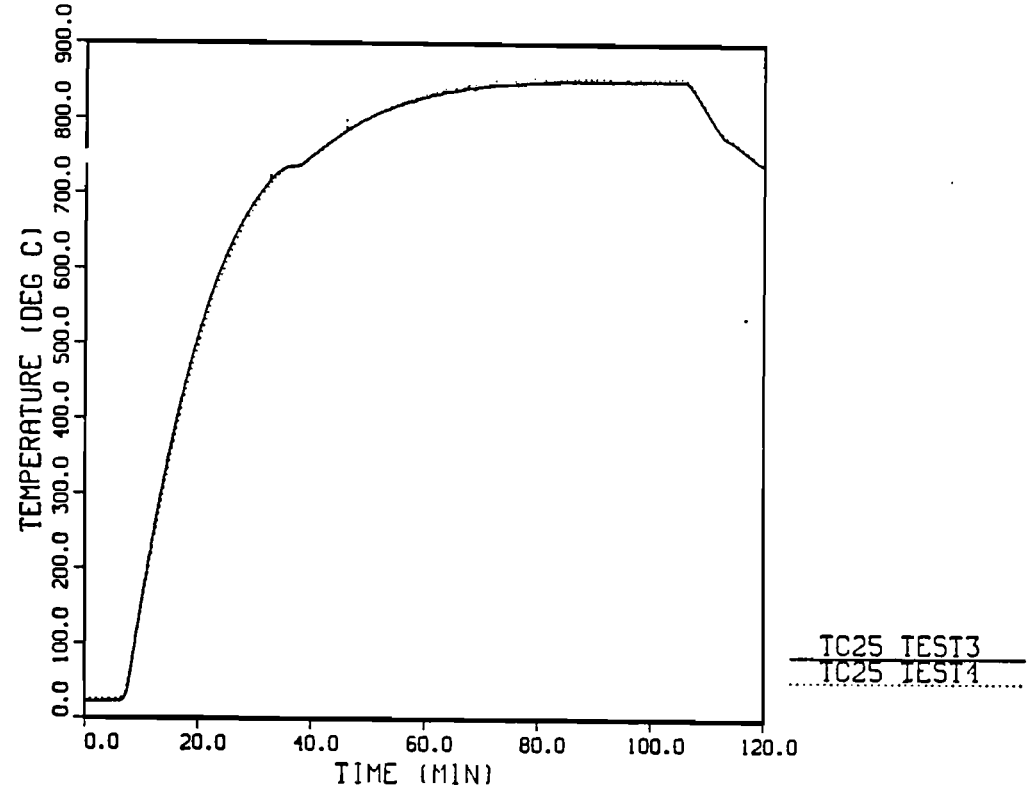

Figure 6.2-16 Temperature Profile for TC25, Tests 3 and 4

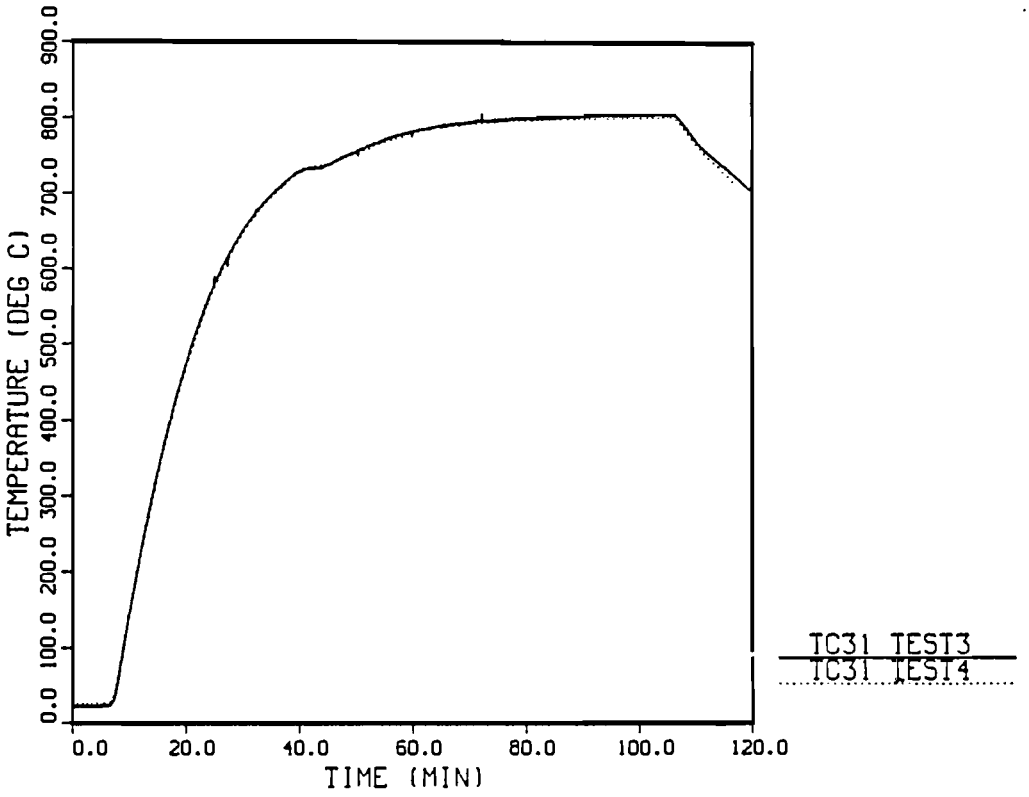

Figure 6.2-17 Temperature Profile for TC31, Tests 3 and 4

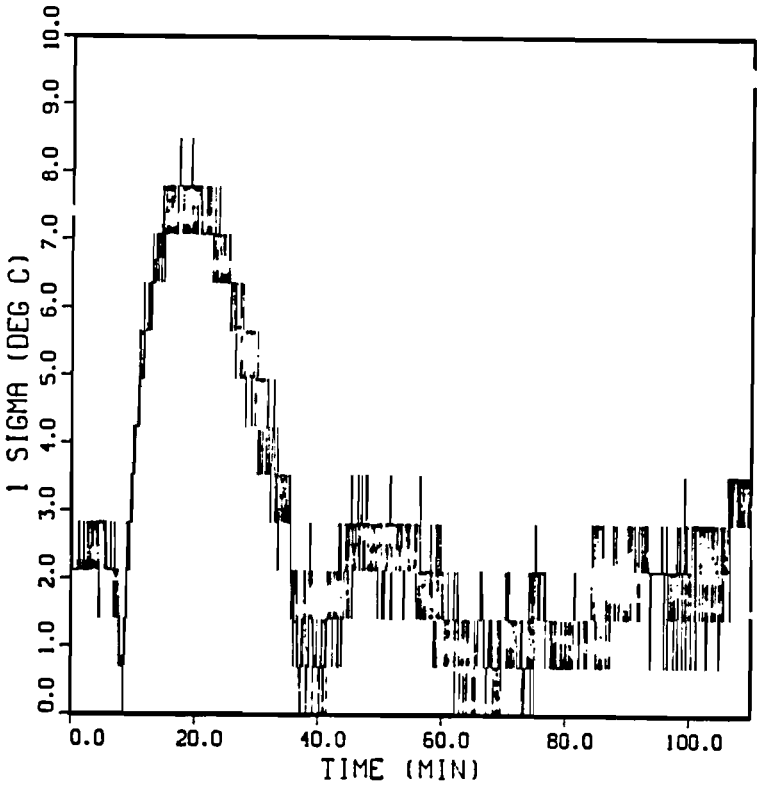

Figure 6.2-18 One Sigma Error Bound as a Function of time for TC1, Tests 3 and 4

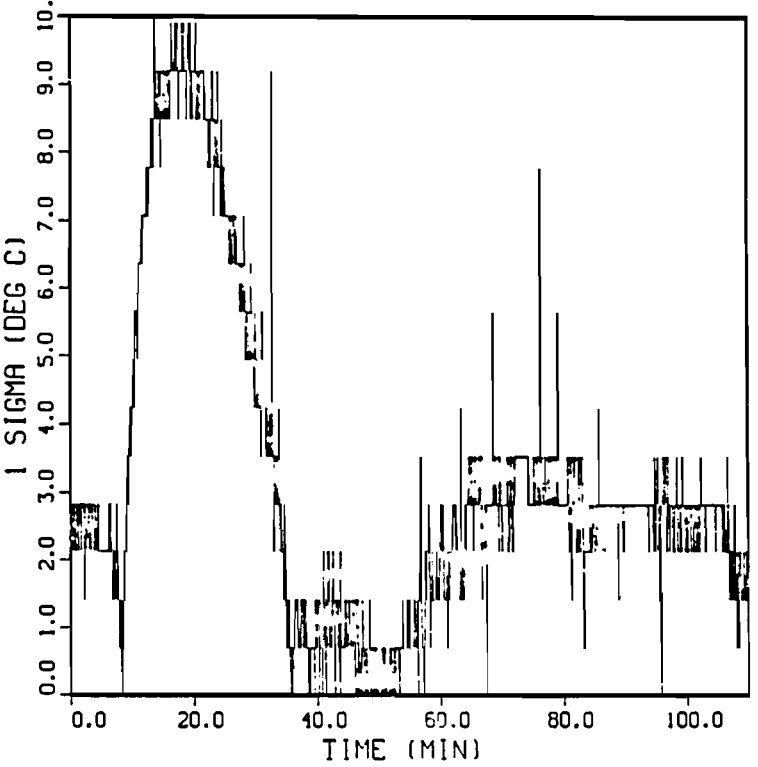

Figure 6.2-19 One Sigma Error Bound as a Function of Time for TC25, Tests 3 and 4

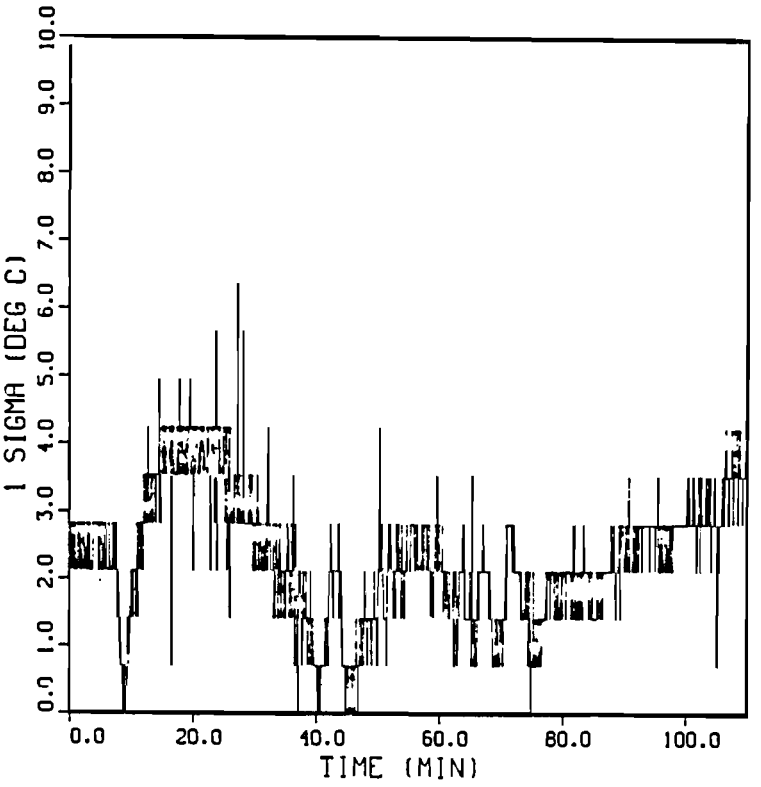

Figure 6.2-20 One Sigma Error Bound as a Function of Time for TC31, Tests 3 and 4

TABLE 6.2-2

Maximum Temperatures, Maximum Absolute Difference,
and Mean Absolute Difference for
Thermocouple Locations TC1, TC25, and TC31
for Both 870°C, 100-Minute Radiant Heat Tests

Thermocouple Station	Test #	Max Temperature (°C)	MAX $\lvert\Delta T\rvert$ (°C)	$\lvert\bar{\Delta T}\rvert$[a] (°C)
TC1	3	844	12.0	4.0 ± 3.0
	4	841		
TC25	3	855	15.0	4.7 ± 3.6
	4	857		
TC31	3	806	9.0	3.2 ± 1.4
	4	805		

[a]The plus or minus value represents the estimated standard deviation of the sample.

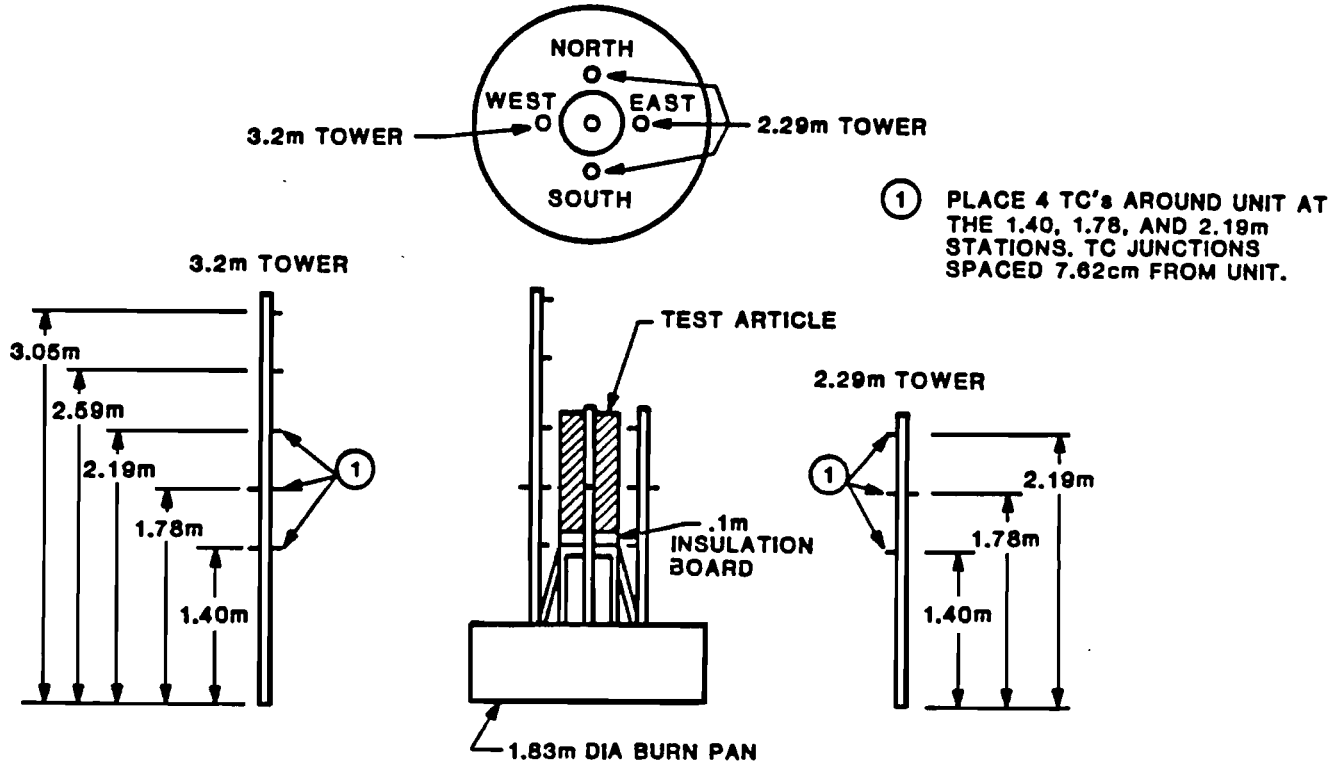

Figure 6.3-1 Locations of Poles Instrumented with Thermocouples for Test 5, Engulfing Fire Test

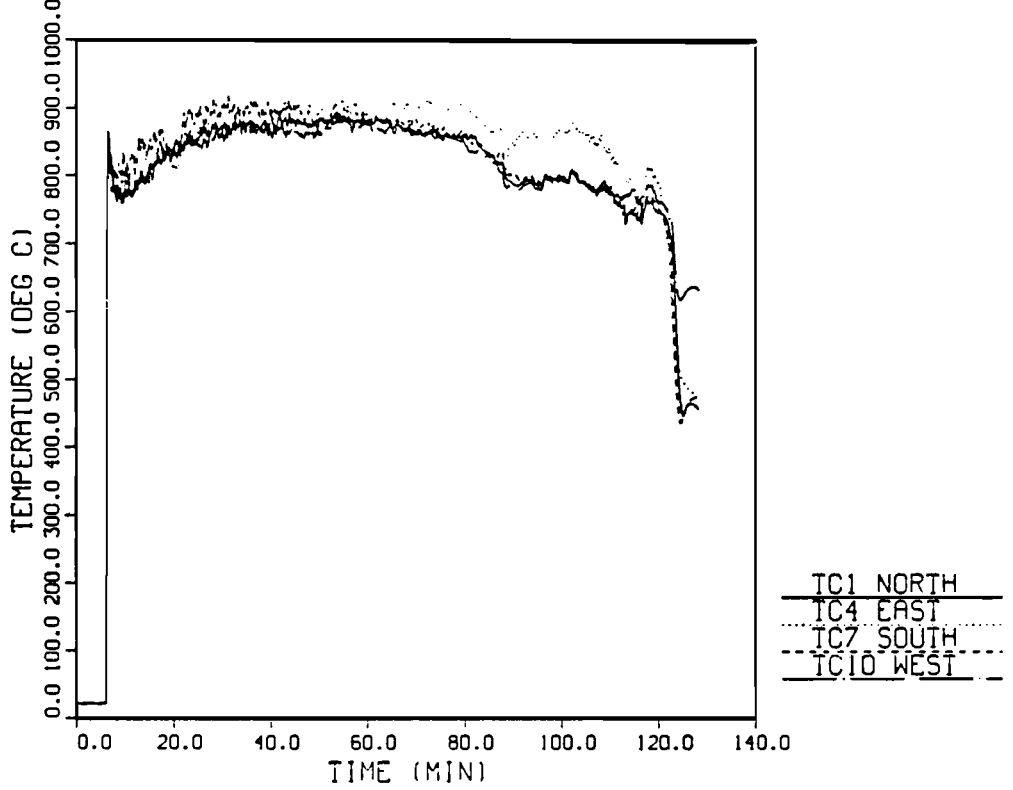

Figure 6.3-2 Flame Temperature Profile, Bottom Axial Plane, Test 5

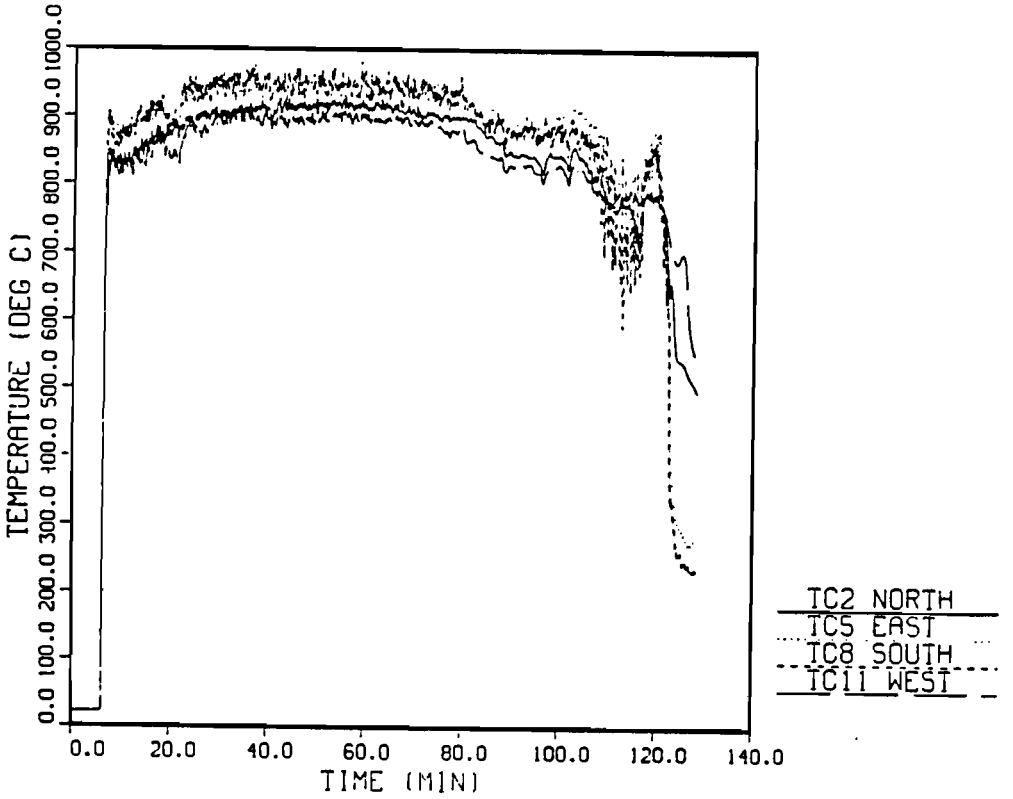

Figure 6.3-3 Flame Temperature Profile, Center Axial Plane, Test 5

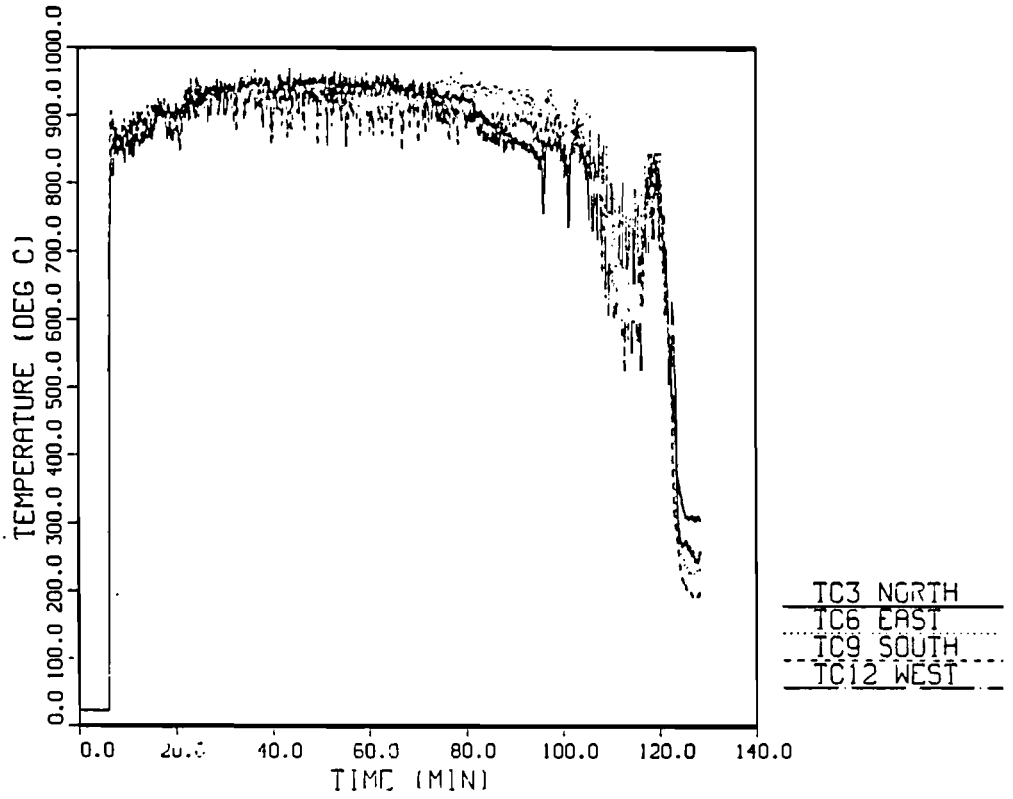

Figure 6.3-4 Flame Temperature Profile, Top Axial Plane, Test 5

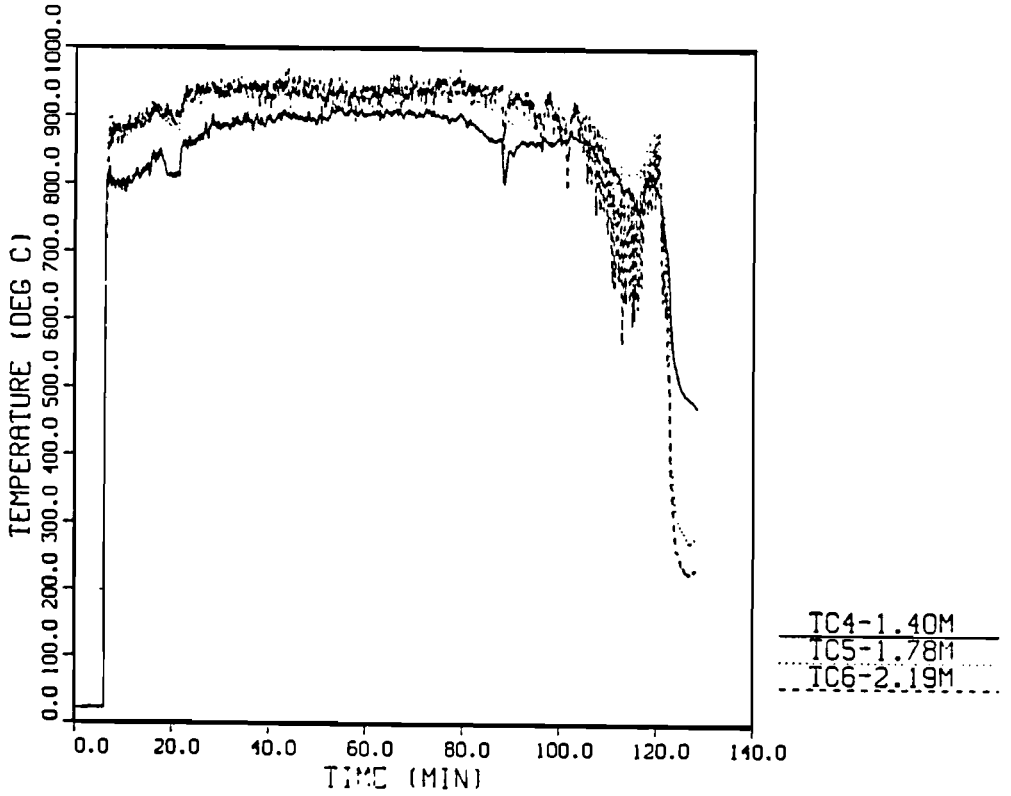

Figure 6.3-5 Flame Temperature Profile, East Circumferential Location, Bottom, Center, and Top Axial Planes, Test 5

TABLE 6.3-1

Sample Mean ($\bar{Y}$) and Standard Deviation(s) for Flame Temperatures Measured During Test 5

Thermocouple Location Station	$\bar{Y}$ (°C)	S(°C)
Bottom Axial Plane		
1	844.0	36.8
4	875.9	31.5
7	857.7	38.5
10	838.7	34.5
Circumferential Mean	854.1	16.6
Center Axial Plane		
2	884.3	31.64
5	918.1	19.6
8	918.4	31.7
11	867.2	31.6
Circumferential Mean	897.0	25.5
Top Axial Plane		
3	906.4	43.2
6	923.3	26.5
9	903.4	27.2
12	898.1	39.4
Circumferential Mean	907.8	10.9

TOTAL $\bar{Y}$ = 886.3°C S = 29.5°C

Flame temperature variability was much greater than radiant heat shroud temperature variability. Circumferential flame temperature variability was slightly greater than the radiant heat results except when considering the control plane. Here circumferential flame temperature variability was 75 percent greater than radiant heat results (percentages are based upon estimated standard deviations). Axial variabilities however are reduced for the fire test by 32 percent over radiant heat test results.

6.3.2 Test Article Temperature Results for Test 5

Figure 6.3-6 through 6.3-9 show temperature profiles for the test article for Test 5. Refer to Figure 3.2-3 for thermocouple locations. Figure 6.3-6 shows temperature profiles for the axial center plane of the test article. The maximum temperature difference on this plane was 93°C between TC13 and TC7. TC13 was the hottest thermocouple on this plane reaching 834°C. The inflection point shown in all test article temperature histories is caused by a solid phase change that occurs at the Curie point. Figure 6.3-7 shows temperature profiles at the top axial plane of the test article. The maximum difference in temperature between any two thermocouples in the top axial plane was approximately 81°C between TC26 and TC28. TC28 reached a maximum temperature of 831°C, the hottest for this plane. Figure 6.3-8 shows temperature profiles for the bottom axial plane. A maximum difference in temperature of 99°C occurred between TC32 and TC34. TC34 was the hottest thermocouple on this plane reaching 820°C. Figure 6.3-9 graphically shows the temperature differences between the three axial planes. The maximum difference in temperature was 43°C between TC25 and TC31.

6.3.3 Surface Heat Flux Results for Test 5

Figures 6.3-10 through 6.3-15 show the surface heat flux as a function of time and surface temperature for thermocouple locations TC1, TC25, and TC31. As in Tests 1 and 3, the curves are smooth indicating the absence of wind induced variability. The data shown in the figures is calculated using a filter strength of 1 to provide the best resolution. The reported estimated

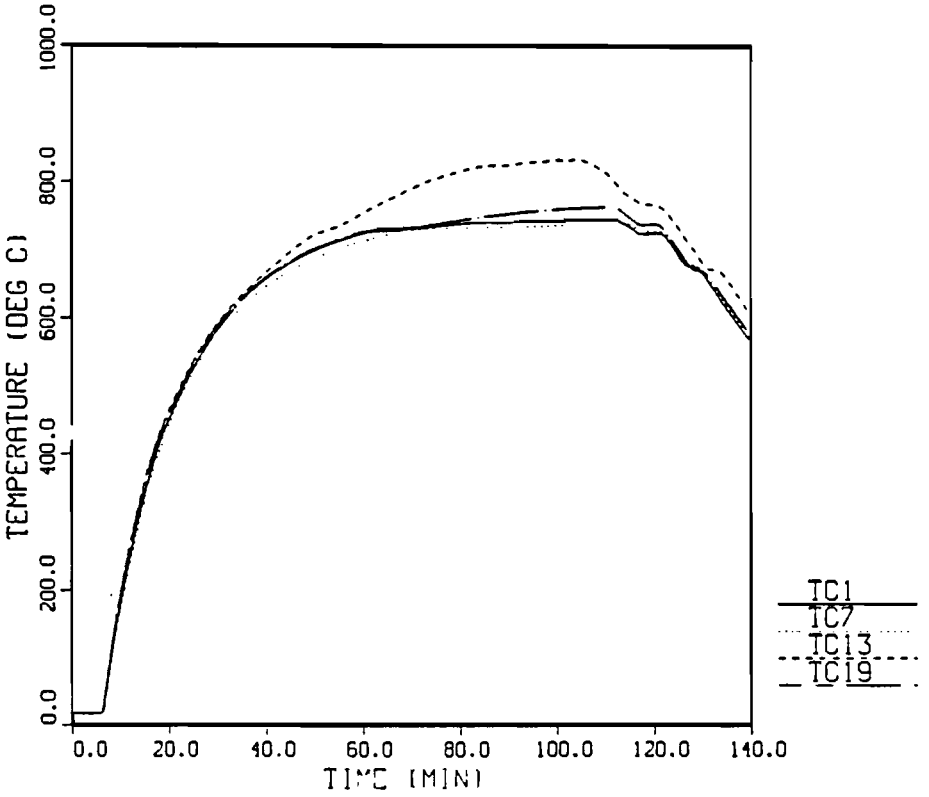

Figure 6.3-6 Test Article Temperature Profile, Center Axial Plane, Test 5

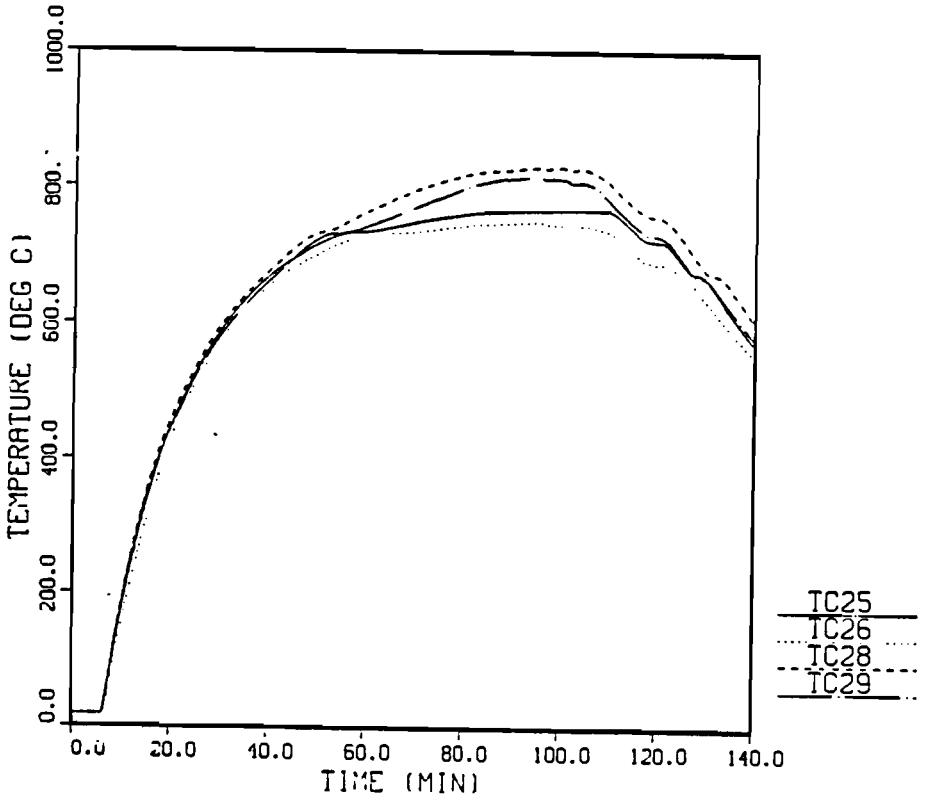

Figure 6.3-7 Test Article Temperature Profile, Top Axial Plane, Test 5

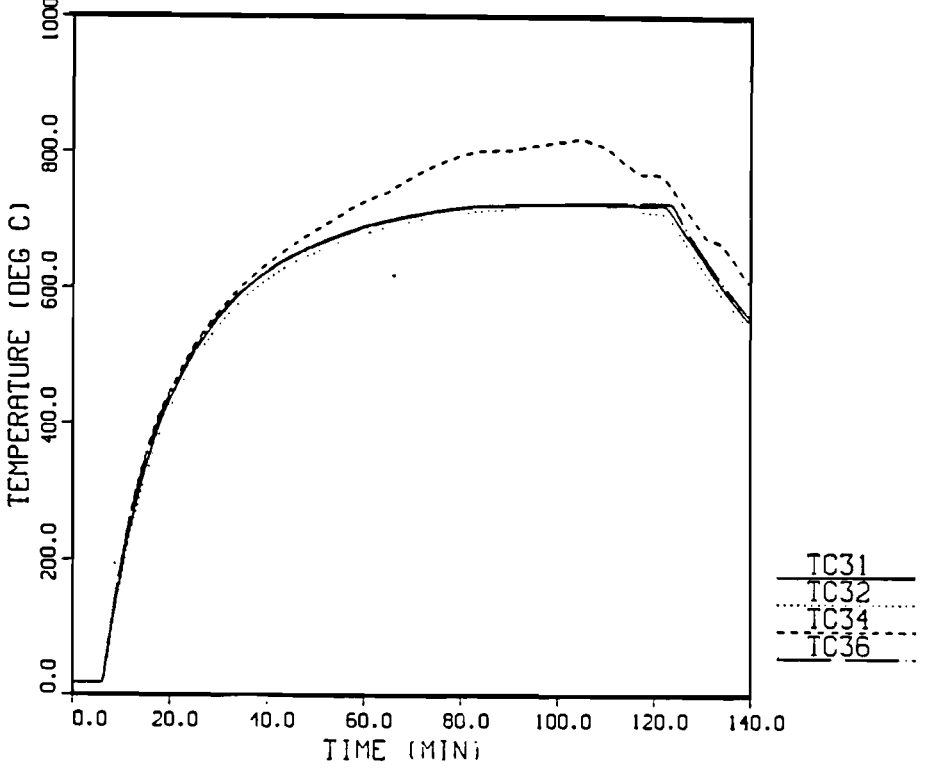

Figure 6.3-8 Test Article Temperature Profile, Bottom Axial Plane, Test 5

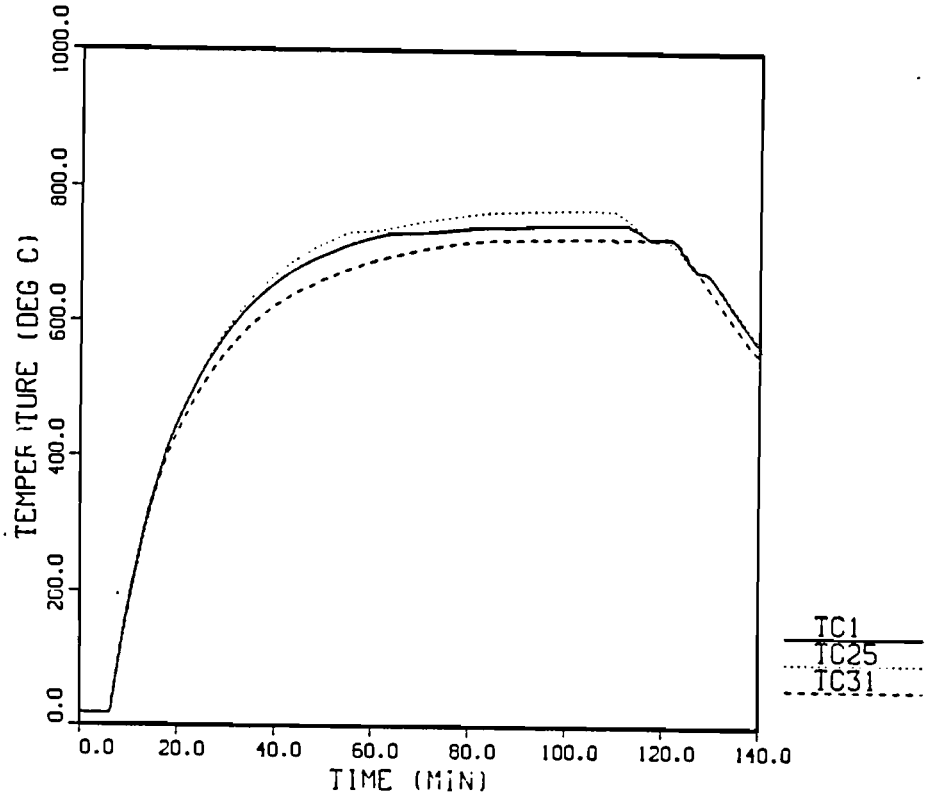

Figure 6.3-9 Test Article Temperature Profile, Bottom, Center, and Top Axial Planes, Test 5

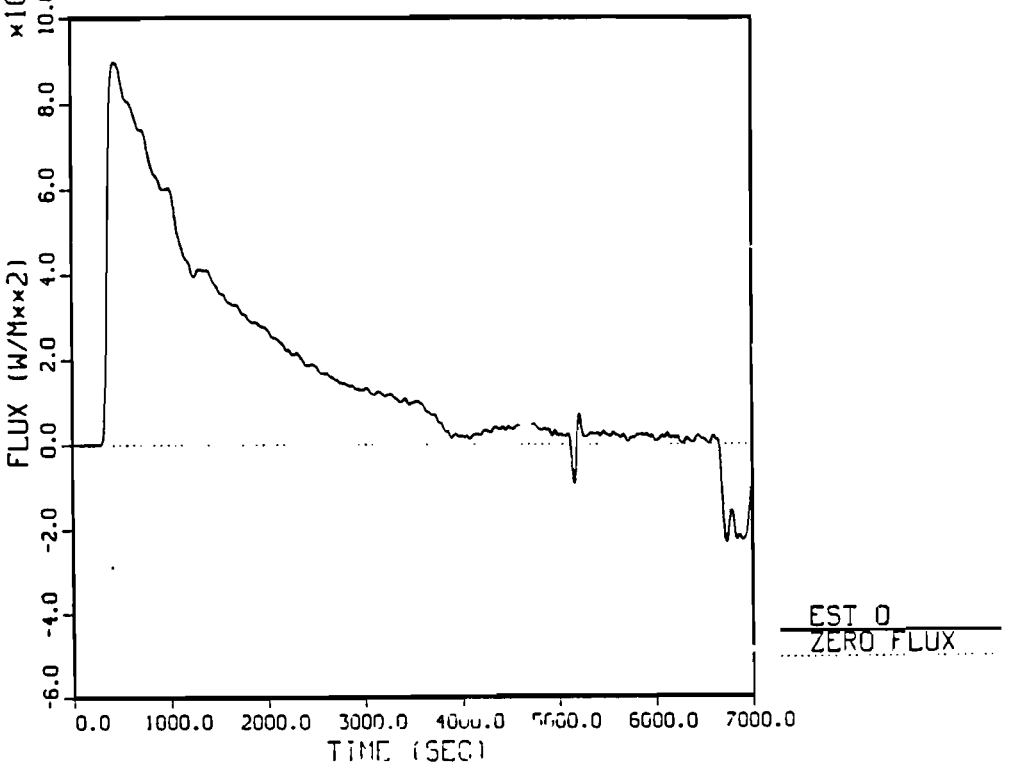

Figure 6.3-10 Local Surface Heat Flux History for TC1, Test 5

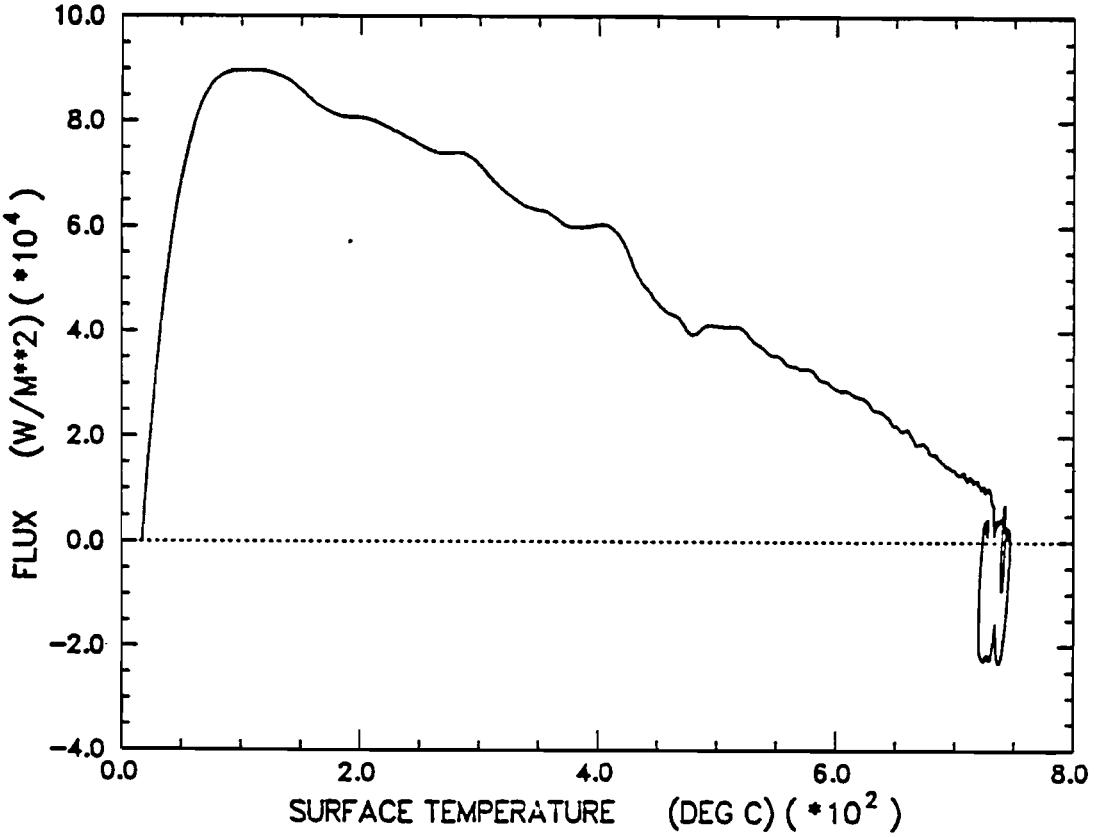

Figure 6.3-11 Local Surface Heat Flux as a Function of Surface Temperature for TC1, Test 5

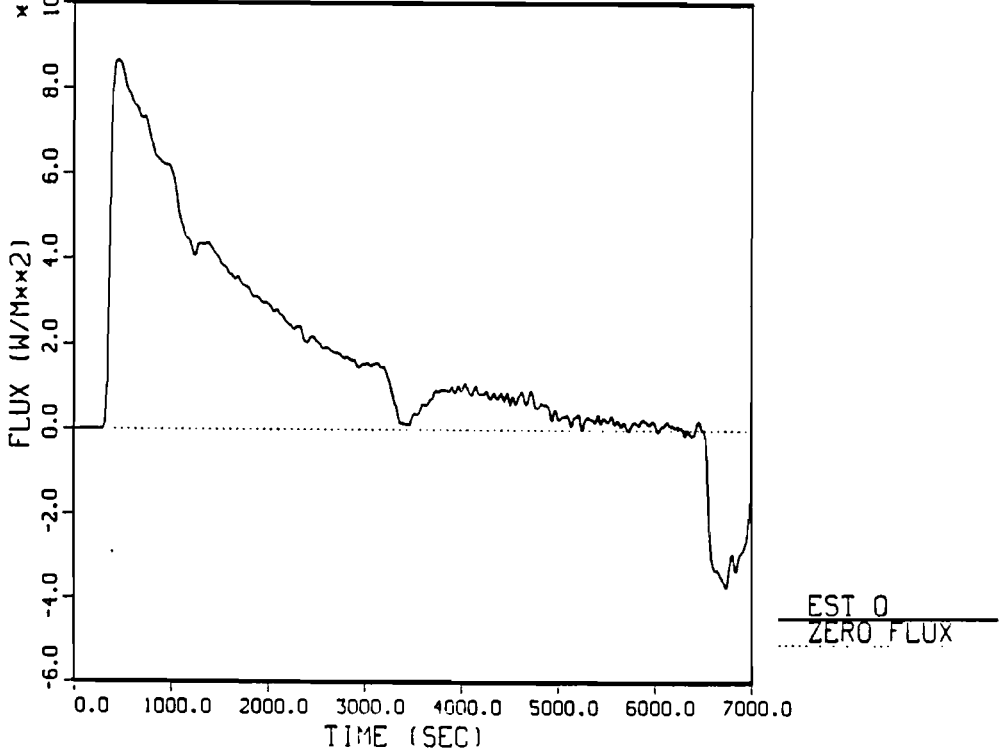

Figure 6.3-12 Local Surface Heat Flux History for TC25, Test 5

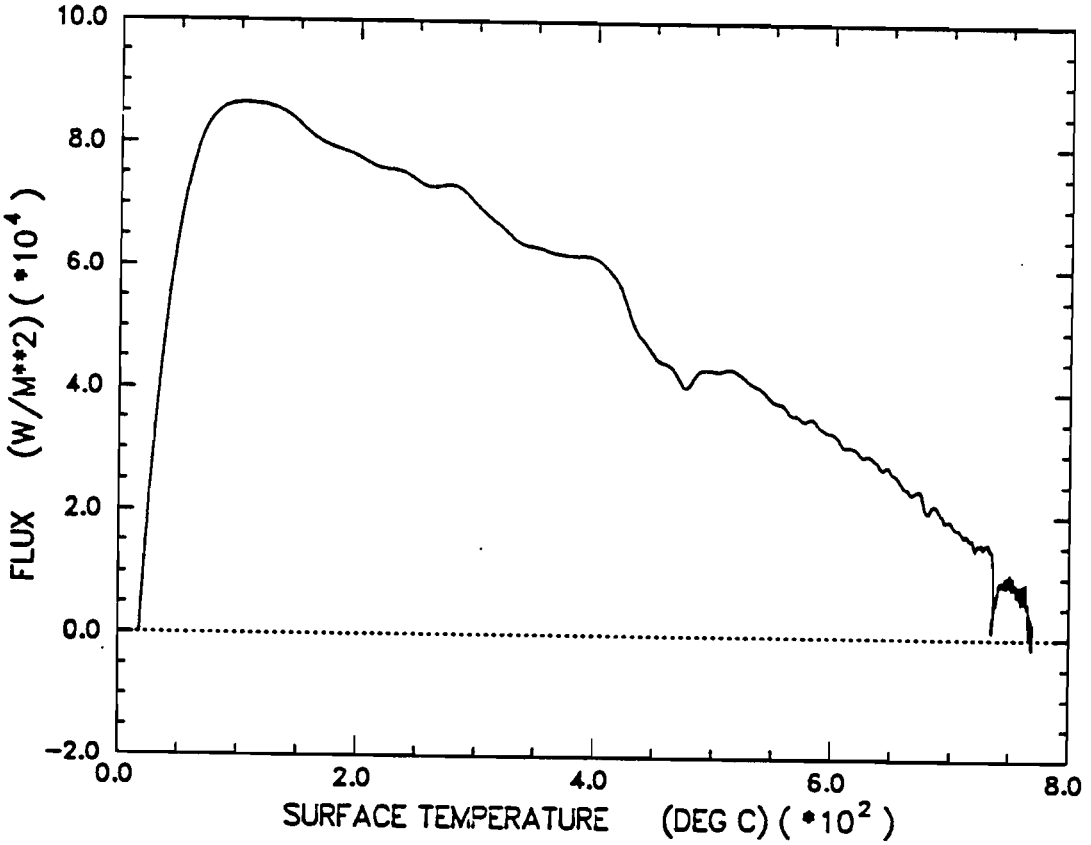

Figure 6.3-13 Local Surface Heat Flux as a Function of Surface Temperature for TC25, Test 5

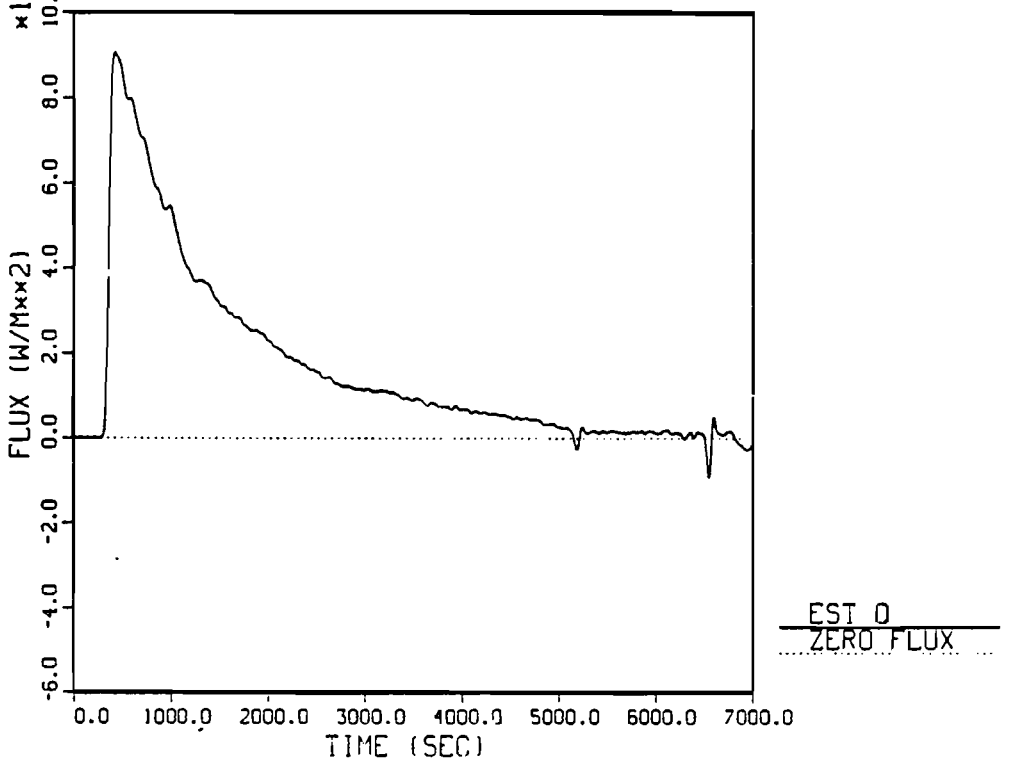

Figure 6.3-14 Local Surface Heat Flux History for TC31, Test 5

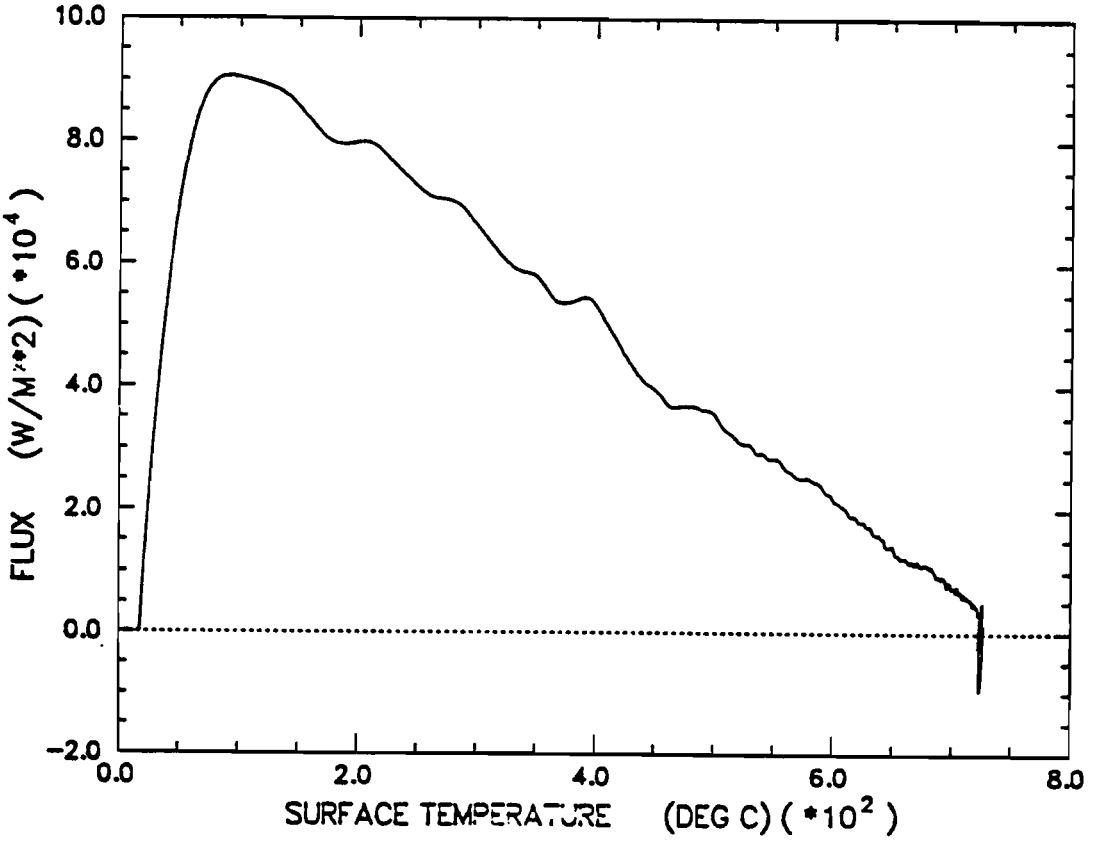

Figure 6.3-15 Local Surface Heat Flux as a Function of Surface Temperatures for TC31, Test 5

heat flux values and estimated surface temperatures, along with their uncertainties, were calculated using a filter strength of 3. Appendix E explains the details. The maximum flux at thermocouple location TC1 was 85.8 KW/m^2 for a surface temperature of 132°C. The time-integrated heat flux at TC1 was 117.50 MJ/m^2. The maximum flux at thermocouple location TC25 was 83.2 KW/m^2 for a surface temperature of 133°C. The time-integrated heat flux was 125.20 MJ/m^2. The maximum flux at thermocouple TC31 was 85.6 KW/m^2 for a surface temperature of 130°C. The time-integrated heat flux was 111.28 MJ/m^2.

6.4 Comparative Results

This section will provide a comparative analysis of the three different thermal environments. Several methods of comparison are considered. Temperature histories, as well as maximum temperatures, are given. Time-integrated surface heat flux is used as a percent difference comparison of environment performance.

6.4.1 Comparison of Test Article Temperature History

Figures 6.4-1 through 6.4-3 show temperature histories from thermocouple locations TC1, TC25, and TC31 for the three different environments. Table 6.4-1 shows maximum temperatures for TC1, TC25, and TC31. As expected prior to the tests, the 870°C, 100-minute radiant heat environment produced much higher test article temperatures than the 800°C, 30-minute test. However, unexpected results occurred between the 870°C radiant heat environment and the engulfing fire environment. Even though measured flame temperatures from the engulfing fire test were greater than shroud temperatures recorded during the 870°C radiant heat test, the heat input to the test article was greater for the 870°C radiant heat environment. Several possible explanations can be given to explain this phenomenon. First, it was mentioned earlier that experimental measurements of flame temperature can have large uncertainties primarily due to the radiative exchange between the hot thermocouple junction and the cold test article surface. This would indicate that the measured

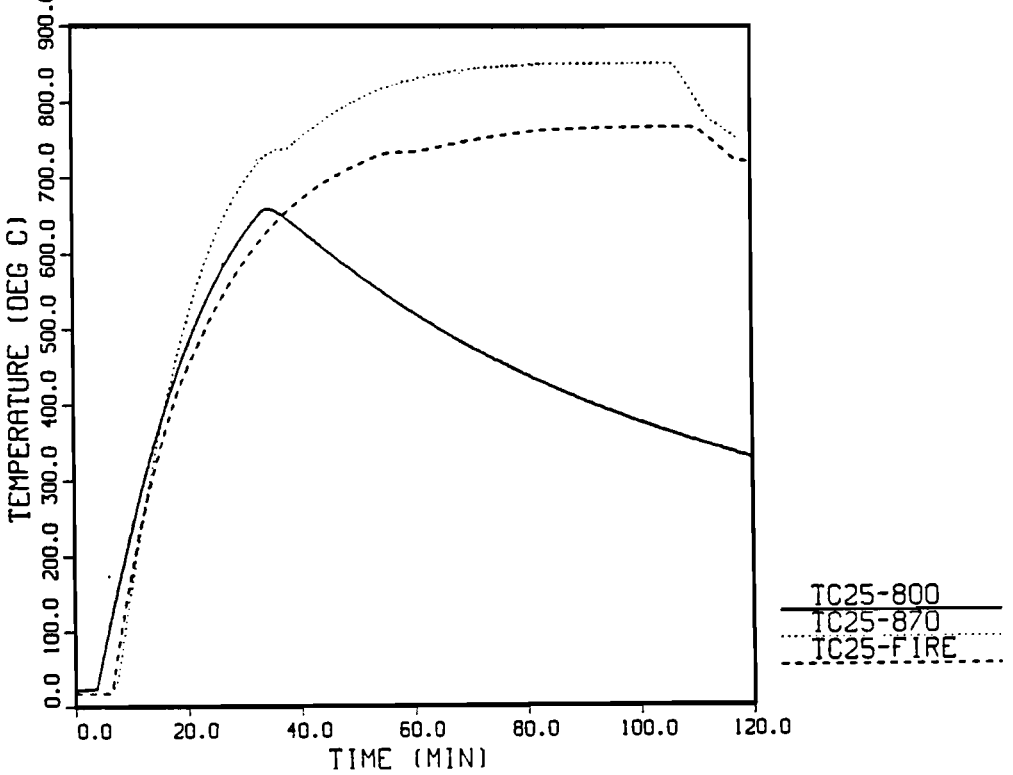

Figure 6.4-1 Comparative Temperature Histories for TC1, Three Different Thermal Environments

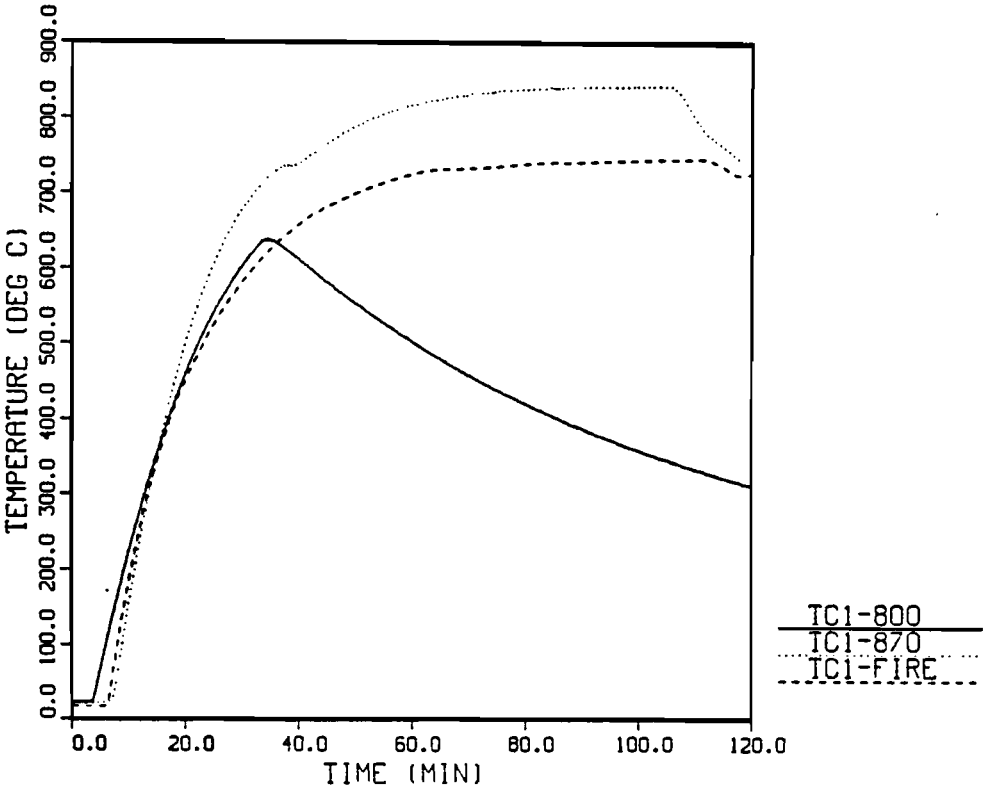

Figure 6.4-2 Comparative Temperature Histories for TC25, Three Different Thermal Environments

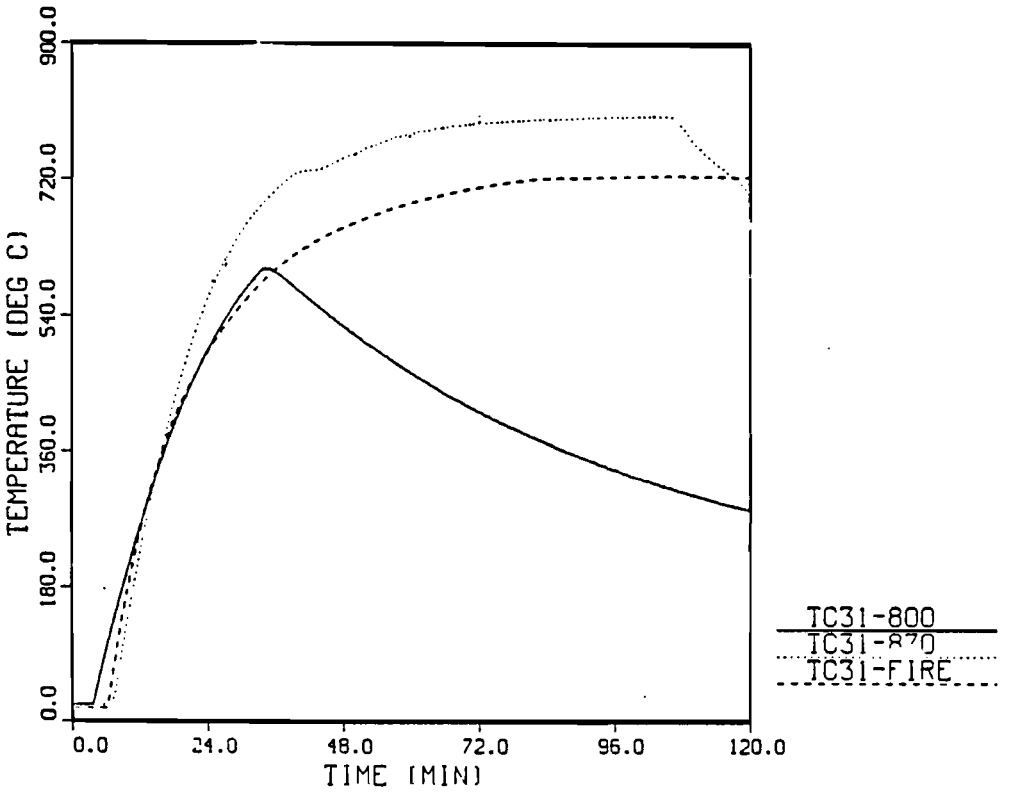

Figure 6.4-3 Comparative Temperature Histories for TC31, Three Different Thermal Environments

TABLE 6.4-1

Maximum Temperatures for Thermocouple Locations TC1, TC25, and TC31 for Three Different Thermal Environments

Thermocouple Location	Thermal Environment	Maximum Temperature (°C)
TC1	800°C, 30-Min Radiant Heat	638
	870°C, 100-Min Radiant Heat	844
	Engulfing Fire, ~100 Min	746
TC25	800°C, 30-Min Radiant Heat	659
	870°C, 100-Min Radiant Heat	855
	Engulfing Fire, ~100 Min	769
TC31	800°C, 30-Min Radiant Heat	602
	870°C, 100-Min Radiant Heat	806
	Engulfing Fire, ~100 Min	726

flame temperatures were lower than the true flame temperatures until the test article surface was sufficiently hot. Another more probable explanation considers the optical thickness [13] of the fire relative to the test article. The optical thickness defines the ability of the medium (in this case a fire) to attenuate energy. If the optical thickness is large enough, the test article that is engulfed in flames will only see and interact with the hot gases of the flames. If the optical thickness is small enough, the test article will interact not only with the enveloping flame but also with the walls of the test facility that are much colder than the hot gases surrounding the test article. The end result is a lower heat input to the test article. Absorption coefficients of sooty flames have been determined experimentally within a large scale open sooty pool fire [14]. Analysis indicates that an object engulfed in flames is influenced by a gas volume extending outward 1 to 2 meters. Experimental results indicate that the flame was not optically thick; the actual flame thickness was less than 1 meter.

The purpose of the enclosed fire facility was to provide an engulfing fire environment to be representative of an open pool engulfing fire. In an open pool engulfing fire environment, wind effects play a dominant role in reducing the heat input to a test article. If a test article were completely engulfed in flames with an optical thickness such that the test article would interact only with the surrounding flames, then the heat input would have been considerably higher. However, open pool engulfing fires represent real environments where wind affects and other uncontrolled variables reduce the heat input to a test article.

The test article in this test series represented a small scale shipping cask. Because of the size of most shipping casks relative to the flames that envelope them, optical depths will be less than optimal in which case the heat input will be reduced. With all these factors considered, the results of the engulfing fire test are realistic. The degree of accuracy of the engulfing fire test results is hard to determine because of the lack of information.

6.4.2 Comparisons of Test Article Surface Heat Flux

Figures 6.4-4 through 6.4-9 show surface heat flux as a function of time and surface temperature for thermocouple locations TC1, TC25, and TC31. The heat flux values were estimated using an inverse heat conduction code SMICC [10]. All three thermal environments are represented in these curves. The maximum surface heat flux at thermocouple locations TC1, TC25, and TC31, along with the time-integrated surface heat flux, is summarized in Table 6.4-2. Again, results indicate that the 870°C, 100-minute radiant heat test was more severe than both the 800°C, 30-minute radiant heat test and the engulfing fire test. In terms of heat absorbed, the data for TC1 indicate that the test article absorbed 21 percent (this value is based on integrated heat flux in units of MJ/m^2) more energy during the 870°C, 100-minute radiant heat test than during the engulfing fire test. This percentage increases to 60 percent when comparing the 870°C, 100-minute radiant heat test with the 800°C, 30-minute radiant heat test. The other two thermocouple stations yielded approximately the same results. It should be emphasized again that these tests do not represent regulatory environments.

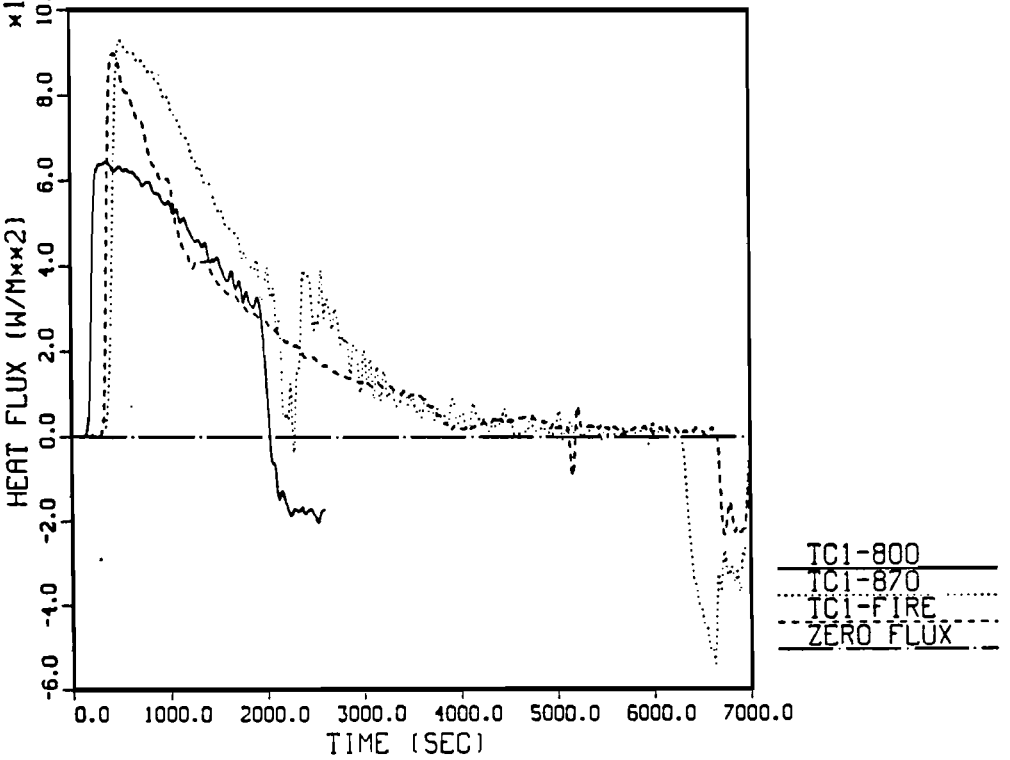

Figure 6.4-4 Surface Heat Flux Histories for TC1, Three Different Thermal Environments

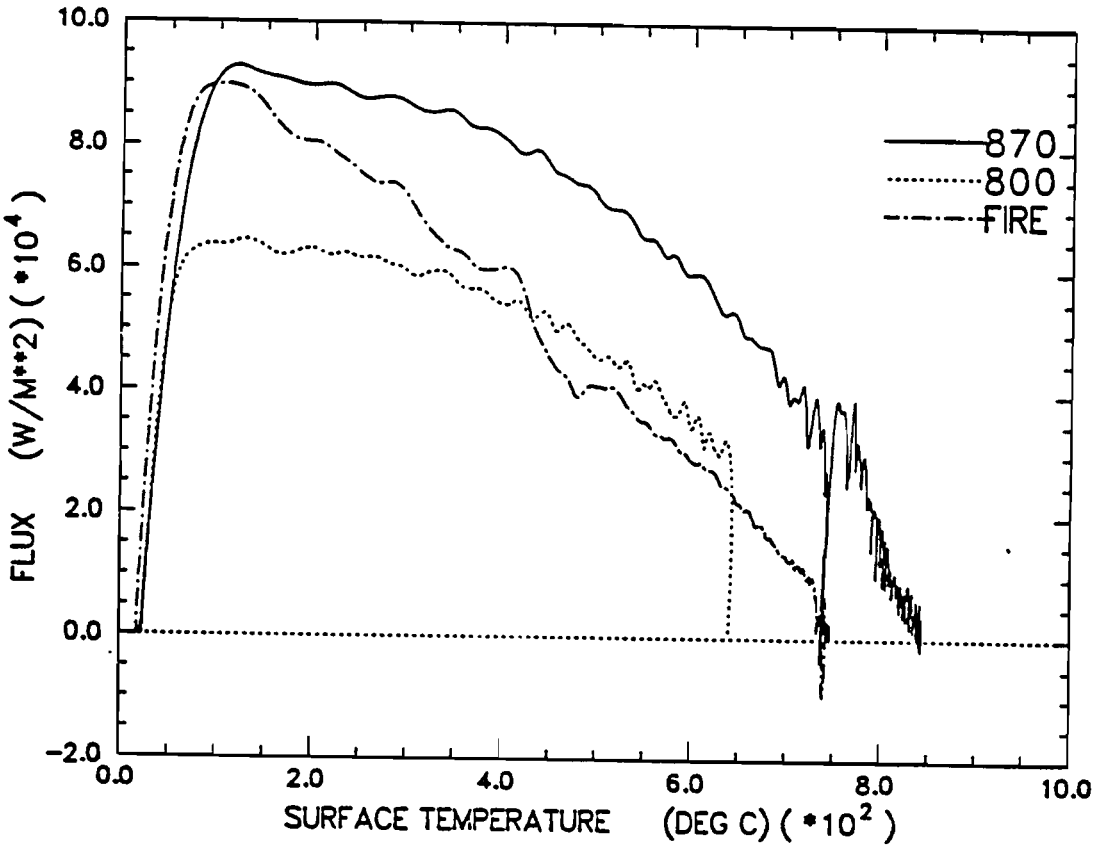

Figure 6.4-5 Surface Heat Flux as a Function of Surface Temperature for TC1, Three Different Thermal Environments

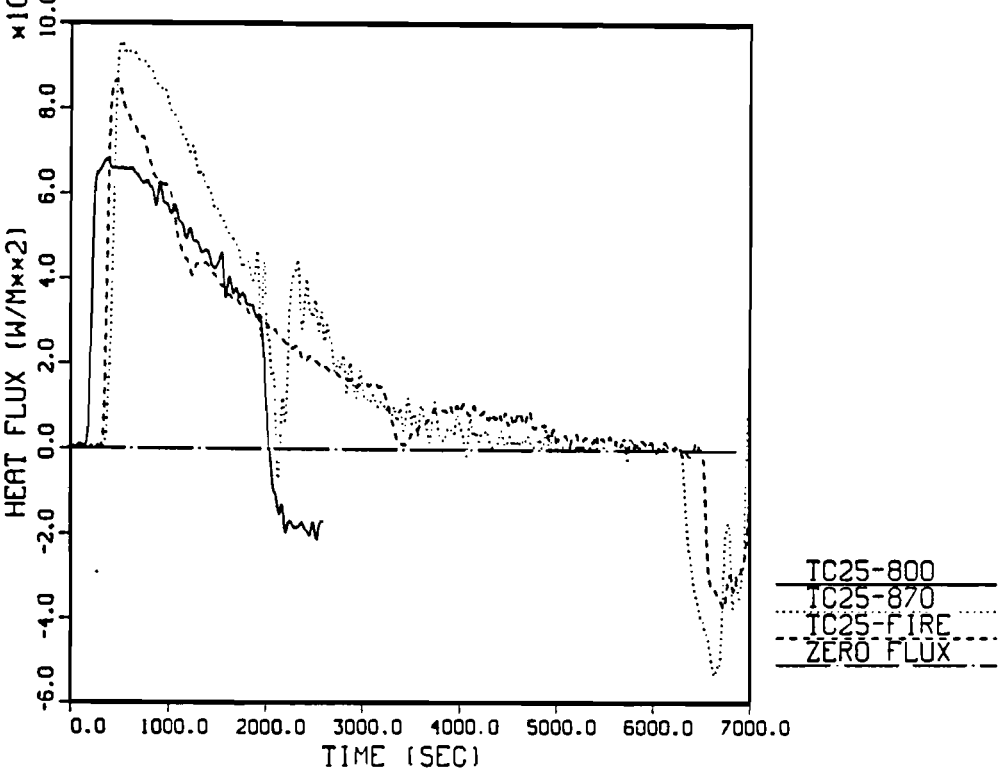

Figure 6.4-6 Surface Heat Flux Histories for TC25, Three Different Thermal Environments

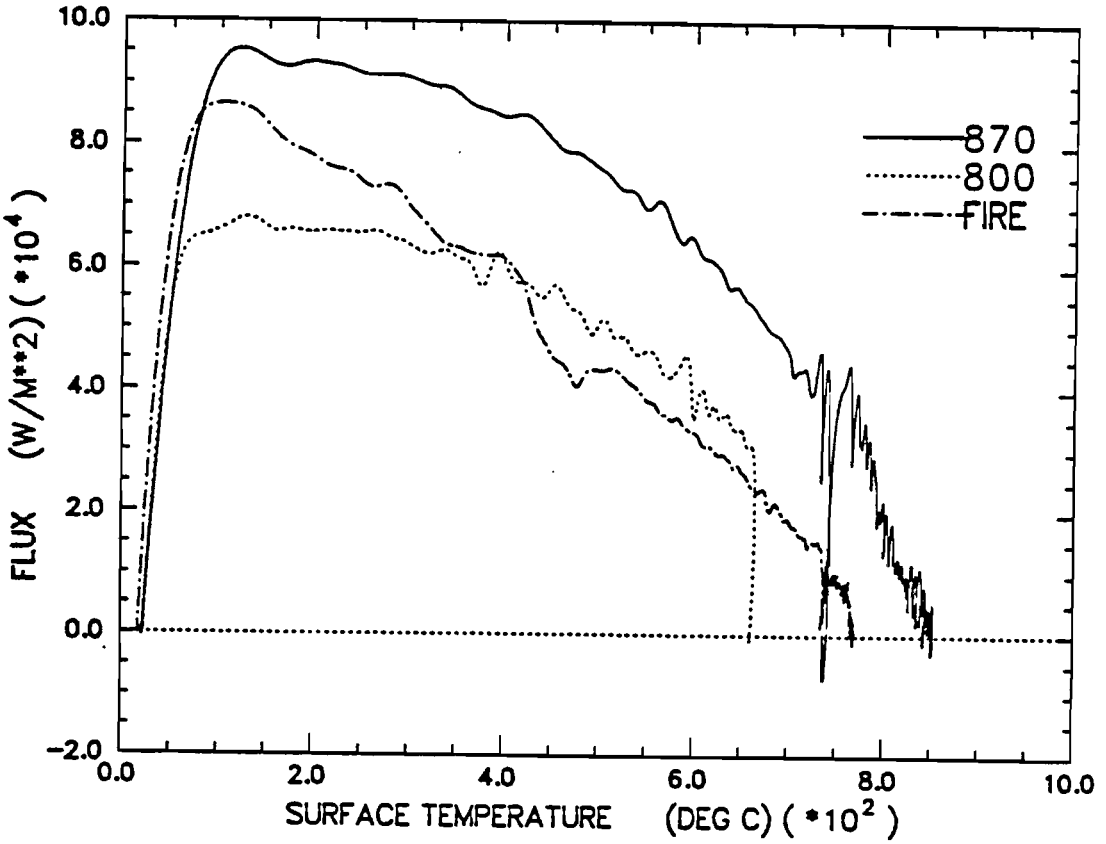

Figure 6.4-7 Surface Heat Flux as a Function of Surface Temperature for TC25, Three Different Thermal Environments

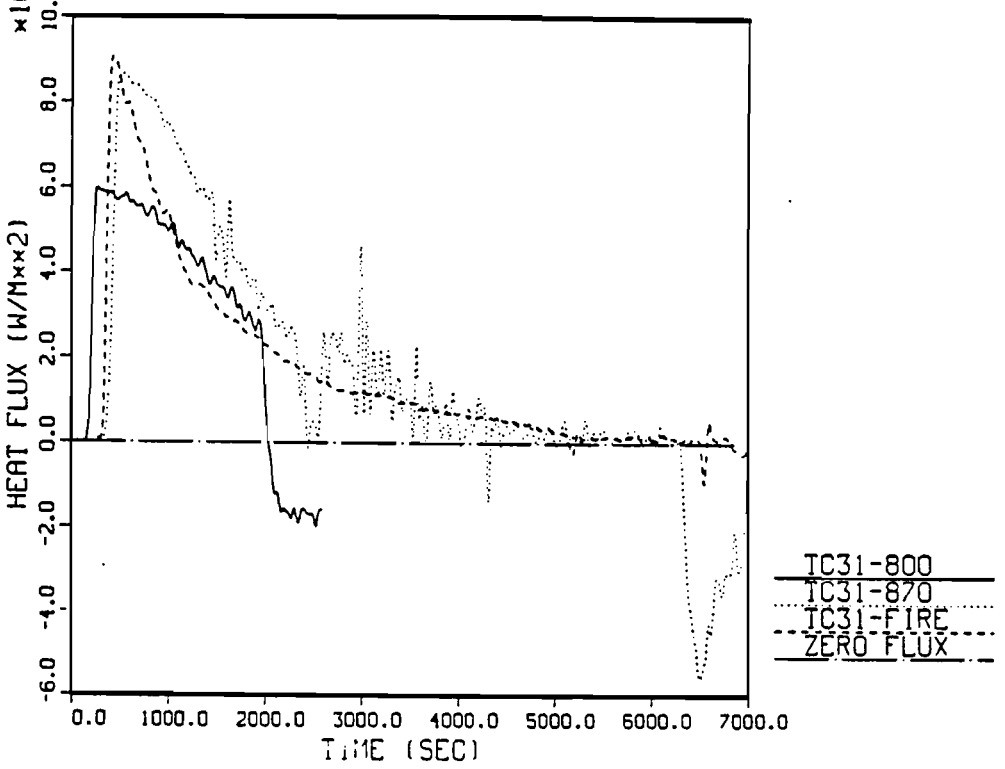

Figure 6.4-8 Surface Heat Flux Histories for TC31, Three Different Thermal Environments

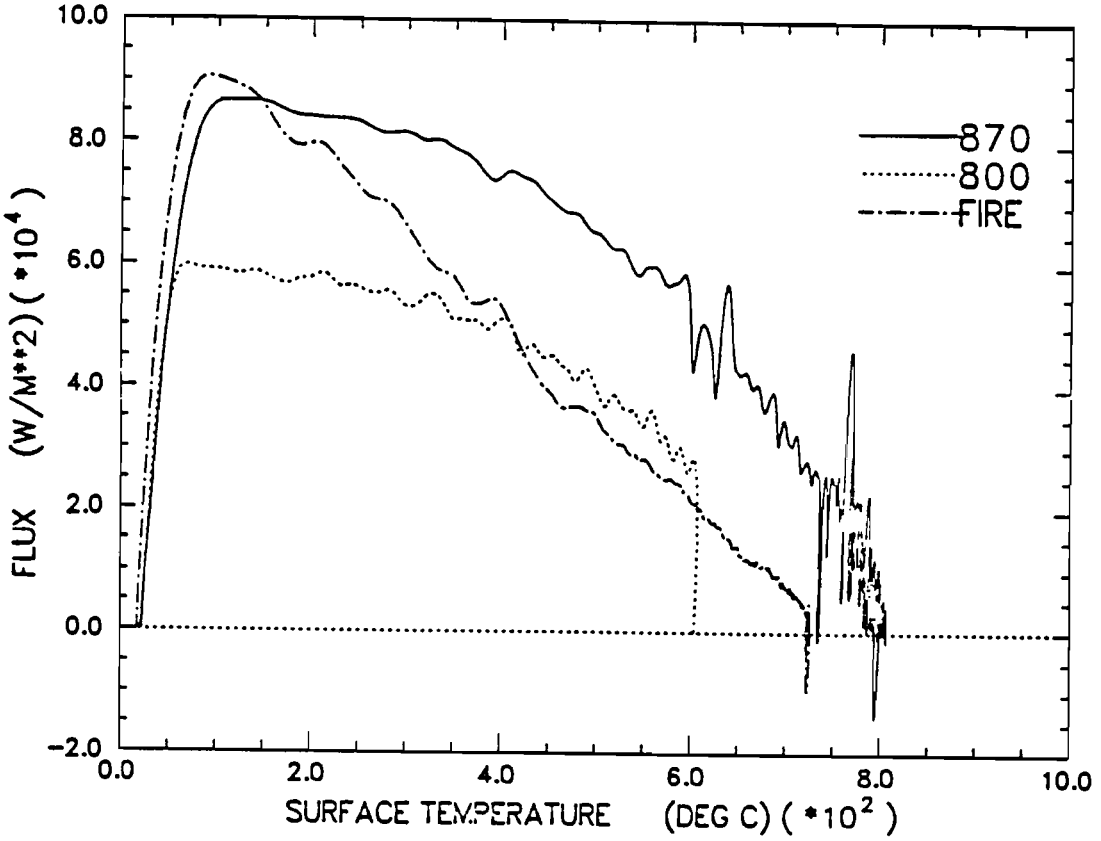

Figure 6.4-9 Surface Heat Flux as a Function of Surface Temperatures for TC31, Three Different Thermal Environments

TABLE 6.4-2

Maximum Surface Heat Flux and Time-integrated Surface Heat Flux from Thermocouple Stations TC1, TC25, and TC31 for Three Thermal Environments

Thermocouple Station	Thermal Environment	Maximum Heat Flux (kW/m^2)	Surface Temp. at Maximum Heat Flux (°C)	Integrated Heat Flux (MJ/m^2)
TC1	800°C, 30-Min[a] Radiant Heat	64.2	124	88.62
	870°C,100-Min[b] Radiant Heat	90.4	166	142.02
	Engulfing Fire[b] ~Min[b]	85.8	132	117.50
TC25	800°C, 30-Min[a] Radiant Heat	67.3	131	92.87
	870°C,100-Min[b] Radiant Heat	93.1	180	143.59
	Engulfing Fire[b] ~Min[b]	83.2	133	125.20
TC31	800°C, 30-Min[a] Radiant Heat	59.0	98	81.81
	870°C,100-Min[b] Radiant Heat	85.3	155	134.92
	Engulfing Fire[b] ~Min[b]	85.6	130	111.28

[a]Data obtained using a filter strength of 2.

[b]Data obtained using a filter strength of 3.

6.4.3 Maximum and Minimum Experimental Results

In this section maximum and minimum experimental results are presented. Figures 6.4-10 through 6.4-12 show maximum and minimum surface heat flux as a function of surface temperature for all three experimental environments. Figure 6.4-10 shows results from the 800°C, 30-minute radiant heat test. The maximum heat flux was obtained from thermocouple location TC26. The minimum surface heat flux was obtained from thermocouple location TC31.

Figure 6.4-11 shows results from the 870°C, 100-minute test. The maximum flux was obtained at thermocouple location TC28. The minimum heat flux for the 870°C, 100-minute test was achieved at thermocouple location TC31.

For the engulfing fire test, maximum heat flux was obtained from thermocouple location TC13. Minimum heat flux was obtained from thermocouple location TC32.

Table 6.4-4 summarizes the results in terms of maximum and minimum surface heat flux as well as the maximum and minimum integrated values.

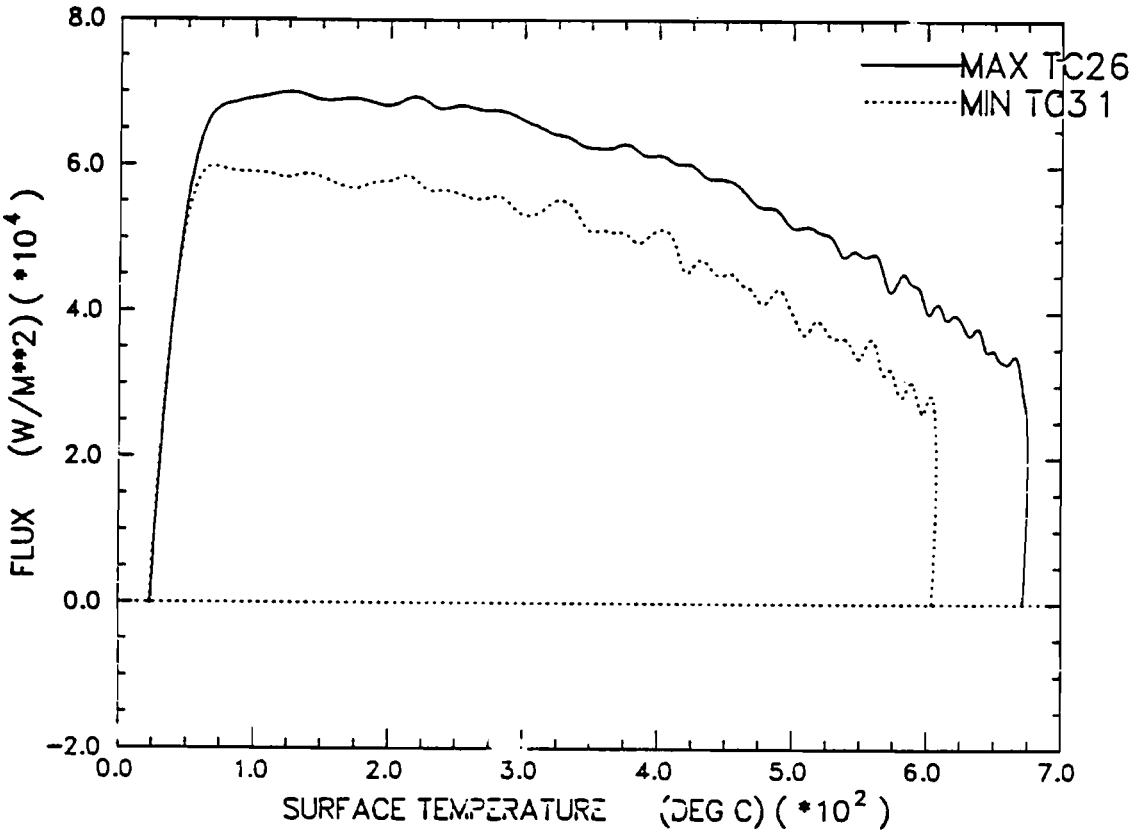

Figure 6.4-10 Maximum and Minimum Surface Heat Flux as a Function of Surface Temperature Obtained from the 800°C, 30-Minute Radiant Heat Test

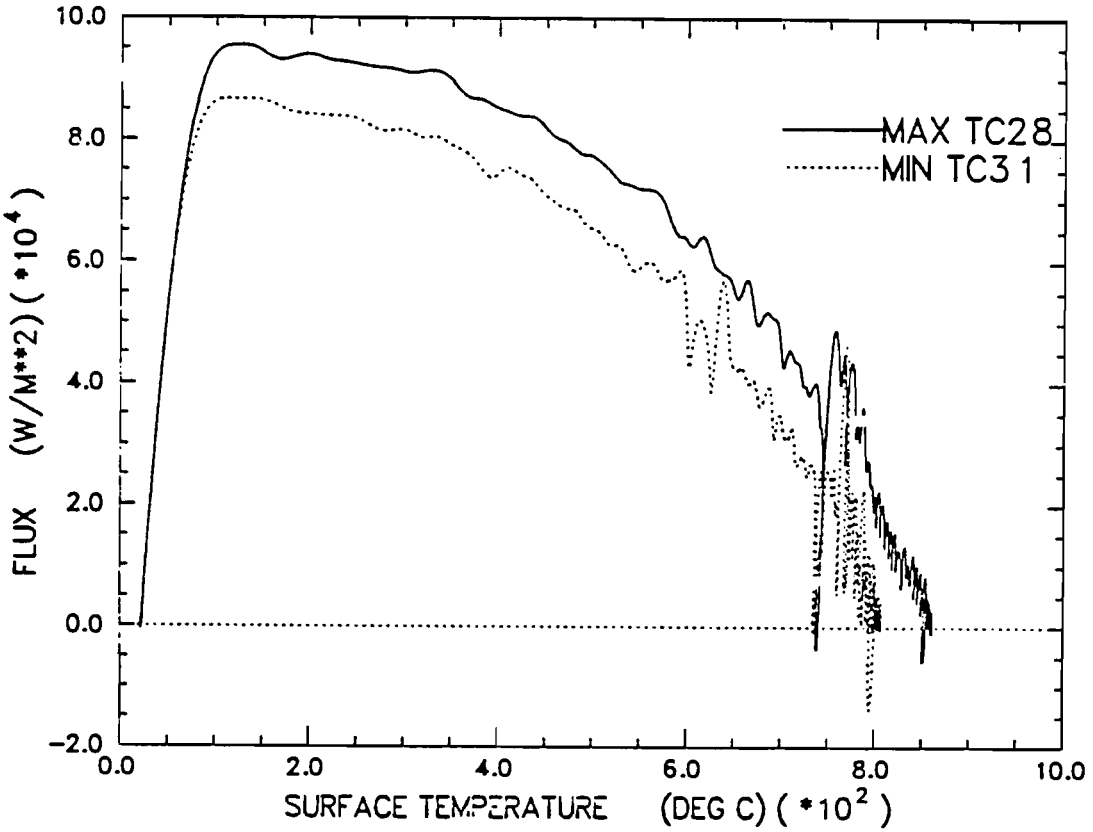

Figure 6.4-11 Maximum and Minimum Surface Heat Flux as a Function of Surface Temperature Obtained from the 870°C, 100-Minute Radiant Heat Test

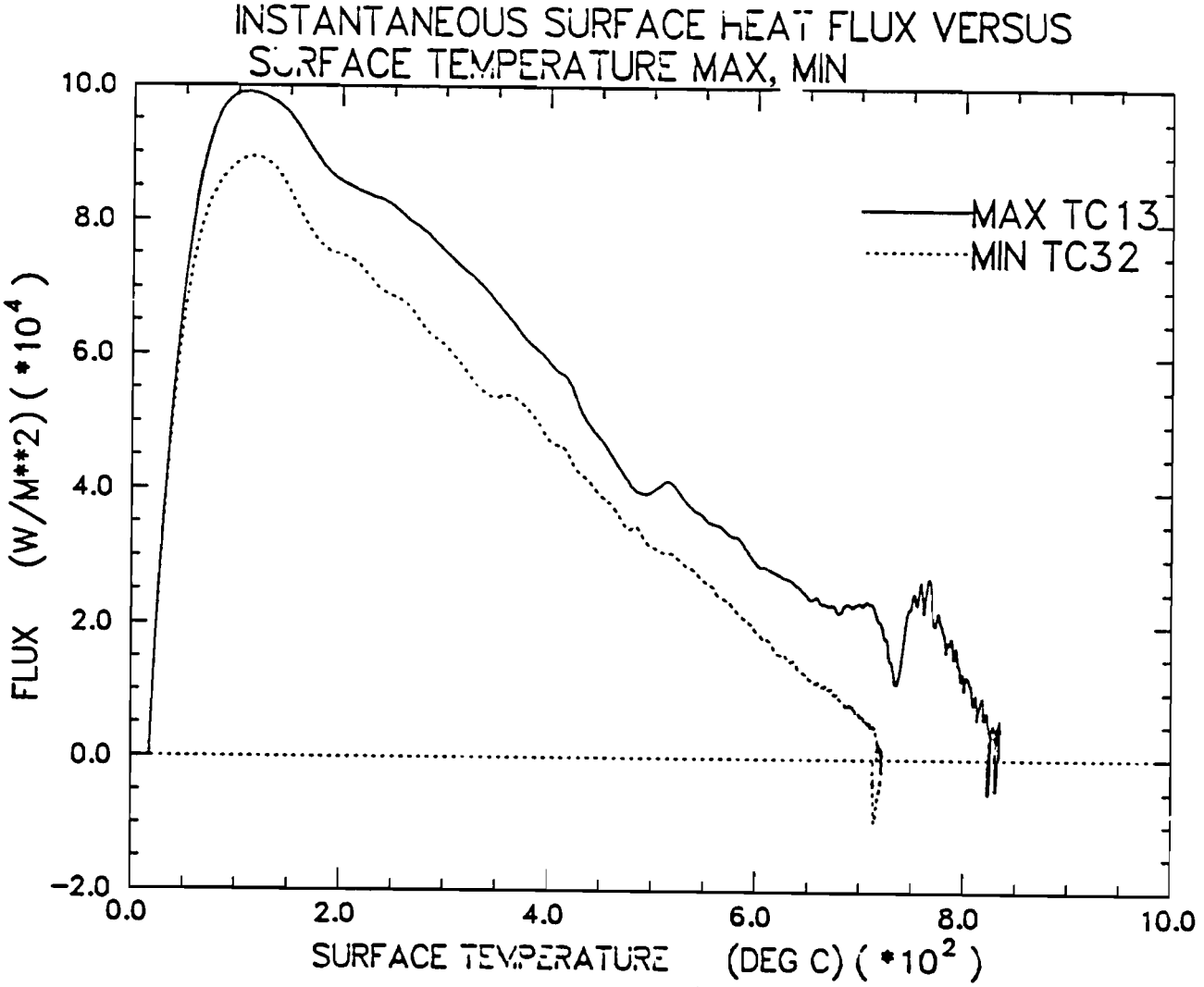

Figure 6.4-12 Maximum and Minimum Surface Heat Flux as a Function of Surface Temperature Obtained from the Engulfing Fire Test

TABLE 6.4-4

Maximum and Minimum Surface
Heat Flux and Time-integrated Surface Heat
Flux from Five Different Thermal Environments

Environment	Maximum Heat Flux (KW/m^2)	Minimum Heat Flux (KW/m^2)	Maximum Integrated Heat Flux (MJ/m^2)	Minimum Integrated Heat Flux (MJ/m^2)
800°C, 30-min[a] Radiant Heat	69.5	59.0	94.83	81.81
870°C, 100-min[b] Radiant Heat	93.0	84.4	144.82	134.92
Engulfing Fire[b] ~ 100 min	89.8	80.7	140.55	110.12

[a]Data obtained using a filter strength of 2.
[b]Data obtained using a filter strength of 3.

7.0 SUMMARY

In this experimental series the response of a cask-like test article to three different thermal environments was investigated. The cask-like features of the test article include a cylindrical cross section as well as a thick wall design.

To compare test performance, the maximum and minimum heat input to the test article was determined. Results indicated that the test article absorbed more energy in the 870°C, 100-minute radiant heat environment than in any other environment investigated. The total heat input to the test article was 58 percent greater during the 870°C, 100-minute radiant heat test than during the 800°C, 30-minute radiant heat test. The total heat input to the test article was 12 percent greater during the 870°C, 100-minute radiant heat test than during the engulfing fire test. These percentages are based on average heat input to the test article in units of MJ/m^2.

It was determined during this test series that test performance analysis is highly dependent upon test article configuration as well as test article thermal mass. Results indicate that the test article had sufficient thermal mass to alter both the radiant heat environment as well as the engulfing fire environment. Therefore, the results of this test series are specific to this test article and are not applicable to real shipping cask geometries. This test series does not conform to regulatory environments.

During the course of this analysis, the question was asked what parameter was more important to the severity of the tests: environment temperature or test duration? This question was initiated because two different test durations and two different environment temperatures were investigated. Before this question is answered, one must recall the test article design objectives. One of the test article design constraints was that the test article should have enough thermal mass such that steady-state conditions are approached at the end of a step change from near ambient conditions to 870°C for a 100-minute period. This would mean that the test article would continue to absorb energy until the end of the 100-minute period at which time the

surface heat flux approaches zero. This design constraint allows one to evaluate both the effects of test duration as well as environment temperature the heat-absorbing capability of the test article.

For the test article configuration used in this test series, it was determined that environment temperature was more important to test severity than test duration. These results are not surprising because the test article has absorbed approximately 77 percent of the total energy absorbed in the first 30 minutes of a 100-minute test. Again, these results are specific to this test article configuration.

To determine if these results were applicable to other test article configurations, a numerical model of the test article was generated using Q/TRAN [3]. Two different boundary conditions were applied:

1) Environment temperature - 800°C
   Environment emittance - 0.9
   Surface absorptance - 0.8
   Test duration - 100 minutes
2) Environment temperature - 870°C
   Environment emittance - 0.9
   Surface absorptance - 0.8
   Test duration - 100 minutes

Results of this analysis were based on integrated heat flux for the first 30 minutes of the test and total integrated heat flux. For the 30-minute integrated heat flux, Boundary Condition 2 (BC2) produced a 22 percent greater heat input than Boundary Condition 1 (BC1). For the total integrated heat flux, the heat input from BC2 was only 12 percent greater than the heat input from BC1. These results support earlier conclusions that environment temperature is more important to test severity than test duration. Now, if the thermal mass of the test article is increased by a factor of 3, the results are different. For the 30-minute integrated heat flux, the heat input

from BC2 was 21 percent greater than the heat input from BC1. For the total integrated heat flux, the heat input from BC2 was 27 percent greater than the heat input from BC1. These results indicate that test duration is more important to test severity than environment temperature.

The final results of this analysis indicate that test severity depends not only on test duration and environment temperature but more importantly on the thermal mass of the object that is being tested.

REFERENCES

[1] Gregory, J. J., R. Mata, and N. R. Keltner. "Thermal Measurements in a Series of Large Pool Fires," SAND85-0196, Sandia National Laboratories, Albuquerque, NM, August 1987.

[2] "Packaging of Radioactive Material for Transport and Transportation of Radioactive Material Under Certain Conditions," U. S. Nuclear Regulatory Commission, Title 10, Code of Federal Regulations, Part 71, revised as of August 1983.

[3] Rockenbach, F. A. "Q/TRAN, Version 1.2 User's Manual," PDA Engineering, Inc., Santa Ana, CA, May 1986.

[4] Sanchez, L. C. "Performance Testing of Thermal Analysis Codes for Nuclear Fuel Casks," SAND84-1854, TTC-0509, Sandia National Laboratories, Albuquerque, NM, January 1987.

[5] Sanchez, L. C. "Solutions Obtained to International Heat Transfer Benchmarking Problems for Nuclear Fuel Casks Using Q/TRAN," SAND85-2621, TTC-0631, Sandia National Laboratories, Albuquerque, NM, February 1987.

[6] Manteufel, R. D., D. E. Klein, and H. R. Yoshimura. "Benchmarking the Q/TRAN Thermal Analysis Computer Code," IAEA-SM-286/95P, Proceedings of PATRAM '86, Davos, Switzerland, June 16-20, 1986 p. 465-474.

[7] Glass, R. E. "Thermal Benchmarking: A Status Report," IAEA-SM-286/100P, Proceedings of PATRAM '86, Davos, Switzerland, June 16-20, 1986 p. 497-499.

[8] Hensel, E. C. "Multidimensional Inverse Heat Conduction," Ph.D. Dissertation, Mechanical Engineering Department, New Mexico State University, Las Cruces, NM, August 1986.

[9] Nakos, J. T. "Response of a 4-Inch Diameter Thick Wall Cylindrical Calorimeter Using Intrinsic and Ungrounded Junction Thermocouples," Internal Memorandum, Sandia National Laboratories, Albuquerque, NM, February 1988.

[10] Hills, R. G., and E. C. Hensel. "Space Marching Inverse Conduction Code," SAND84-1563, Sandia National Laboratories, Albuquerque, NM, July 1986.

[11] Blackwell, B. F. "Radiant Heat Test of a Simulated Cross Section of a DOT Fuel Cask," Internal Memorandum RS7537/82/2m, Sandia National Laboratories, Albuquerque, NM, August 1, 1982.

[12] Nelsen, J. M. "Determination of Net Heat Fluxes and Assessment of Test-to-Test Thermal Input Variation for Three Large Engulfing Open Pool Fire/Calorimeters Tests," SAND85-1821, Sandia National Laboratories, Albuquerque, NM, November 1986.

[13] Siegel, R. and J. R. Howell. Thermal Radiation Heat Transfer, New York: McGraw Hill Book Company, 1972.

[14] Longenbaugh, R. S., and L. K. Matthews. "Experimental and Theoretical Analysis of the Radiative Transfer Within a Sooty Pool Fire," SAND86-0083, Sandia National Laboratories, Albuquerque, NM, March 1988.

APPENDIX A

Thermal Properties of Test Article Materials

The heat transfer analysis of the calorimeter test article required thermal properties for 1010/1020 mild steel and Cera-blanket . The recommended properties are given in Tables A.1 and A.2 and Figures A.1 through A.3. Since thermal properties for the 1010/1020 mild steel were not available, the properties of A517 mild steel were used. The thermal properties of A517 were obtained experimentally.

Thermal Conductivity Measurements of A517 Mild Steel

The thermal conductivity of A517 mild steel was measured as a function of temperature in the Dynatech thermal comparator [A-1,A-2] Table A.1 and Figure A.1 give the thermal conductivity as a function of temperature.

Specific Heat Measurement of A517 Mild Steel

The specific heat of A517 mild steel was measured as a function of temperature using differential scanning calorimetry (DSC) [A-3]. The measured specific heat values are shown in Table A.1 and Figure A.3. Since inverse heat transfer calculations are fairly sensitive to specific heat at temperatures near the curie point, detailed resolution was used in obtaining specific heat values.

TABLE A.1
Thermophysical Properties of A517 Mild Steel(a)
Density = 8,020. (kg/m^3)

T (°C)	Thermal Conductivity (W/m-°C)	Specific Heat (J/kg-°C)
21.9 (295.1 K)	(b)	431.
51.9 (325.1 K)	(b)	469.
101.9 (375.1 K)	(b)	486.
139.0 (412.2 K)	45.8	(b)
149.0 (422.2 K)	45.7	(b)
151.9 (425.1 K)	(b)	502.
199.0 (472.2 K)	45.3	(b)
201.9 (475.1 K)	(b)	528.
249.0 (522.2 K)	44.7	(b)
251.9 (525.1 K)	(b)	548.
299.0 (572.2 K)	44.0	(b)
301.9 (575.1 K)	(b)	565.
349.0 (622.2 K)	43.2	(b)
351.9 (625.1 K)	(b)	582.
399.0 (672.2 K)	42.2	(b)
401.9 (675.1 K)	(b)	611.
449.0 (722.2 K)	41.1	(b)
451.9 (725.1 K)	(b)	641.
499.0 (772.2 K)	39.9	(b)
501.9 (775.1 K)	(b)	662.
549.0 (822.2 K)	38.6	(b)
551.9 (825.1 K)	(b)	703.
599.0 (872.2 K)	37.2	(b)
601.9 (875.1 K)	(b)	758.
649.0 (922.2 K)	35.6	(b)
650.9 (924.1 K)	(b)	833.
684.9 (958.1 K)	(b)	904.
699.0 (972.2 K)	34.0	(b)
730.0 (1003.2 K)	(b)	1097.
740.0 (1013.2 K)	(b)	1294.
749.0 (1022.2 K)	32.3	(b)
750.0 (1023.2 K)	(b)	1457.
760.0 (1033.2 K)	(b)	1499. Curie Point
770.0 (1043.2 K)	(b)	1415.
780.0 (1053.2 K)	(b)	1231.
790.0 (1063.2 K)	(b)	1063.
799.0 (1072.2 K)	30.5	(b)
800.0 (1073.2 K)	(b)	934.
825.0 (1098.2 K)	(b)	749.
850.0 (1123.2 K)	(b)	662.
850.9 (1124.1 K)	28.5	(b)
900.0 (1173.2 K)	(b)	603.
900.9 (1174.1 K)	27.7	(b)

(a) Data taken from Reference A-4
(b) Data not available in Ref. A-4

TABLE A.2

Thermophysical Properties of Cera-Blanket[R]
Density x Specific Heat = 144,757 (J/m^3-°C)

T (°C)		Thermal Conductivity (W/m-°C)
-17.8	(255.4 K)	0.026
93.3	(366.5 K)	0.032
204.4	(570.9 K)	0.045
315.6	(588.8 K)	0.064
426.7	(699.9 K)	0.087
546.8	(820.0 K)	0.113
648.9	(922.1 K)	0.144
760.0	(1033.2 K)	0.176
871.1	(1144.3 K)	0.210
982.2	(1255.4 K)	0.249

[R] Registered trademark of CERABLANKET, Manville Refractory Products Department, Denver, Colorado.

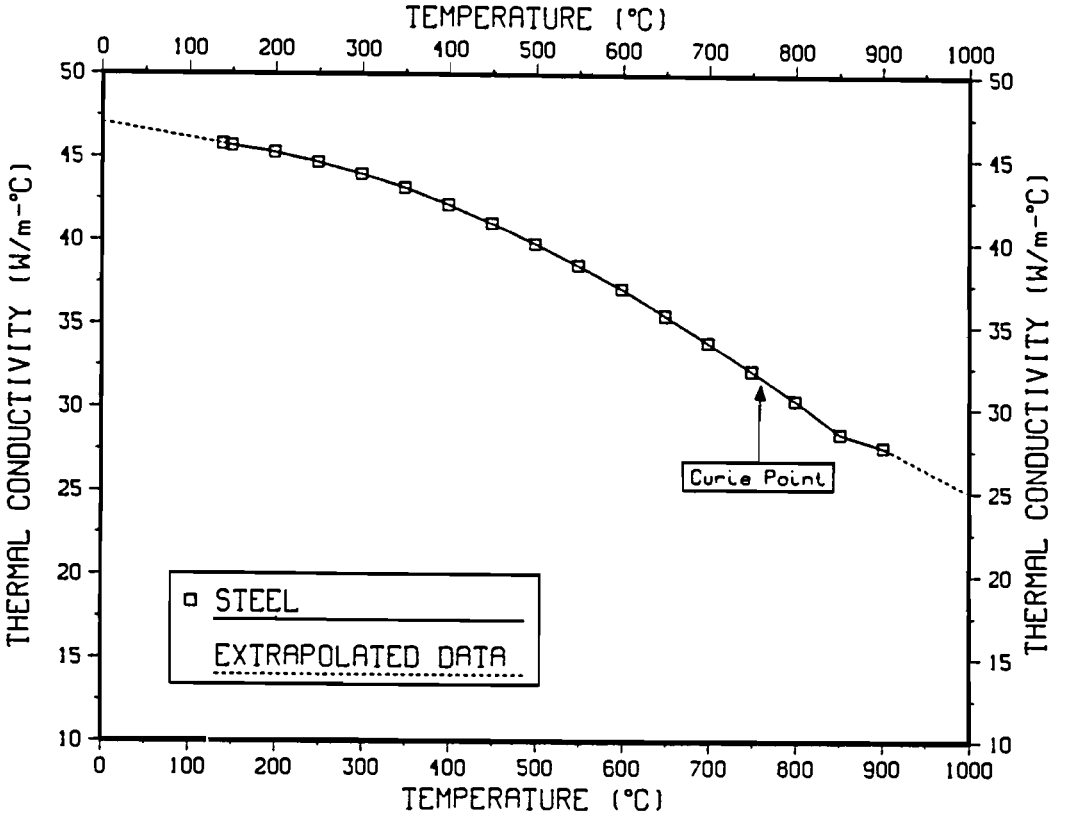

Figure A.1 Thermal Conductivity of A517 Mild Steel [A-4].

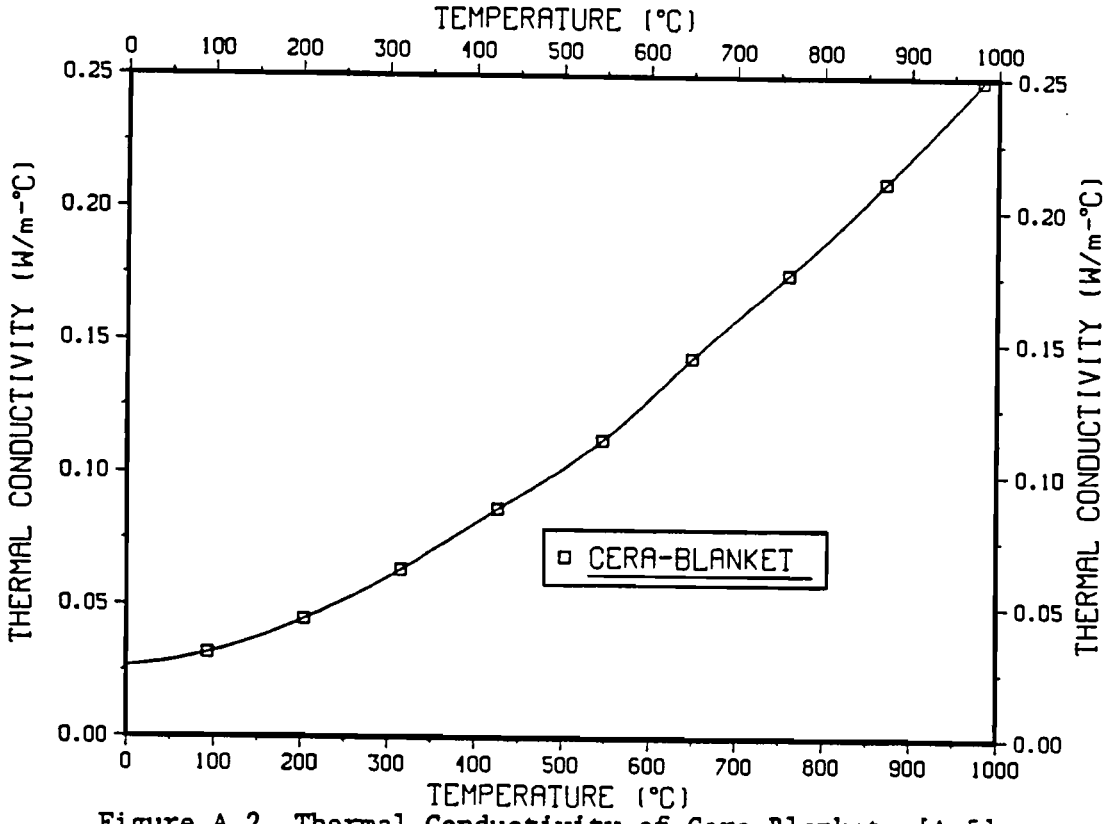

Figure A.2 Thermal Conductivity of Cera-Blanket [A-5].

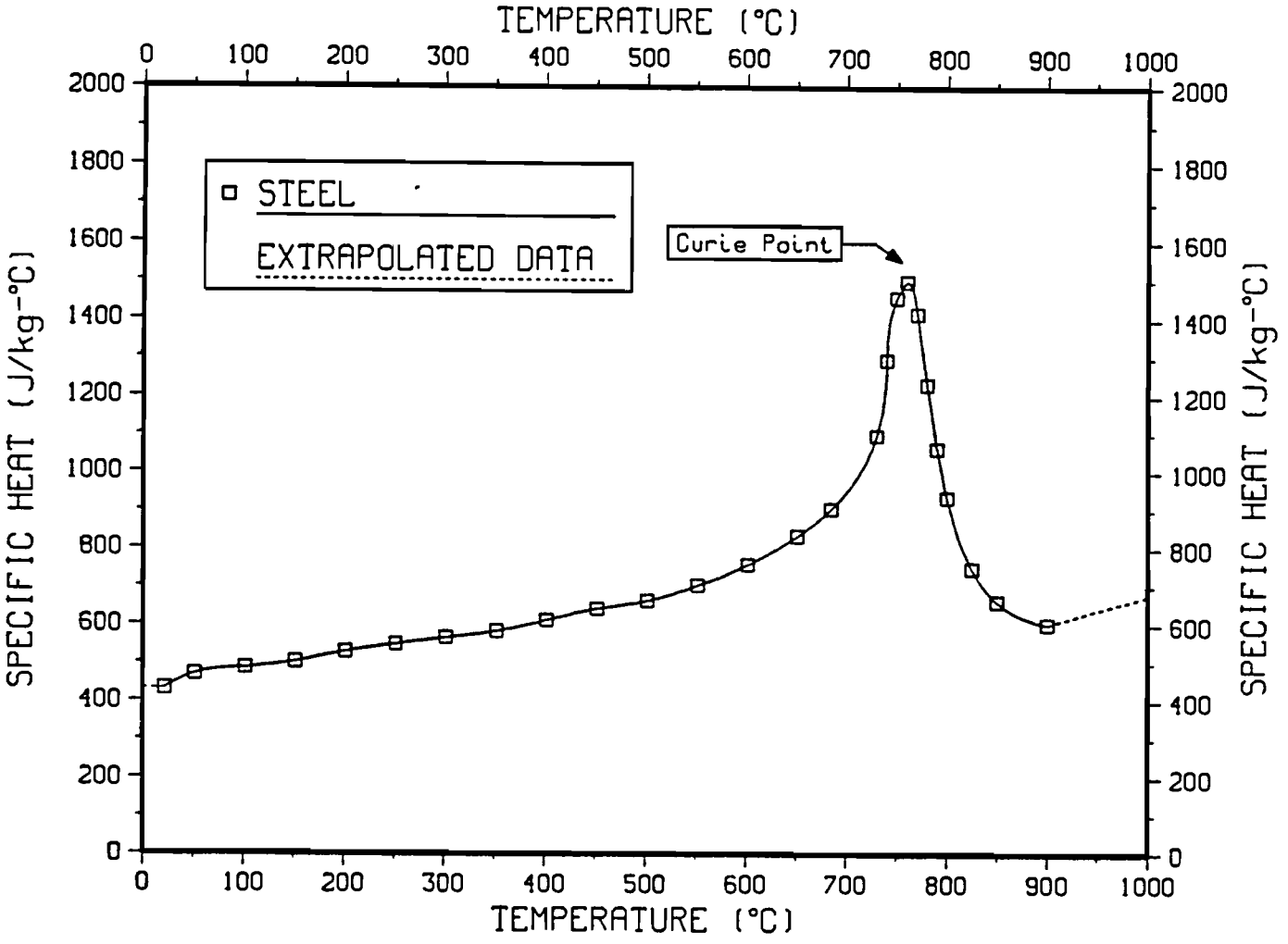

Figure A.3 Specific Heat of A517 Mild Steel [A-4].

REFERENCES

[A-1] Moss, M., J. A. Koski, and G. M. Haseman. "Measurements of Thermal Conductivity by the Comparative Method," SAND82-0109, Sandia National Laboratories, Albuquerque, NM, March 1982.

[A-2] Sweet, J. N., et al. "Comparative Thermal Conductivity Measurements at Sandia National Laboratories," SAND86-0840, Sandia National Laboratories, Albuquerque, NM, June 1986.

[A-3] Callanan, J. E., and S. A. Sullivan. "Development of Standard Operating Procedures for Differential Scanning Calorimeters," Rev. Sci. Instrum., Vol. 57, No. 10, October 1986, pp. 2584-2592.

[A-4] Roth, E. P., et al. "Thermal Properties Measurements of ASTM A517 Steel," Internal Memorandum, Sandia National Laboratories, Albuquerque, NM, January 20, 1983.

APPENDIX B

Thermal Radiative Properties of Pyromark Series 2500 Black Paint

In order to more accurately model the thermal characteristics of various metal components coated with Pyromark Series 2500 high temperature black paint, detailed optical properties of the painted surface were necessary. The various testing conditions, which are described in the main body of this appendix, were implemented as part of the Sandia National Laboratory contract with the Department of Transportation - Federal Railroad Administration (DOT-FRA) to study the thermal environment during simulated fire conditions. Historically, Pyromark high temperature paints (manufactured by Tempil, a division of Big Three Industries) have been utilized by thermal testing groups, as well as the space, nuclear, and solar industries because of both high temperature stability and desirable optical characteristics. Pyromark black paint, as an example, exhibits both a high solar absorptance (~0.97) and a high emissivity (~0.88) when properly applied to Inconel substrates and operated at temperatures < 550° C. The specific Pyromark paint that will be addressed in this appendix is Series 2500 black paint (manufacturer recommended maximum operating temperature of 1300° C (2500° F) and will be referred to as Pyromark paint throughout the text that follows.

For the particular application addressed by this article, the paint was applied to a variety of metal components to retain a uniform, highly emissive surface (> 0.80) during the extreme temperatures (> 700° C) encountered during either fire testing or under simulated conditions. Historically, testing personnel have assumed that the Pyromark coating exhibited high emittance characteristics (> 0.80) even though significant visual color changes have occurred. In the section that follows, both field and laboratory optical measurement and data analysis techniques

that were used to characterize the paint will be described. During field measurements, significant paint color changes (from black to blue) were observed for Pyromark applied to a mild steel substrate and subjected to temperatures > 600° C. The observed color change was accompanied by a decrease in both the solar averaged absorptance (from 0.97 to 0.84) and emissivity at 600° C (from 0.88 to 0.85). In addition to the color change, subsequent laboratory measurements on similar Pyromark samples, removed from a fire site at SNLA, indicated that the paint spectral reflectance properties had been dramatically altered, as expected. As a result of this and other similar solar related observations, the author will address the following Pyromark issues: 1) the significance of the visual appearance upon the emittance characteristics, 2) the expected optical properties as a function of the two substrate types (Inconel and mild steel) investigated, and 3) suggest possible mechanisms for the coating color change observed on the mild steel substrates.

INSTRUMENTATION AND DATA AVERAGING

Field Measurements

Since the Pyromark painted components were too large to easily measure with laboratory equipment, two types of portable instruments were used to characterize the optical properties in the field. One portable instrument was used to obtain the solar average hemispherical reflectance values, R_s (D&S), while the other instrument determined the normal emittance values, $E_{N\text{-}GD}$ (100 °C or 300 °C), for black body temperatures of 100 °C and 300 °C. Both field and laboratory determined values are listed in Tables B-1 and B-2. The field measured values provided the necessary data points to compare to our Pyromark data base values determined using spectral reflectance properties obtained from laboratory instrumentation. The spectral properties were needed to determine the temperature dependent normal emittance characteristics, see explanation in the Data Analysis section below.

TABLE 1.

PYROMARK SERIES 2500 BLACK PAINT APPLIED TO
INCONEL AND MILD STEEL SUBSTRATES

FIELD (PORTABLE) INSTRUMENT DETERMINED VALUES

FILE :: DOTAPX1

SAMPLE FILE ID	COMMENT	BLACKBODY SOURCE TEMP (DEG K)	BLACKBODY SOURCE TEMP (DEG C)	BLACKBODY SOURCE TEMP (DEG F)	BLACKBODY PEAK WAVELENGTH (MICRONS)	DB-100 PORTABLE INFRARED REFLECTOMETER VALUES R (T) N-GD	DB-100 PORTABLE INFRARED REFLECTOMETER VALUES A (T) N-GD	D&S SSR SOLAR ENERGY AVERAGED VALUES (AM 2.0) R (2π) S	D&S SSR SOLAR ENERGY AVERAGED VALUES (AM 2.0) A (2π) S
PYROMARK (SERIES 2500) INCONEL SUBSTRATE	"BLACK"	373	100	212	7.8	0.19	0.81	0.03	0.97
						std dev +/- 0.04		std dev +/- 0.002	
TEST ARTICLE SHROUD		573	300	572	5.1	0.24	0.76		
						std dev +/- 0.03			
NUMEROUS TEMP CYCLES TO > 850C	"BLACK/BLUE"	373	100	212	7.8	0.21	0.79	0.09	0.91
						std dev +/- 0.01		std dev +/- 0.012	
		573	300	572	5.1	0.25	0.75		
						std dev +/- 0.01			
PYROMARK (SERIES 2500) MILD STEEL SUBSTRATE	"BLUE/BLACK"	373	100	212	7.8	0.19	0.82	0.12	0.88
						std dev +/- 0.04		std dev +/- 0.01	
TEST ARTICLE		573	300	572	5.1	0.20	0.81		
						std dev +/- 0.03			
TEMP CYCLE TO > 850C	"BLUE"	373	100	212	7.8	0.23	0.77	0.15	0.85
						std dev +/- 0.02		std dev +/- 0.01	
		573	300	572	5.1	0.21	0.79		
						std dev +/- 0.02			

TABLE 1. (CONT)

SAMPLE FILE ID	COMMENT	BLACKBODY SOURCE TEMP (DEG K)	(DEG C)	(DEG F)	BLACKBODY PEAK WAVELENGTH (MICRONS)	DB-100 PORTABLE INFRARED REFLECTOMETER VALUES R (T) N-GD	A (T) N-GD	D&S SSR SOLAR ENERGY AVERAGED VALUES (AM 2.0) R (2π) S	A (2π) S
PYROMARK (SERIES 2500) MILD STEEL SUBSTRATE	"BLUE"	373	100	212	7.8	0.12	0.88	0.09	0.91
						std dev +/- 0.04			std dev +/- 0.05
TEST ARTICLE	AFTER REPAINT TEMP CURE TO 850C	573	300	572	5.1	0.13	0.87		
						std dev +/- 0.04			
TEMP CYCLE TO > 850C	"BLUE"	373	100	212	7.8	0.18	0.82	0.11	0.89
						std dev +/- 0.04			std dev +/- 0.05
	AFTER REPAINT TEMP CURE TO 850C + ADDITIONAL TEMP CYCLE TO 850C	573	300	572	5.1	0.19	0.81		
						std dev +/- 0.04			

****

TABLE 2.

PYROMARK SERIES 2500 BLACK PAINT APPLIED TO
INCONEL AND MILD STEEL SUBSTRATES

LABORATORY INSTRUMENT DETERMINED VALUES

FILE :: DOTAPX2

SAMPLE FILE ID	COMMENT	BLACKBODY SOURCE TEMP (DEG K)	(DEG C)	(DEG F)	BLACKBODY PEAK WAVELENGTH (MICRONS)	BLACKBODY INTEGRATED VALUES R (T) BB	A (T) BB	SOLAR ENERGY AVERAGED VALUES (AM 2.0) R (2π) S	A (2π) S
"BLACK"	PYROMARK (SERIES 2500) INCONEL SUBSTRATE 540C CURE	300	27	81	9.7	0.098	0.902	0.027	0.974
		350	77	171	8.3	0.108	0.892		
		400	127	261	7.2	0.117	0.883		
		450	177	351	6.4	0.124	0.876		
		500	227	441	5.8	0.129	0.871		
		550	277	531	5.3	0.132	0.868		
		600	327	621	4.8	0.132	0.868		
		650	377	711	4.5	0.132	0.868		
		700	427	801	4.1	0.130	0.870		
		750	477	891	3.9	0.128	0.872		
		800	527	981	3.6	0.125	0.875		
		850	577	1071	3.4	0.122	0.878		
		900	627	1161	3.2	0.118	0.882		
		950	677	1251	3.1	0.115	0.885		
		1000	727	1341	2.9	0.111	0.889		
		1050	777	1431	2.8	0.107	0.893		
		1100	827	1521	2.6	0.104	0.896		
		1150	877	1611	2.5	0.100	0.900		
		1200	927	1701	2.4	0.097	0.903		
		1250	977	1791	2.3	0.094	0.906		
		1300	1027	1881	2.2	0.091	0.909		
"BLUE" PAINT FLAKE	PYROMARK (SERIES 2500) MILD STEEL SUBSTRATE FIRE SITE FLAKE ~1000C	300	27	81	9.7	0.181	0.819	0.159	0.841
		350	77	171	8.3	0.168	0.833		
		400	127	261	7.2	0.159	0.841		
		450	177	351	6.4	0.154	0.846		
		500	227	441	5.8	0.151	0.849		
		550	277	531	5.3	0.149	0.851		
		600	327	621	4.8	0.147	0.853		
		650	377	711	4.5	0.147	0.853		

TABLE 2. (CONT)

BLACKBODY SOURCE TEMP (DEG K)	(DEG C)	(DEG F)	BLACKBODY PEAK WAVELENGTH (MICRONS)	BLACKBODY INTEGRATED VALUES R (T) BB	A (T) BB
700	427	801	4.1	0.146	0.854
750	477	891	3.9	0.146	0.854
800	527	981	3.6	0.147	0.853
850	577	1071	3.4	0.147	0.853
900	627	1161	3.2	0.147	0.853
950	677	1251	3.1	0.147	0.853
1000	727	1341	2.9	0.149	0.851
1050	777	1431	2.8	0.148	0.852
1100	827	1521	2.6	0.148	0.852
1150	877	1611	2.5	0.149	0.851
1200	927	1701	2.4	0.149	0.851
1250	977	1791	2.3	0.150	0.850
1300	1027	1881	2.2	0.150	0.850

The portable instrument used to measure R_s (D&S) was a Solar Spectrum Reflectometer (SSR), manufactured by Devices & Services Company, Dallas, TX. This reflectometer is designed to measure the solar averaged (Air Mass 2.0) hemispherical reflectance of flat opaque materials. Note that because the Pyromark coated components measured were both large cylinders (~ 24 in. diameter), no correction for the non-flat geometry was necessary. The SSR measures the hemispherical reflectance by diffusely illuminating a sample placed over the measurement port and viewing the sample surface with a detector assembly consisting of four separate detectors [B-1]. To approximate the solar (Air Mass 2.0) distribution, the output of the four separately filtered (to tailor spectral response) detectors are electronically weighted and summed. The wavelength range encompassed by the detection system is from 0.300μm to 2.500μm. When properly calibrated, the reflectometer has a measurement uncertainty of ± 0.015 reflectance units for these types of samples [B-2].

The other portable instrument used for the field measurements was a portable infrared reflectometer, Model DB-100, manufactured by Gier-Dunkle, Inc. The reflectometer is designed to measure the normal infrared emittance, $E_{N\text{-}GD}$ (100° C or 300° C), of flat opaque samples placed over the measurement port for 100 °C and 300° C black body radiation. Again note that no correction was necessary for the non-flat sample surface because both painted components were of large cylindrical geometries. The DB-100 determines the infrared reflectance (emittance = 1.00 - reflectance) by viewing the sample (with a single detector) while the surface is alternately irradiated with black body radiation from a rotating slit-cavity at differing temperatures. To obtain a measured value, the difference in the detector ac signal is integrated and weighted for either a 100° C or 300° C black body by placing a filter into the detector optical path. When calibrated to a known standard, the measurement uncertainty should be ± 0.035 reflectance units for these types of samples [B-3].

Laboratory Measurements

The hemispherical reflectance properties, covering the wavelength range from 0.265μm to 2.400μm, were measured using a Beckman 5270 spectrophotometer equipped with an integrating sphere accessory. All data obtained using this instrument were referenced to NBS calibrated standard material and should have a measurement uncertainty of ± 0.005 reflectance units (1.000 reflectance units = 100% reflectance). From the data measured within this wavelength region, the solar averaged hemispherical reflectance values, R_s (2π), were calculated using the following expression:

$$R_s(2\pi) = \frac{\int_{\lambda_1}^{\lambda_2} S_\lambda(E)\ \rho_\lambda(2\pi)\ d\lambda}{\int_{\lambda_1}^{\lambda_2} S_\lambda(E) d\lambda} \qquad \text{B-1}$$

where S_λ (E) is the solar energy distribution (Air Mass 2.0) value for wavelength λ, $\rho_\lambda(2\pi)$ is the measured hemispherical reflectance value for wavelength λ, and the integration interval is λ_1 = 0.265μm to λ_2 = 2.400$_\mu$m.

Since the samples measured were opaque, the solar averaged absorptance value, $A_s(2\pi)$, was calculated using equation (2) below:

$$A_s(2\pi) = 1.000 - R_{sn}(2\pi) \qquad \text{B-2}$$

A listing of the various optical properties for a variety of surface conditions using both the field and laboratory instruments is provided in Tables B-1 and B-2, as previously mentioned. In order to provide a correlation between the field, R_s (D&S), and laboratory, R_s (2π), measured values, the solar averaged reflectance was used as the

correlation parameter. This quantity was selected because: 1) the SSR provided the more accurate measured values of the two portable instruments, and 2) Pyromark black paint has been well characterized in this wavelength region [B-4]. Note that properly prepared (i.e. thermal cured following modified manufacturer recommendations, see Conclusion IV.) "regular black" Pyromark should exhibit a solar averaged absorptance of 0.97 when applied to stainless steel alloy substrates. The absorptance spectra for both the "black" and "blue" Pyromark paint coatings through the solar wavelength range are provided, for reference, in Figure B-1. The significance (upon the optical properties) of the "black" and "blue" Pyromark observed colors will be addressed in the Discussion section below.

For the optical properties covering the wavelength range from 2.400μm to 20.0μm, a recently developed system was employed. A Perkin-Elmer Model 1800 FTIR (Fourier Transform Infrared) spectrophotometer has been modified using an integrating sphere arrangement to enable the measurement of both hemispherical reflectance and transmittance properties over the near to mid-infrared wavelength region [B-5]. By merging the reflectance spectra from the two laboratory instruments, material properties can be optically characterized over the combined wavelength range to within a measurement uncertainty of ± 0.010 units. Using the spectral information obtained by this method, black body averaged values as a function of temperature were calculated using the equation below:

$$R_{BB}(T) = \frac{\int_{\lambda_1}^{\lambda_2} BB_\lambda(T)\ \rho_\lambda(2\pi)\ d\lambda}{\int_{\lambda_1}^{\lambda_2} BB_\lambda(T)\ d\lambda} \qquad \text{B-3}$$

where R_{BB} (T) is the calculated black body averaged reflectance value for temperature T (°K) and an integration interval of λ_1 = 0.265μm to λ_2 = 20.0μm, BB_λ (T) is the Planck distribution value for temperature T (°K)

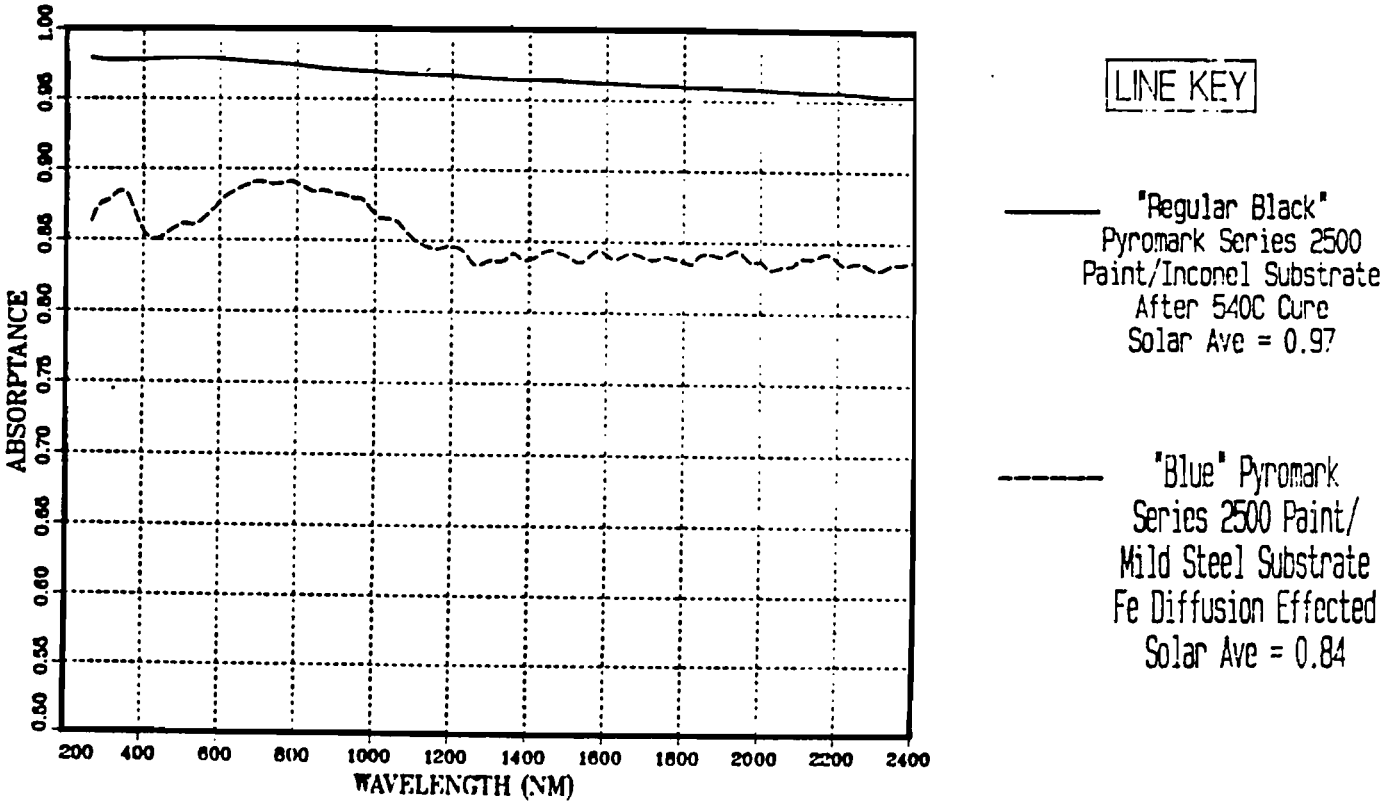

Figure B-1. "Regular Black" and "Blue" Pyromark Paint Absorptance Spectra Through Solar Wavelength Range (265 nm to 2400 nm)

and wavelength λ, $\rho_\lambda(2\pi)$ is the measured hemispherical reflectance value at wavelength g.

Finally, since the samples were opaque, the black body averaged absorptance value, A_{BB} (T), was calculated using equation B-4 below:

$$A_{BB}(T) = 1.000 - R_{BB}(T) \qquad \text{B-4}$$

Note that the A_{BB} (T) values also represent the normal emittance, E_N (T), since the measurements were taken at near normal incidence for both spectrophotometers (Beckman [6°]; Perkin-Elmer [15°]). A plot of the spectral absorptance and black body averaged normal emittance properties are provided in Figures B-2 and B-3, for both the regular "black" and "blue" Pyromark coatings. Notice that the normal emittance characteristics are also listed in Table B-2.

Discussion of Optical Properties

It should be noted that the radiative properties of a material can be determined in the manner described above only if the surface optical properties remain stable. One mechanism that can significantly alter the optical characteristics of the material surface is a crystallographic phase transformation. Evidence now suggests that the optical properties of Pyromark (Series 2500 high temperature black) paint are both substrate and temperature dependent. Findings indicate that Pyromark black paint, when applied to mild steel substrates, apparently undergoes a phase transformation at ~ 800° C.

The "black-to-blue" paint phase transformation, observed on the mild steel substrate, significantly altered the spectral absorptance properties, as shown in Figure B-2. X-ray diffraction data, comparing the "black" and "blue" coating, indicated a significant paint crystallographic change. The complete transformation mechanism is not known at this time, but is probably related to the diffusion of Fe into

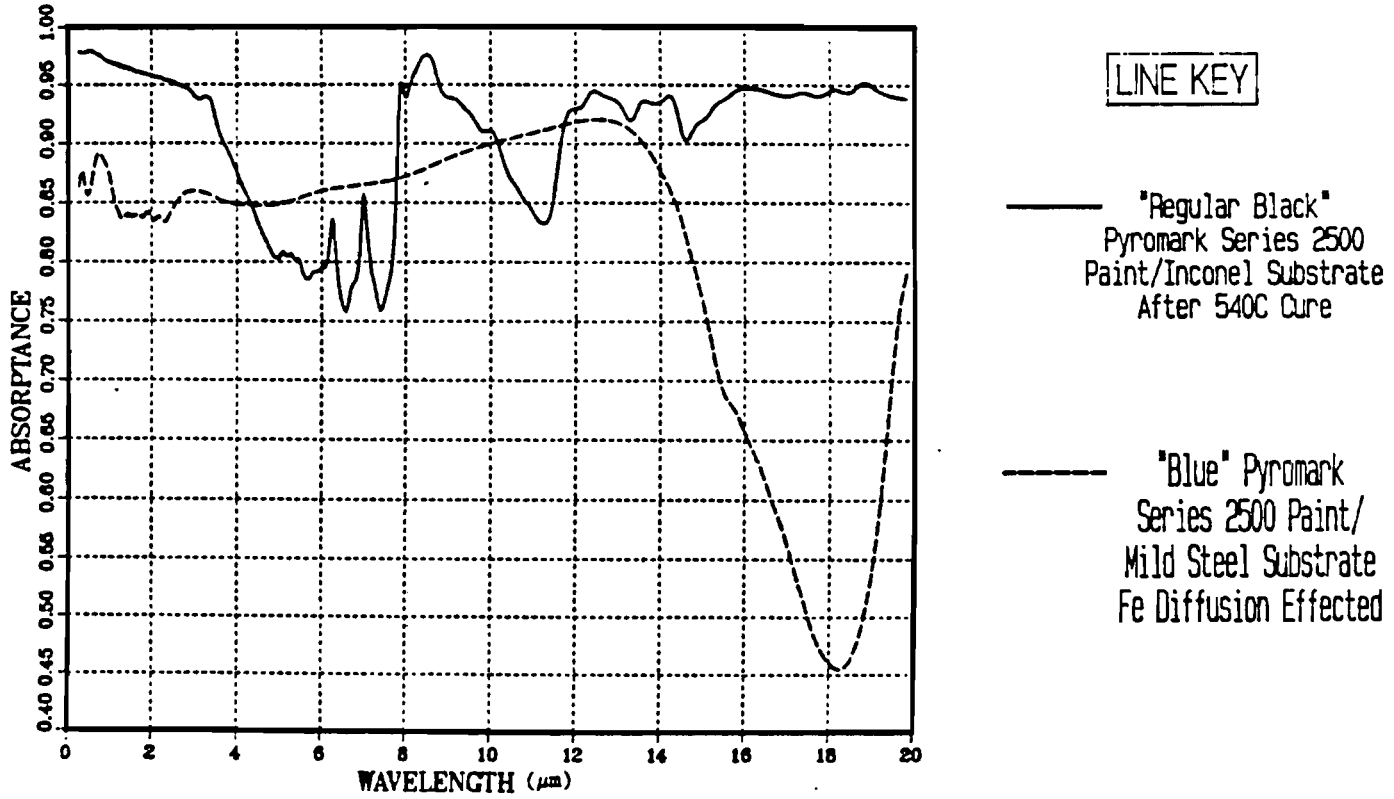

Figure B-2. "Regular Black" and "Blue" Pyromark Paint Absorptance Spectra from 0.265 μm (265 nm) to 20.0 μm (20,000 nm)

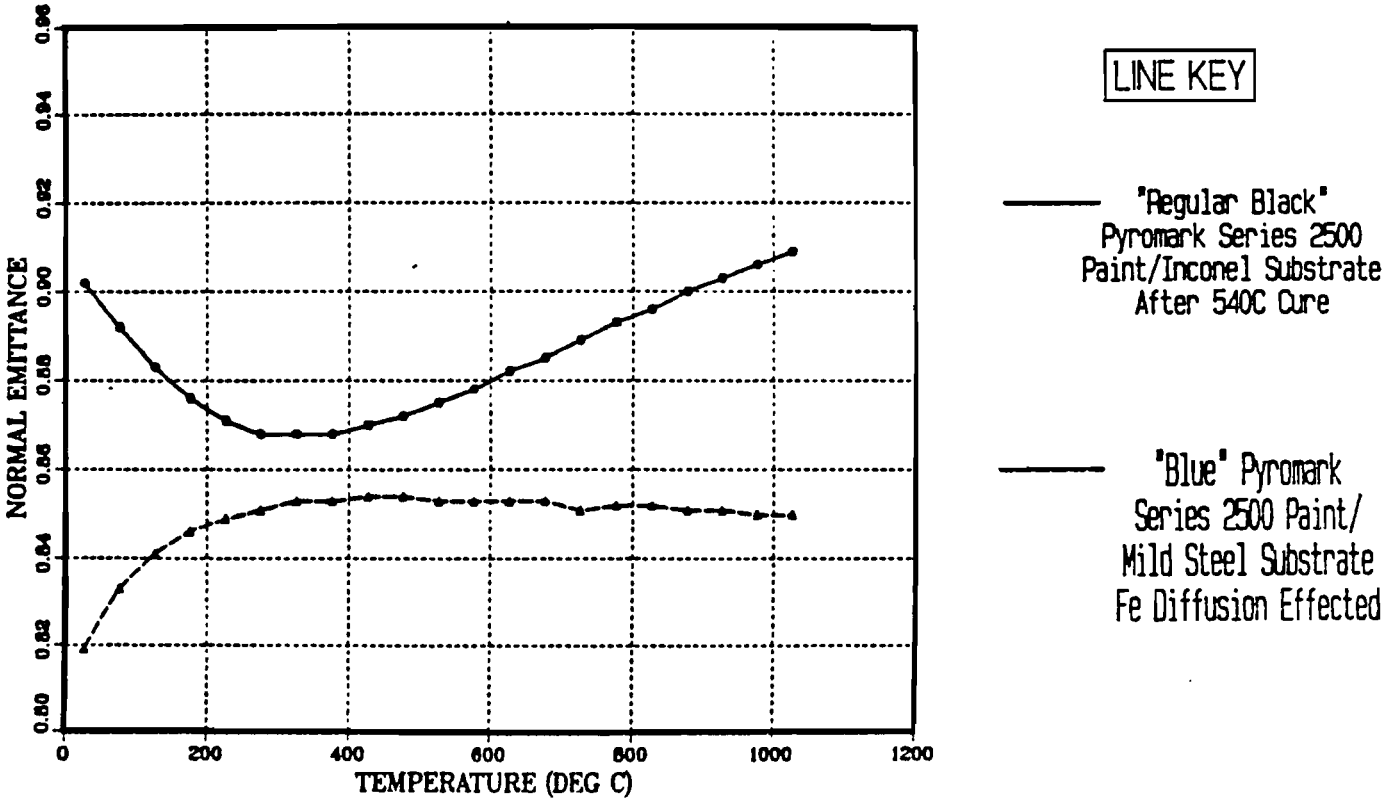

Figure B-3. Calculated Normal Emittance Versus Temperature for "Regular Black" and "Blue" Pyromark Paint

the paint matrix (consisting of primarily Fe-Mn oxides) shifting the balance of the solid solution into a different phase. The temperature dependent emittance characteristics (calculated using the spectral absorptance), shown in Figure B-3, exhibited a slight change between the two phases with emittance values above 0.80 for all temperatures. The reason for the relative non-sensitivity of the black body averaged values, especially at elevated temperatures, is due to both the inherent broad wavelength dependence of the Planck distribution and the limited spectral difference between the two paint phases for wavelengths below 14μm.

A comparison of the field and laboratory determined solar averaged values demonstrated good agreement for both the "black" and "blue" Pyromark regions. Typical A_S values for the "black" regions (Inconel substrate) were 0.97, while the "blue" regions (mild steel) ranged from 0.84 to 0.89. A comparison of the field and laboratory determined emittance values is shown in Figure B-4. Note that the measurement uncertainty for the portable instrument is also provided in the figure. Because of the following factors: 1) the relatively large uncertainty in the portable infrared instrument measured values, 2) the non-uniformity of the Pyromark coated surfaces measured in the field, and 3) the good agreement between the field and lab measured solar averaged values; the laboratory determined emittance values should be taken as typical "best" (black) and typical "worst" (blue) case values. Clearly, even the "blue" Pyromark coating exhibited emittance values > 0.80 for above ambient temperature conditions.

Conclusions

I. The optical properties of Pyromark Series 2500 high-temperature black paint are both substrate and temperature dependent.

II. Findings indicate that Pyromark black paint, when applied to mild steel substrates, apparently undergoes a phase transformation at -

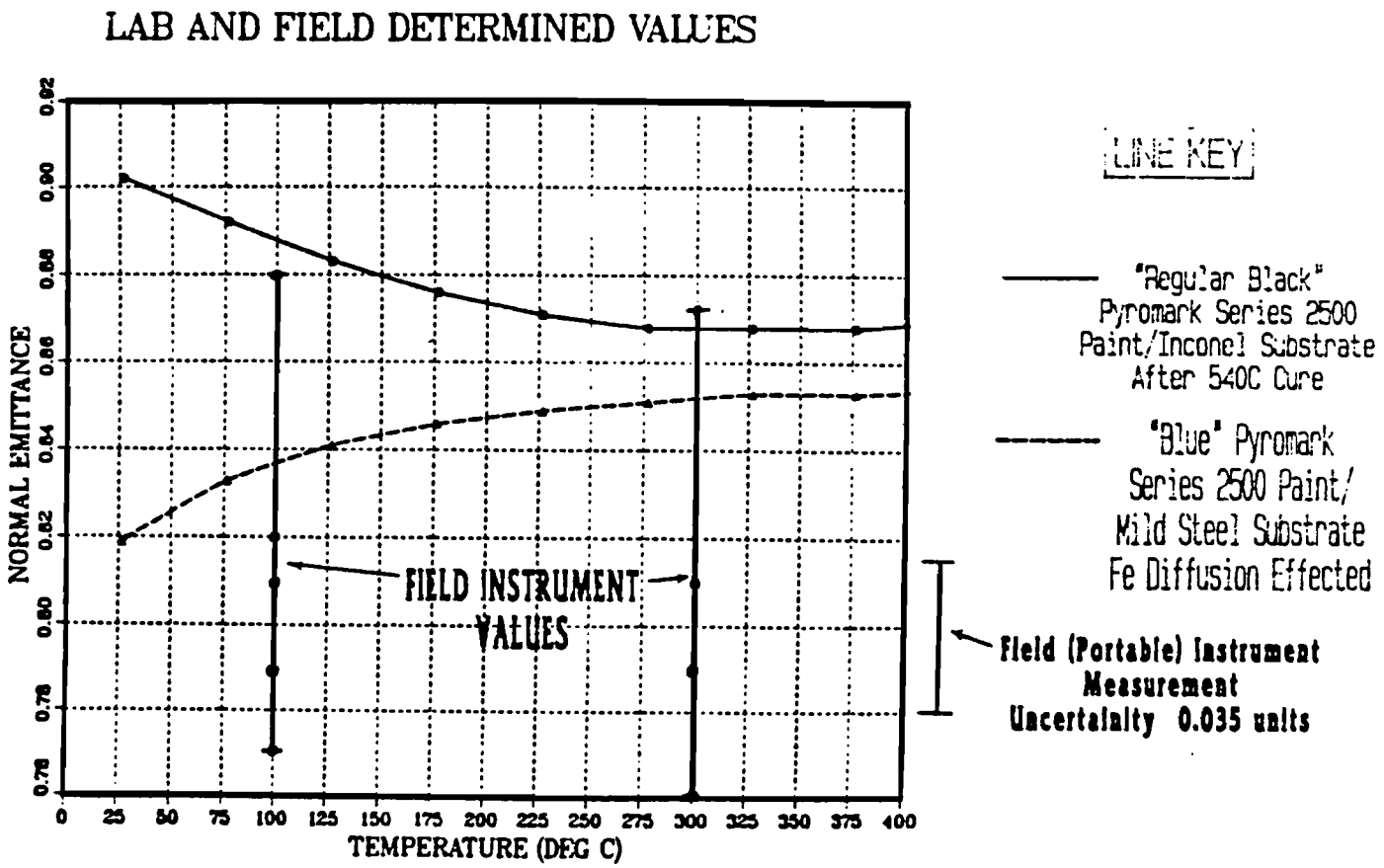

Figure B-4. Calculated Normal Emittance Versus Temperature for "Regular Black" and "Blue" Pyromark Paint Including Field (Portable) Instrument-Measured Values

800° C. The "black-to-blue" transformation significantly altered the spectral absorptance properties of the paint. Typical solar averaged absorptance values decreased from 0.97 (black) to 0.84 (blue). Calculated normal emittance characteristics were also effected but remained above 0.80 for above ambient temperature conditions.

III. Other transformations, which could significantly effect the optical properties, could occur on other substrates and other temperatures. Studies are continuing on a variety of substrates and temperatures and will be subsequently published [B-6]. Note, however, that the limited information that is available suggests that an irreversible transformation (on the mild steel substrates) occurs very rapidly at ~ 800° C and that the "blue" Pyromark coating remains optically stable (after the transformation) within the operating temperature range of the test article, i.e. ambient to ~ 870° C.

IV. For Pyromark paint operation temperatures above 540° C (1000 °F), the following modified curing technique is recommended:

1. Clean substrate as per manufacturer recommendations and apply paint with either brush or spray (spray gun preferred).
2. AIR DRY ~ 2 hours or until tack-free (or over night).
3. All heating rates should be no greater than 10° C per minute whenever possible.
4. Heat to 120° C (250° F), hold for ~ 2 hours.
5. Heat to 250° C (480° F), hold for ~ 2 hours.
6. Heat to 540° C (1000° F), hold for ~ 1 hour.
7. Heat to MAXIMUM OPERATING TEMPERATURE + 50° C, hold for ~ 1 hour.

REFERENCES

[B-1] Mahoney, A. R. "Solar Hemispherical Reflectometer Modification for Second Surface Mirror Materials," SAND 82-0934, March 1982.

[B-2] Pettit, R. B. "Optical Measurement Techniques Applied to Solar Selective Coatings," SAND-77-0421, August 1977.

[B-3] Pettit, R. B., and A. R. Mahoney. "Portable Instrumentation for Solar Absorptance and Emittance Measurements," (80-1541C) Proc Line Focus Solar Thermal Energy Tech. Dev. Conf. USDOE, Albuquerque, NM, 1980, pp. 437-447.

[B-4] Nelson, B., and A. R. Mahoney. "The Effect of Vitrification Temperature on the Solar Averaged Absorptance Properties of Pyromark Series 2500 Black Paint," SAND 86-0675, June 1986.

[B-5] Tardy, H. L., and R. G. Dunn. "Spectral Hemispherical Reflectometer for the Mid-Infrared," SAND 86-2886J, 1987.

[B-6] Mahoney, A. R., and H. L. Tardy. "Thermal Degradation of Pyromark High-Temperature Solar Absorbing Paint," to be published.

APPENDIX C

Comparison of Measured Surface Temperature With Estimated Surface Temperature

Obtaining accurate measurement of surface temperature of an object exposed to a severe environment has been difficult. This is primarily due to radiative exchange that occurs between the temperature probe and the environment, soot buildup on the sensing surface, and convective effects.

An alternative method of estimating the surface conditions is to place temperature sensing devices on the inside wall of the object and use the measured interior temperature histories to infer the surface condition variation as a function of space and time. This method is called inverse heat conduction [C-1]. Recently a different type of temperature measuring sensor has been considered for severe environment application. This sensor, called the Nanmac surface thermocouple [C-2], differs considerably in its operating principles, as well as installation, from the standard sheathed type thermocouple (see Figure 2.2-3).

By comparing two different methods of obtaining surface temperature, one can get a better understanding of the accuracy of the surface temperature measurements. However, because of the uncertainties involved with inverse heat conduction, as well as with direct measurement using Nanmac thermocouples, the results of this analysis do not indicate the actual accuracy of these methods. Only the difference in the two methods is compared. Thermocouple TC1 and TC40 are used for the comparison. Other locations yielded approximately the same results. Data for all three environments are included.

The two measurement locations, TC1 and TC40, represent the same measurement point but were slightly offset from each other to minimize interference (see Figure 2.2-3). The Nanmac thermocouple (TC40) was flush with the surface of the test article, and the intrinsic Type K thermocouple (TC1) was mounted on the back face of 3.18 cm (1.25 inches) of steel. The temperature history from TC1 was used in an inverse heat conduction analysis [C-1] to estimate the surface temperature.

To compare the two temperature histories, TC40 and TC1, absolute difference between the two temperature histories was used.

Results from the 800°C, 30-minute radiant heat test are shown in Figures C.1-1 and C.1-2. The first figure, C.1-1, shows the temperature history for TC40 and the estimated surface temperature using data for TC1. Agreement seems good. The Nanmac temperature lags slightly behind the estimated temperature for the first 1200 seconds and then is slightly greater for the duration of the test. Figure C.1-2 shows the absolute difference between the two temperatures as a function of time. Largest differences (approximately 7.0°C) occur during the beginning of the heat up phase. The average absolute difference for the entire test was 2.5 ± 1.6°C. The Nanmac thermocouple has a relatively fast response time (in the millisecond region), and the data scanning rate was 5 seconds, which eliminates response time as a possible cause for lagging behind the estimated surface temperature for early times. Since installation is critical to Nanmac performance, this could be another possible cause. However, the more probable cause is the inverse approximation. The Nanmac thermocouple can respond immediately to the environment because it can see the environment. The thermocouple used in the inverse calculation is located on the back face of 3.175 cm (1.25 inches) of steel. Therefore, its response is delayed because of the thermal lag effect. This does explain why there are large differences during early times but does not explain why the estimated temperature is ahead of the measured surface temperature.

Figures C.1-3 and C.1-4 show the results of the 870°C, 100-minute radiant heat test, and Figures C.1-5 and C.1-6 show results from the engulfing fire test. Results from all three tests are summarized in Table C.1-1.

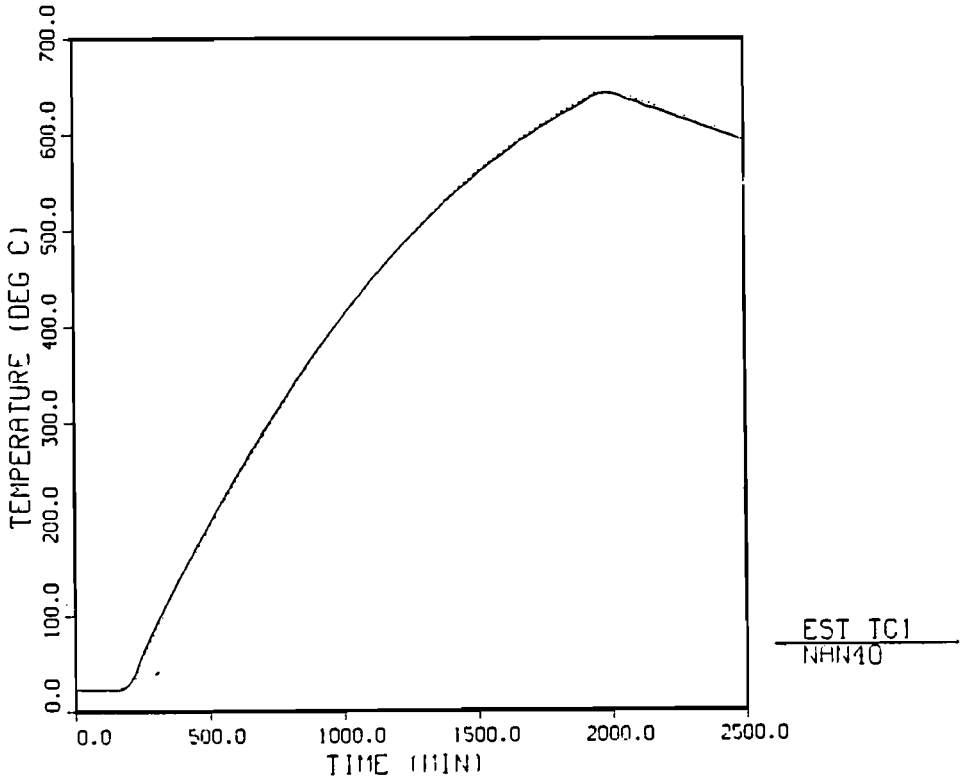

Figure C.1-1 Temperature History from NAN40 Versus Estimated Surface Temperature from TC1, Test 1

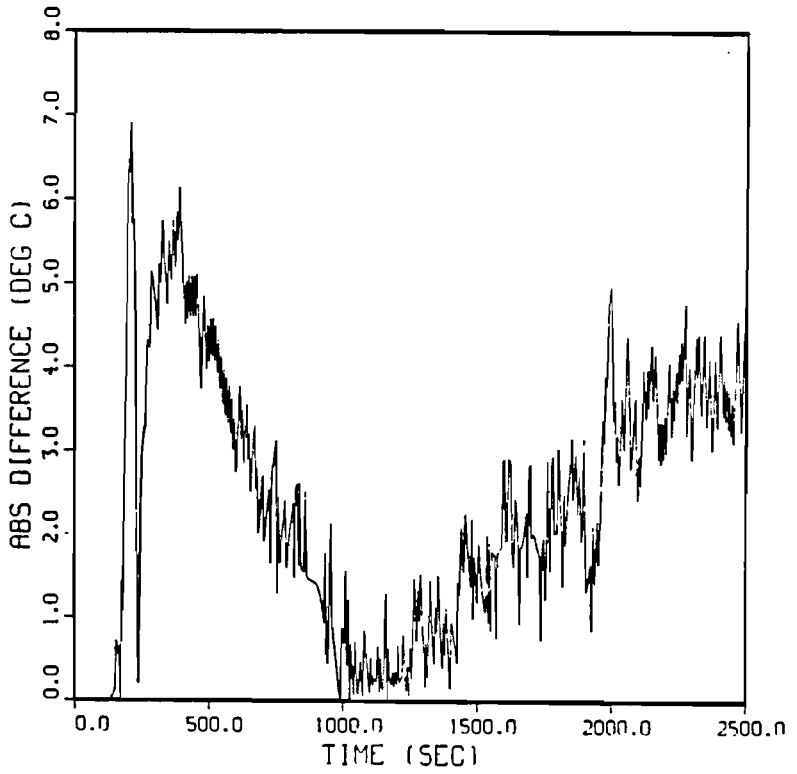

Figure C.1-2 Absolute Difference Between Measured Surface Temperature from NAN40 and Estimated Surface Temperature from TC1, Test 1

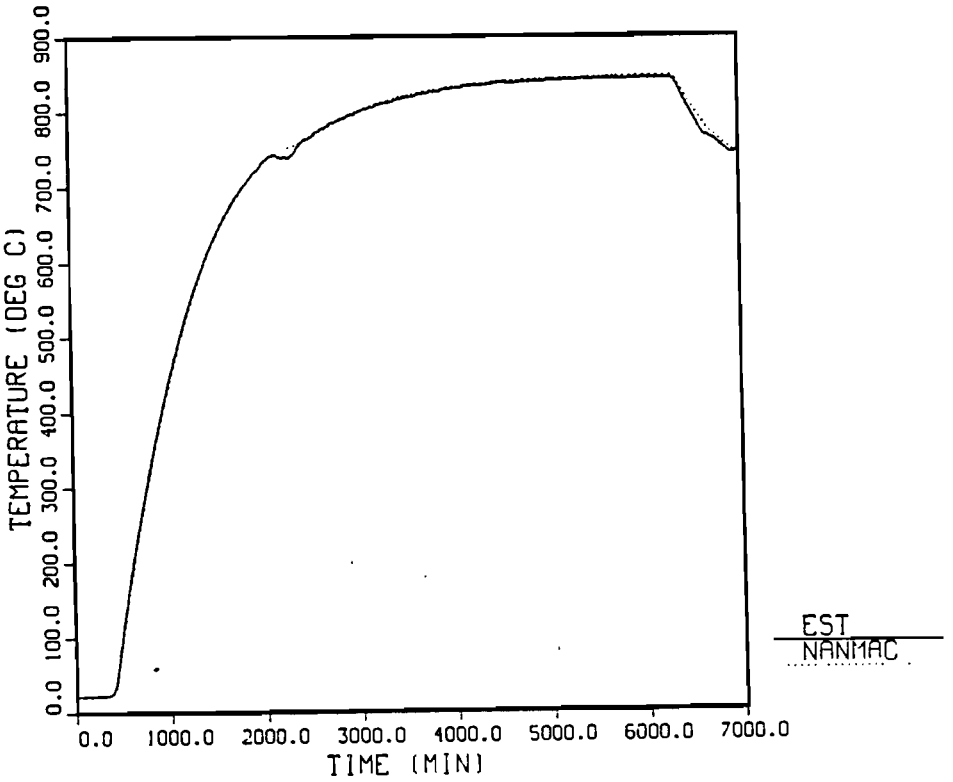

Figure C.1-3 Temperature History from NAN40 Versus Estimated Surface Temperature from TC1, Test 3

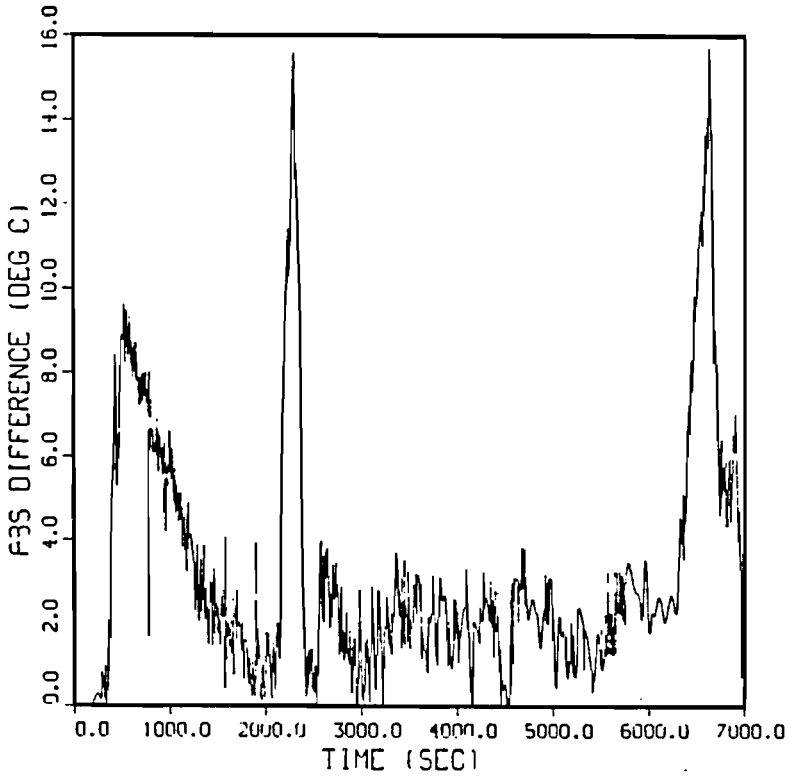

Figure C.1-4 Absolute Difference Between Measured Surface Temperature from NAN40 and Estimated Surface Temperature from TC1, Test 3

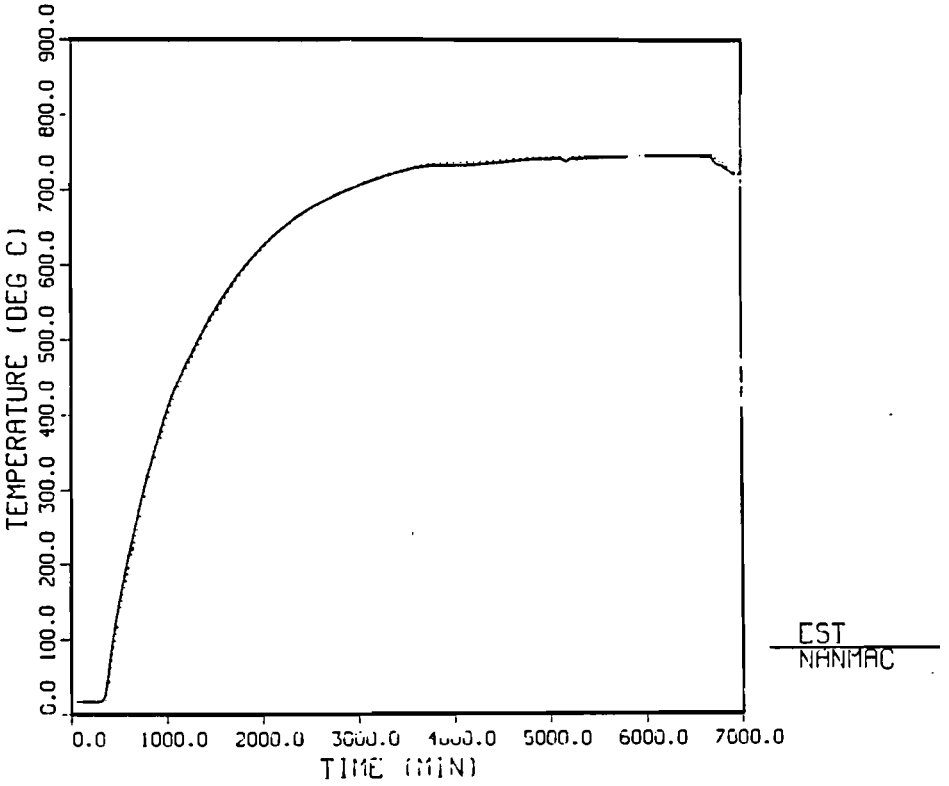

Figure C.1-5 Temperature History from NAN40 Versus Estimated Surface Temperature from TC1, Test 5

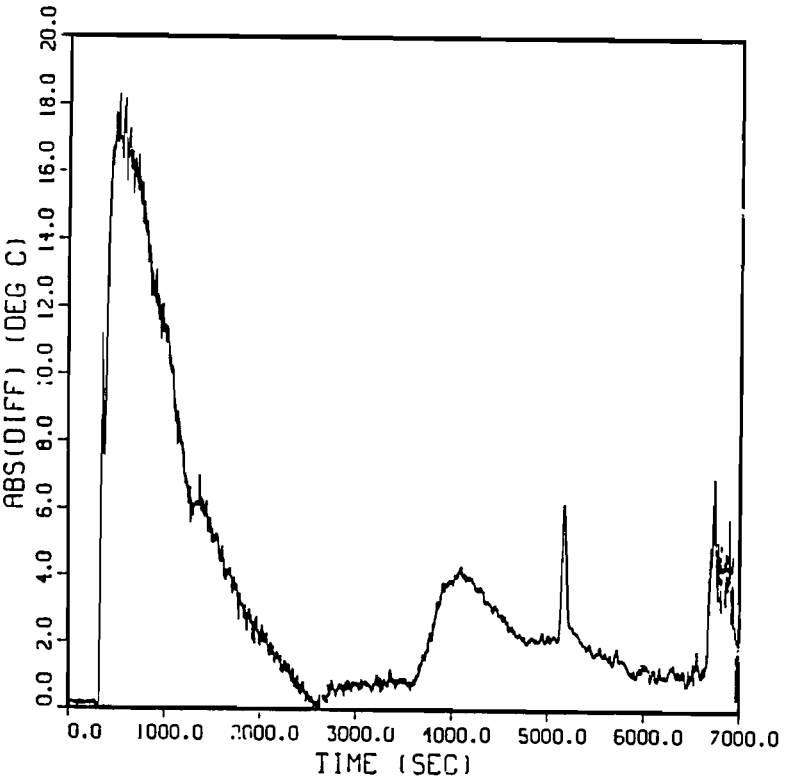

Figure C.1-6 Absolute Difference Between Measured Surface Temperature from NAN40 and Estimated Surface Temperature from Test 5

TABLE C.1-1

Comparative Results of Measured Surface Temperatures Obtained from Nanmac Thermocouples and Estimated Surface Temperatures Obtained from Backface Intrinsic Thermocouples

Thermal Environment	Max $\|\Delta\|$ (°C)	Avg $\|\Delta\|$[a] (°C)
800°C, 30 min Radiant Heat	7.0	2.5±1.6
870°C, 100 min Radiant Heat	15.5	3.2±2.9
Engulfing Fire, ~ 100 min	18.0	3.5±4.1

[a]The ± values represent the estimated standard deviation associated with the sample mean.

REFERENCES

[C-1] Hills, R. G., and E. C. Hensel. "Space Marching Inverse Conduction Code," SAND84-1563, Sandia National Laboratories, July 1986.

[C-2] Bainbridge, B. L. "Performance of Nanmac Surface Thermocouples," Internal Memorandum, Sandia National Laboratories, Albuquerque, NM, December 24, 1985.

APPENDIX D

Uncertainty Analysis Using the Inverse Heat Conduction Code SMICC

This appendix describes the analysis performed to determine the uncertainty associated with estimated surface heat flux and estimated surface temperature. A resolution analysis is given to indicate the effects of digital filtering on the resolution of the surface estimates. For a complete discussion of inverse heat conduction variance and resolution analysis see Reference [D-1]. An assessment of the uncertainty in material properties and their affect on surface estimates is given.

Resolution Analysis

Uncertainties in surface estimates depend largely upon random measurement uncertainties and the time step of the differencing scheme, as well as on the resolution of surface estimates [D-1]. Resolution is a term that defines how the surface estimates are smoothed or "blurred" over time. Digital filters are used here to effectively smooth, or average, the input data over time. The estimated surface temperatures are less sensitive to random measurement uncertainty than surface heat flux estimates [D-1]. Therefore, the main thrust of the uncertainty analysis focuses on the uncertainty of estimated surface heat flux. Biased or systematic uncertainties were not analyzed in this report.

Figure D.1-1 graphically shows the effects of filtering on the resolution of surface estimates. In this figure three different filter strengths were analyzed at a time node of 500 seconds for thermocouple location TC1 during Test 1. The filter strength indicates the number of future and past times used. The surface resolution is "blurred" as filter strength increases. This "blurring" increases the time domain at which surface conditions are determined. As filter strength is increased, the surface resolution decreases. The resolution coefficients indicate how each time is weighted in determining surface conditions at 500 seconds. The algebraic sum of those coefficients is one. If no filter were used, Figure D.1-1 would contain a vertical line of magnitude one centered at 500 seconds indicating that only time node 500 is used to estimate surface conditions at 500 seconds.

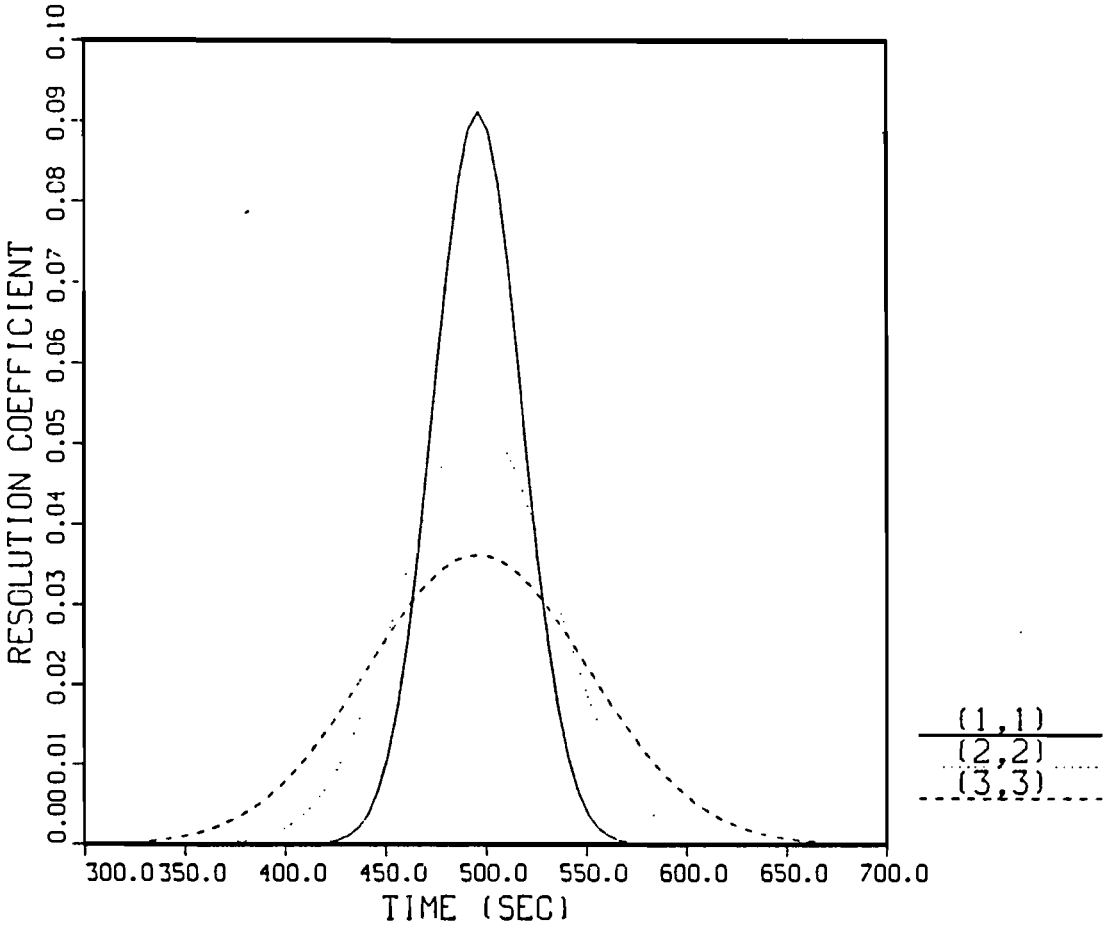

Figure D.1-1 Resolution Coefficients for a $\Delta t = 5.0$, as a Function of Filter Strength

Figures D.1-2 and D.1-3 show estimated surface conditions when no filter is used. It is difficult to determine the shape of the surface heat flux history because of large variations. The estimated surface temperature history, on the other hand, is relatively smooth and well defined. Figure D.1-4 shows the effects of filtering on the estimated surface heat flux as a function of filter strength. As filter strength is increased, the estimated surface heat flux shows more stability and less variation; however, the ability to resolve sharp peaks is degraded. This, in turn, reduces maximum values of heat flux.

The problem arises as to how much filtering should be used to effectively estimate the uncertainties of surface estimates that are representative of the test. Basically one has to consider the trade offs between surface resolution and uncertainty magnitude. The methodology that was used to decide on a filter strength is relatively simple. The main criteria used to evaluate test performance is time-integrated surface heat flux because this represents the total heat input to the test article for a given test. Therefore, the filter strength should not greatly affect this value. Table D.1-1 shows the integrated surface heat flux uncertainty and the time integrated surface heat flux as a function of filter strength. This table shows that a 87 percent reduction in uncertainty accompanies a 0.6 percent change in time integrated heat flux. Therefore, the filter strength does not greatly affect integrated flux.

As filter strength is increased to larger values, the surface heat flux, as a function of time, becomes greatly distorted causing large changes in integrated heat flux. Therefore, filter strengths beyond 5 were not considered.

Going back to Figure D.1-4 one can see how the curves are distorted as filter strength is increased. Filtering is required to estimate the surface heat flux. Without filtering one cannot determine the shape of the surface heat flux versus time curve because of large variations (see Figure D.1-2). A

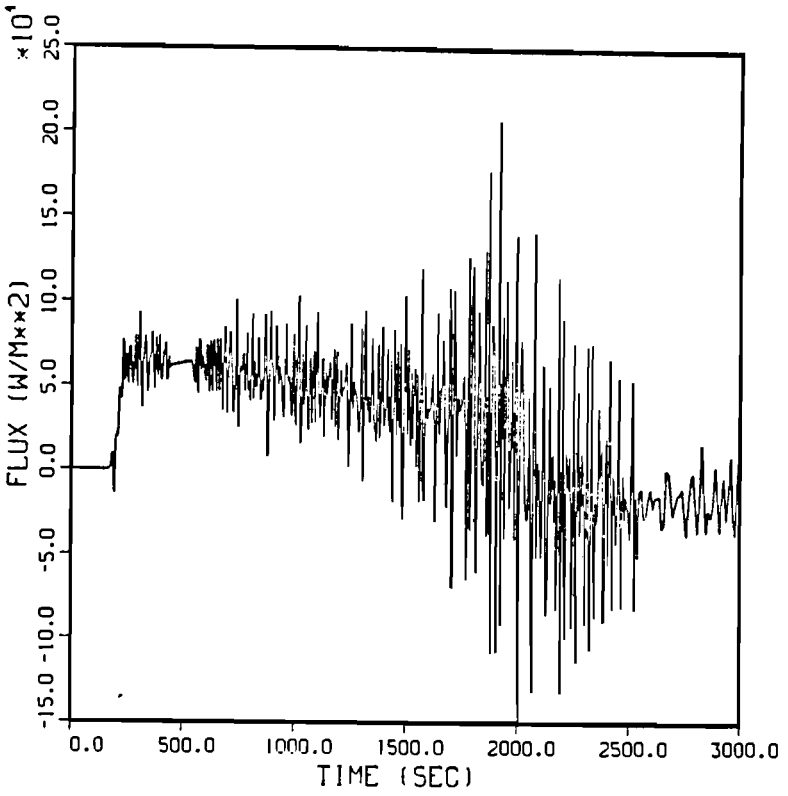

Figure D.1-2 Estimated Surface Heat Flux History Using No Filter for TC1, Test 1

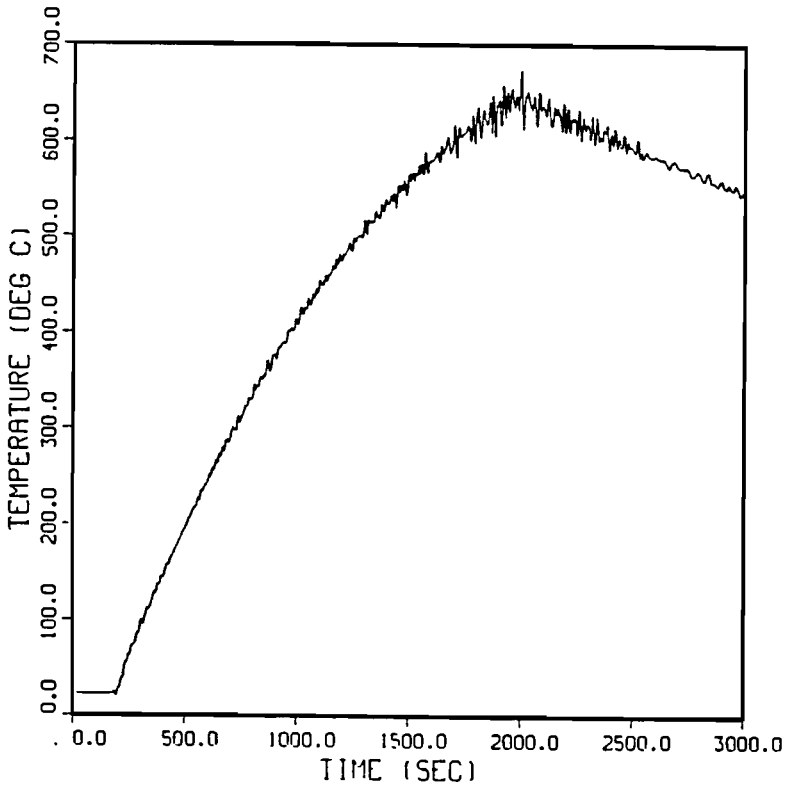

Figure D.1-3 Estimated Surface Temperature History Using No Filter for TC1, Test 1

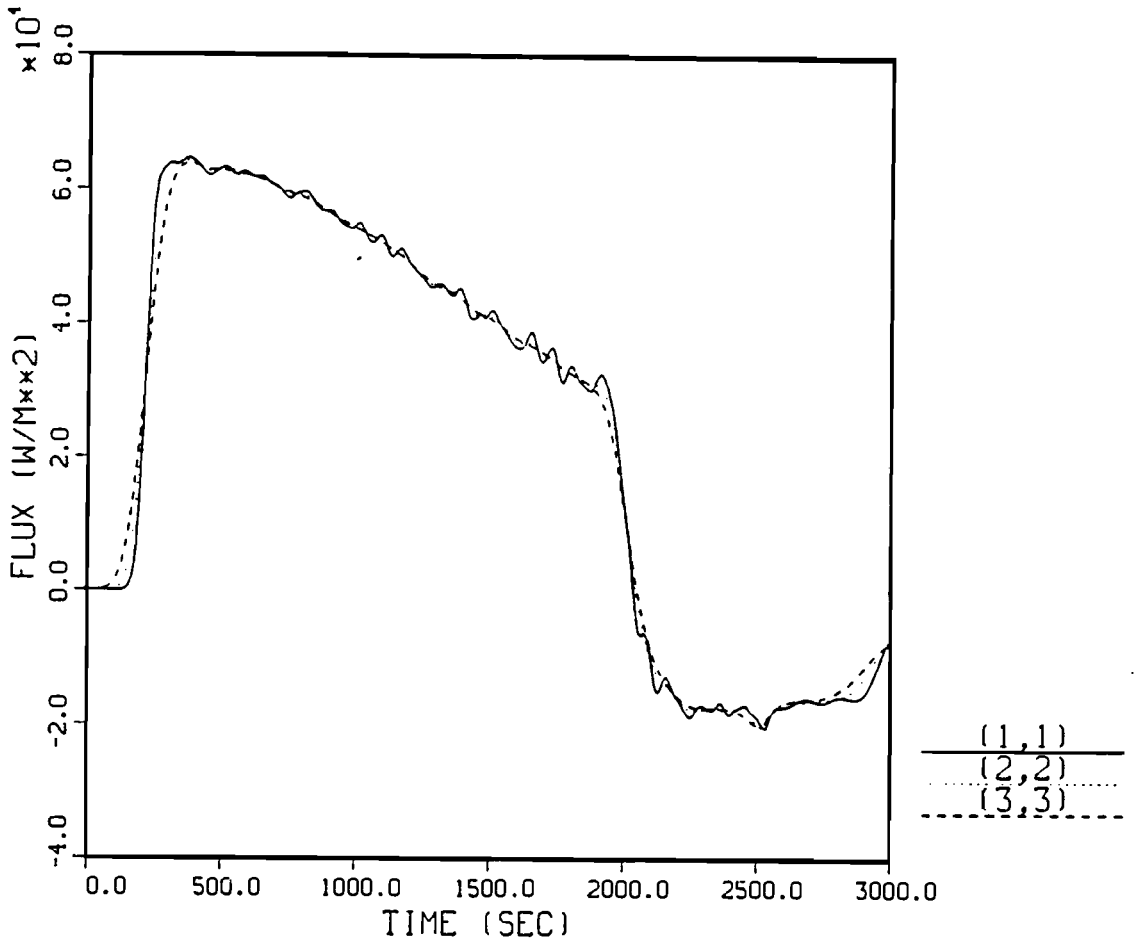

Figure D.1-4 Surface Heat Flux Histories as a Function of Filter Strength for TC1, Test 1

TABLE D.1

The Effect of Filter Strength on Relative Uncertainties and Time Integrated Surface Heat Flux[a]

Filter Strength	Surface Heat Flux Uncertainty ± (MJ/m^2)	Integrated Heat Flux (MJ/m^2)
1	16.24	88.76
2	6.10	88.62
3	3.30	88.43
4	2.14	88.20

[a]This information was obtained from TC1 during Test 1.

filter strength of 1 provides the best resolution at the expense of large uncertainty which, in some cases, is larger than the estimated surface heat flux. For large filter strengths, a filter strength of 4, for example, uncertainties in surface heat flux become smaller than the random measurement uncertainties that are used to calculate them. For a reasonable uncertainty magnitude and good resolution, a filter strength of 2 was chosen for Test 1 results.

The uncertainty performance for the 870°C, 100-minute radiant heat test was considerably different than for the 800°C, 30-minute test. Figure D.1-5 shows the effects of filter strength on the estimated surface heat flux. The variability of surface heat flux is considerably reduced as filter strength is increased, especially when the test article becomes saturated. A filter strength of 3 was chosen due to the relatively large uncertainty bounds with respect to Test 1 results. A filter strength of 3 was also used for the engulfing fire test results.

Uncertainty Analysis Using Random Measurement Uncertainty

There are four basic sources of uncertainty in the thermocouple measurements at the Radiant Heat Facility [D-2]. Those sources are the data acquisition system (DAS), the thermocouple and extension wire combination, the thermocouple installation, and noise errors induced in the analog wiring. The first two are readily quantified, the third and fourth are not.

The uncertainties resulting from the DAS and the thermocouple and extension wire combination have been studied in depth in [D-2]. The uncertainties resulting from the DAS are "random" in nature and result from items like electrical noise and digitizing of the data. Uncertainties resulting from the thermocouples and extension wires are "systematic" in nature and result from specific calibration of the wire used.

The mounting method uncertainties result from the fact that what is actually being measured is not what is desired to be measured--in this case

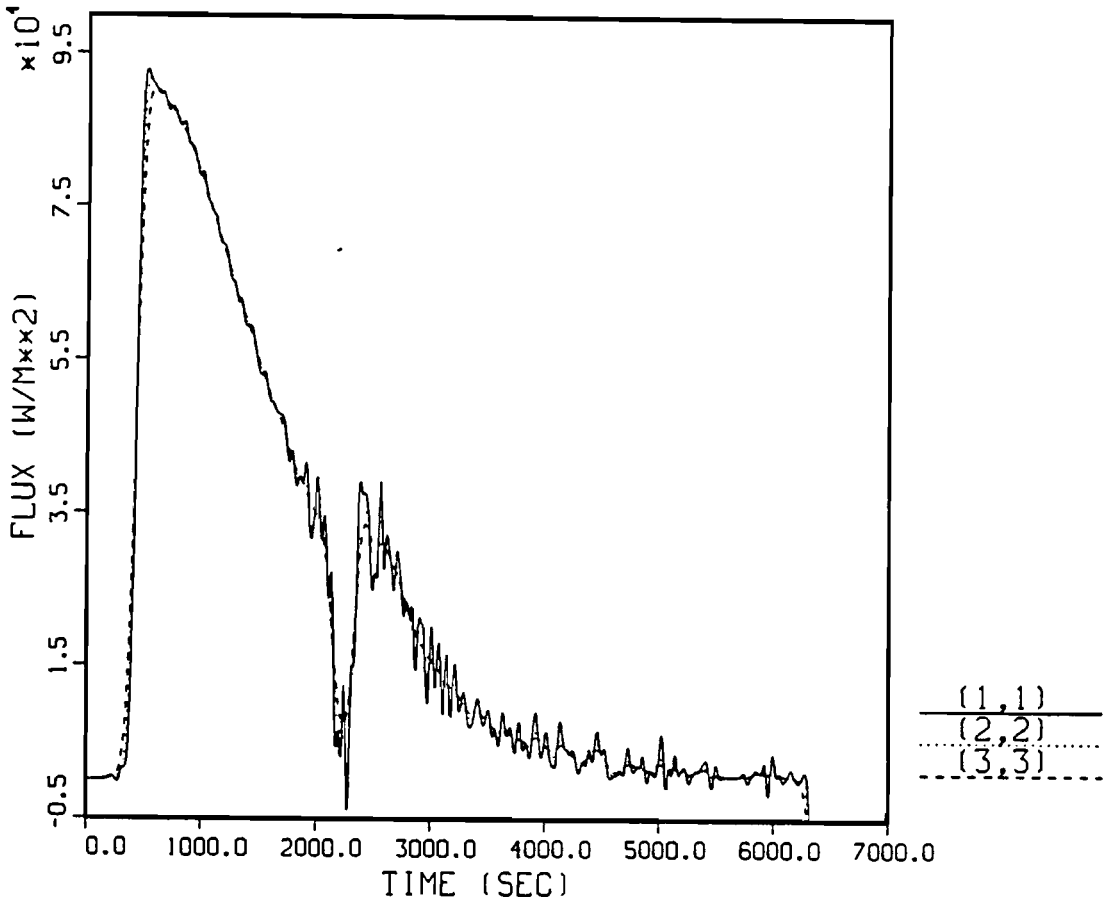

Figure D.1-5 Surface Heat Flux Histories as a Function of Filter Strength for TC1, Test 3

the metal temperature. The mounting method uncertainties are more difficult to quantify, are systematic and transient in nature, depend on the specific test, and are believed to be the single largest source of uncertainty.

The noise-induced errors are caused by the electric power source for the lamps, which generates random signals in the analog lines. These noise uncertainties increase with increasing power level.

The estimation of heat flux from temperature measurements with inverse codes effectively involves taking derivatives of the temperature with respect to space and time. When this is done, the systematic uncertainties are eliminated as a source of uncertainty only in the heat flux calculations because they are either constant or vary slowly. As a result, the random DAS uncertainties and electrically generated noise are the ones that need to be considered.

Tables II and VI in [D-2] discuss the magnitude of these uncertainties. Based on manufacturer's data, it is suggested that a random uncertainty of ± 0.3 percent of full scale reading be used in each of four ranges used in the DAS: ± 10 mv, ± 20 mv, ± 40 mv, and ± 80 mv. Note that 10 mv corresponds to 250°C for the thermocouples used, 20 mv corresponds to 485°C, 40 mv corresponds to 970°C, and 80 mv corresponds to greater than 1370°C. In addition, measurements documented in the above reference suggest that an uncertainty of ± 60 μv be added to each range to account for noise induced from the power system. Totaling these uncertainties in each range one arrives at these values: ± 0.9 percent of FS up to 250°C, ± 0.6 percent of FS up to 485°C, and (lumping the upper two ranges) ± 0.5 percent up to the maximum temperature seen. A single value of about ± 1 percent of the full scale reading in each range (in F or C) can be used as a reasonable estimate of the random uncertainty in the temperature measurements used for calculating heat flux.

The random measurement uncertainty temperature regions are shown below:

Temperature Range (°C)	Uncertainty (°C)
0--250	2.5
251--485	4.85
486--850	8.5

The inverse heat conduction code SMICC [D-1] used for the uncertainty analysis uses an ordinary least squares (OLS) estimator, which estimates the uncertainties of surface conditions. The statistical assumptions about the random measurement errors that are used to develop OLS can be found in Reference [D-3].

The uncertainty reported in this appendix is the uncertainty associated with the total heat input for each test. The time-integrated surface heat flux uncertainty is integrated over time providing an average uncertainty for the entire heatup phase of the test. For the 800°C, 30-minute radiant heat test, the total heat input to the test article was 88.62 ± 6.10 MJ/m^2. The data used for this calculation was obtained from TC1, Test 1. This location is assumed to be representative of the entire test article. The total heat input to the test article during the 870°C, 100-minute test was 143 ± 22.19 MJ/m^2. Again, results are presented for TC1 only. The total heat input to thermocouple location TC1 during the enclosed engulfing fire environment was 125 ± 30.95 MJ/m^2.

Uncertainty Analysis for Material Property Data

To determine the effect of uncertainty in material property data, a sensitivity analysis was performed. The sensitivity analysis varied thermal conductivity and the density-specific heat product to determine the effects on surface estimates. The uncertainty bounds of the material properties that were investigated in the sensitivity analysis were obtained from personal communications with the Thermophysical Properties Division at Sandia National

Laboratories (see Appendix A). Only data from TC1, Test 1 was used for the sensitivity analysis. The results are representative of the test series.

Results of the sensitivity analysis indicate that there is a one-to-one relationship with respect to the sensitivity of estimated surface heat flux to the density-specific heat product. In other words, a 5 percent uncertainty in density-specific heat produces a 5 percent change in estimated surface heat flux. The sensitivity of estimated surface heat flux was considerably less. This means that a 5 percent uncertainty in thermal conductivity produces less than 1 percent change in estimated surface heat flux. The sensitivity of estimated surface heat flux is linear, with respect to uncertainty of material properties, up to an uncertainty of 10 percent. Uncertainties beyond 10 percent were not investigated.

The sensitivity of estimated surface temperature was the same for thermal conductivity uncertainty as well as density-specific heat uncertainty. The calculated relationship was a 5 percent uncertainty in material properties which produced a 2 percent change in estimated surface temperature.

REFERENCES

[D-1] Hills, R. G., and D. C. Hensel. "Space Marching Inverse Conduction Code," SAND84-1563, Sandia National Laboratories, July 1986.

[D-2] Nakos, J. T. and B. G. Strait. "An Error Analysis of Thermocouple Measurements in the Radiant Heat Facility," SAND80-2655, Sandia National Laboratories, December 1980.

[D-3] Beck, J. W., and K. J. Arnold. Parameter Estimation in Engineering Science, New York: John Wiley and Sons, Inc., 1977.